

S2-84273

Copy 552

RM E57C07

79
P

63 16236

Code -1

Classification changed to
Effective 18 April 1961
NASA CCN-3 By J.J.Carron



RESEARCH MEMORANDUM

EXPERIMENTAL INVESTIGATION OF EFFECTS OF COMBUSTION -
CHAMBER LENGTH AND INLET TOTAL TEMPERATURE,
TOTAL PRESSURE, AND VELOCITY ON
AFTERBURNER PERFORMANCE

By Charles R. King

Lewis Flight Propulsion Laboratory
Cleveland, Ohio

CLASSIFIED DOCUMENT

This material contains information affecting the National Defense of the United States within the meaning of the espionage laws, Title 18, U.S.C., Secs. 793 and 794, the transmission or revelation of which in any manner to an unauthorized person is prohibited by law.

~~OTS PRICE~~
~~XEROX \$ 7.60/pk~~
~~MICROFILM \$ 2.57/pk~~

NATIONAL ADVISORY COMMITTEE
FOR AERONAUTICS

WASHINGTON

June 3, 1957

~~DECLASSIFIED~~

NACA RM E57C07

NATIONAL ADVISORY COMMITTEE FOR AERONAUTICS

RESEARCH MEMORANDUM

EXPERIMENTAL INVESTIGATION OF EFFECTS OF COMBUSTION-CHAMBER
LENGTH AND INLET TOTAL TEMPERATURE, TOTAL PRESSURE,
AND VELOCITY ON AFTERBURNER PERFORMANCE

By Charles R. King

SUMMARY

The effects of afterburner-inlet total temperature, total pressure, velocity, fuel-air ratio, and afterburner combustion-chamber length on afterburner performance and stability limits were investigated using a 25.75-inch-diameter cylindrical afterburner installed in a duct test rig. This afterburner is typical of current high-performance V-gutter-type afterburners without internal cooling liners. The range of afterburner-inlet conditions investigated was as follows: total temperature, 1260° to 1860° R; total pressure, 750 to 1800 pounds per square foot absolute; velocity, 400 to 650 feet per second; and afterburner fuel-air ratio, lean blowout to higher than stoichiometric. The afterburner combustion-chamber length was varied in 12-inch increments from 30 to 66 inches.

Each of the parameters had a marked effect on combustion efficiency within the range of conditions investigated. For example, changing the afterburner combustion-chamber length from 30 to 66 inches produced large increases in combustion efficiency (from a min. increase of 22 percentage points to a max. increase of 42 percentage points), and changing the afterburner-inlet total temperature from 1260° to 1860° R increased the efficiency as little as 4 and as much as 27 percentage points. The variation in efficiency produced by changing pressure and velocity was somewhat less than that for changes in temperature and length but still significant.

For most conditions investigated, the lean blowout fuel-air ratio of the afterburner was reduced by increasing the afterburner-inlet total pressure and total temperature or by decreasing the afterburner-inlet velocity.

The afterburner total-pressure-loss coefficient was essentially unaffected by changes in the afterburner-inlet total temperature and pressure and only slightly affected by velocity. The total-pressure-loss

coefficient increased as the afterburner temperature ratio increased, and a minimum value was obtained with variations in afterburner combustion-chamber length. As afterburner temperature ratio and velocity increased, there was a decrease in the length at which the pressure-loss coefficient reached a minimum, the major effect being that of temperature ratio.

High-frequency combustion instabilities were encountered more frequently as the afterburner combustion-chamber length and afterburner-inlet total pressure were increased and were absent entirely for the 30-inch afterburner combustion chamber. Low-frequency combustion instabilities occurred more frequently as the afterburner-inlet total pressure was increased and the afterburner length was decreased and were absent entirely for an afterburner combustion-chamber length of 66 inches.

INTRODUCTION

High-performance afterburners and afterburner components have been developed and investigated for specific turbojet engines and operating conditions for many years. As a result of these investigations (the results of many of which are summarized in ref. 1), much data are available on the performance of these specific afterburners or components for specific sets of operating conditions. In addition to these data, other performance data show the effect of combustion-chamber length (refs. 2 to 4), pressure and velocity (refs. 3 to 9), and other variables on afterburner performance. However, a systematic evaluation of the individual effects of afterburner-inlet conditions and length on afterburner performance has not been made heretofore on a single afterburner configuration, making it impossible to evaluate completely the individual effects of inlet conditions and length on afterburner performance.

This investigation, conducted on a high-performance afterburner configuration (representative of current medium- to high-fuel-air-ratio designs), determines systematically the individual effects of afterburner-inlet total temperature, total pressure, and velocity, and combustion-chamber length on afterburner performance and operating limits. The investigation was conducted in a large-scale afterburner test rig at the NACA Lewis laboratory to determine the effect of these variables on combustion efficiency (for three afterburner fuel-air ratios), combustion-chamber pressure-loss coefficient, lean blowout limits, and combustion instabilities. The range of each of the afterburner-inlet variables investigated is as follows: total temperature, 1260° to 1860° R; total pressure, 750 to 1800 pounds per square foot absolute; velocity, 400 to 650 feet per second; afterburner fuel-air ratio, lean blowout to higher than stoichiometric; and combustion-chamber length (defined as the distance from the flameholder trailing edge to the effective nozzle throat), 30 to 66 inches.

DECLASSIFIED

APPARATUS

Installation

The general arrangement of the afterburner test rig and the afterburner is shown in figure 1. As shown in figure 1(a), the combustion air first enters a preheater (consisting of eight J35 combustor cans simulating a turbojet-engine primary combustion system), where it is heated from approximately 540° R to the desired afterburner-inlet temperature. The heated gas then passes from the preheater into a mixing chamber, which provides a uniform temperature profile at the diffuser inlet. A 44-percent-blockage screen was installed at the diffuser inlet to provide a uniform diffuser-inlet velocity profile and a means of measuring airflow through the afterburner. After passing through the screen, the gas enters the diffuser, which is made up of a conical outer shell and a formed innerbody supported by four streamlined struts located 90° apart. The flow passage through the diffuser was designed to provide a linear area increase with increasing diffuser length up to the discharge end of the blunt innerbody. This diffuser design provides a nearly flat pressure and velocity profile at the afterburner inlet (diffuser exit). After leaving the diffuser, the gas passes through the afterburner combustion chamber and the exhaust nozzle and then is discharged into the exhaust system.

The details of the afterburner are shown schematically in figure 1(b). The afterburner had an inside diameter of 25.75 inches. The afterburner combustion-chamber length was varied from 30 to 66 inches by inserting cylindrical spool pieces between the flameholder and the exhaust nozzle. The fuel-air mixture was ignited with a torch ignitor. An external shroud was provided for cooling the afterburner shell (no internal cooling liner used). The cooling air passing through the shroud was saturated with water sprayed into the air at the shroud cooling-air inlet.

Details of the fuel-injection system (incorporating some of the desirable features of the fuel system described in refs. 8 and 10) are shown in figure 2. Twenty-four spray bars attached to a single manifold and equally spaced circumferentially in the diffuser section of the afterburner were located 30.5 inches upstream of the flameholder. Each spray bar contained seven fuel orifices, four on one side and three on the other. These orifices were 0.031 inch in diameter and injected fuel normal to the direction of the airflow. The spray bars were flattened to reduce the pressure loss, and the orifices were positioned radially to produce a uniform radial fuel-air distribution at the diffuser exit.

The flameholder (fig. 3) was a conventional two-V-gutter-type flameholder (similar to those designed for high performance presented in

refs. 4, 5, and 7). The flameholder was mounted in a spool piece located at the diffuser exit. This spool piece also contained a quartz window used for observing blowouts.

The variable-area exhaust nozzle (fig. 4) consisted of a water-cooled butterfly valve, which allowed the effective flow area of the exhaust-nozzle throat to be varied from approximately 1.77 to 3.05 square feet. The variable-area nozzle is discussed in appendix A.

Instrumentation

Instrumentation stations for the measurement of temperatures and pressures throughout the afterburner are shown in figure 1(b). (All symbols and stations are defined in appendix B.) Pressures were measured on mercury-filled manometers and recorded photographically. Temperatures were measured with thermocouples and recorded on self-balancing potentiometers. Fuel flows were measured with calibrated rotameters. The details of the instrumentation at each station are shown in figure 5.

The locations of the four probes used to measure the total pressure at station 3 are shown in figure 5(a). The locations of the instrumentation used to measure static and total pressures at station 4 (downstream of the airflow measuring screen) are shown in figure 5(b). Thermocouples located as shown in figure 5(c) were used to determine the afterburner-inlet total temperature at station 5. The instrumentation at station 7, located as shown in figure 5(d), was used to calculate the afterburner-inlet total pressure and velocity. Fuel-air-ratio surveys at station 7 were made using an NACA fuel-air-ratio analyzer and a traversing probe as described in reference 10.

Pairs of differential pressure orifices (located at station 8) for detecting high-frequency combustion instabilities (described in ref. 11) were arranged as shown in figure 5(e). The principle of operation of these orifices is, briefly, as follows: For each orifice, the flow coefficient is considerably higher when the gas flows into rather than out of the chamfered side. Inasmuch as the orifices making up a pair are oppositely oriented, their installation in a fluctuating pressure field results in a pressure differential across a U-tube manometer connected to the orifices. This pressure differential was used as the indication of the presence of high-frequency combustion instabilities in the afterburner.

The very-low-frequency combustion instabilities were sensed by the conventional pressure rakes installed in the afterburner and resulted in fluctuations in the indicated pressures on the manometer boards. These instabilities were also audible to the facility operator.

~~DECLASSIFIED~~

The instrumentation located as shown in figure 5(f) was used to measure the total pressure at the exhaust-nozzle inlet (station 11). A total-pressure probe was used to determine the pressure loss through the exhaust nozzle at station 12 (fig. 5(g)). The skin thermocouples shown in this figure were used to determine the thermal expansion of the nozzle shell, because the flow area at this station was used in the computation of the afterburner combustion temperature.

PROCEDURE

The operating procedure for obtaining data was as follows: The afterburner was ignited, the afterburner-inlet flow conditions were set, and then the fuel-air ratio was varied while holding the afterburner-inlet conditions constant by adjusting the exhaust-nozzle area. Just prior to taking each data point, the pressure in the external cooling passage was adjusted so as to be equal to the pressure inside the afterburner, thus reducing leakage through the flanges of the afterburner spool pieces to a minimum. A cold point (nonafterburning) was taken for each combination of conditions to evaluate the nonafterburning pressure losses in the afterburner.

Data were obtained for afterburner lengths of 30, 42, 54, and 66 inches over the following range of afterburner-inlet conditions:

Total temperature, °R	1260 to 1860
Total pressure, lb/sq ft abs	750 to 1800
Velocity, ft/sec	400 to 650
Afterburner fuel-air ratio	Lean blowout to higher than stoichiometric

Stability limits were determined by observation of the flame extinction through the quartz window in the afterburner shell and by the change in afterburner pressure drop at the instant of blowout. Blowouts were approached very slowly by gradually changing the fuel flow and the nozzle area, the values of which were recorded at the instant of blowout.

Radial fuel-air-ratio surveys were made at various circumferential positions at station 7 both at the beginning and near the end of this investigation. The sampling probe radially traversed a path ranging from 1/4 inch from the shell to 2 inches from the afterburner centerline. These surveys were made during afterburner operation.

The airflow was determined from the measured total-pressure drop across the diffuser-inlet screen calibrated against a series of fixed-area exhaust nozzles for each afterburner-inlet temperature investigated. The afterburner-inlet velocity was determined from the wall

static-pressure and stream total-pressure measurements at station 7 (no measurable difference existed between the wall and stream static pressures at this station). The exhaust-nozzle-exit total pressure was determined from pressures measured at stations 11 (exhaust-nozzle inlet) and 12 (exhaust-nozzle exit) as described in detail in appendix A. The afterburner combustion temperature was computed from the effective area of the exhaust-nozzle throat, the exhaust-nozzle-exit total pressure, the afterburner gas flow, and the assumption of a Mach number of 1.0 across the effective area of the nozzle throat. Combustion efficiency was computed as the ratio of actual afterburner temperature rise to the ideal theoretical afterburner temperature rise. Details of these computations are given in appendix C.

The fuel used for this investigation was MIL-F-5624A, grade JP-4, which has a heating value of 18,725 Btu per pound and a hydrogen-carbon ratio of 0.172.

TYPICAL AFTERBURNER PROFILES AND VARIATIONS IN AFTERBURNER PARAMETERS

Data plots are presented in order to show the typical profiles existing at the afterburner and nozzle inlets (figs. 6 and 7) and to give an indication of the experimental variations in the afterburner parameters (fig. 8).

Typical Afterburner Profiles

Inlet gas temperature. - Typical profiles of gas temperature at the afterburner inlet (measured at station 5) are shown in figure 6(a) for three different afterburner-inlet velocities at an afterburner-inlet total temperature of 1660° R and a total pressure of 1270 pounds per square foot absolute. (It was assumed that no change in temperature occurred between station 5 and the afterburner inlet.) The profiles at each rake location for each velocity were relatively uniform, with a slight drop near the diffuser innerbody, and fell within a 110° band in temperature.

Inlet velocity. - Afterburner-inlet (station 7) velocity profiles are shown in figure 6(b) for the same conditions as for the gas temperature profiles with the addition of two nonafterburning runs. These profiles were obtained for average afterburner-inlet velocities from approximately 400 to 600 feet per second. (It was assumed that the fuel sprayed ahead of these rakes had no effect on the pressures measured by the rakes.) In general, the velocity profiles had the same shape for each velocity level for both the afterburning and nonafterburning

~~DECLASSIFIED~~

NACA RM E57C07

7

operating conditions. The curves indicate that the velocity was fairly uniform across the afterburner inlet except near the wall and at the end of the blunt innerbody. The difference in the velocity profile from one side to the other of the afterburner centerline is believed to result from a slight misalignment of the centerlines of the diffuser centerbody and outer shell.

Outlet pressure. - Exhaust-nozzle-inlet (afterburner-exit) total-pressure profiles as measured at station 11 for afterburner fuel-air ratios of 0, 0.040, and 0.059 are shown in figures 6(c) and (d) for the extreme afterburner lengths of 30 and 66 inches, respectively. These data were obtained at an afterburner-inlet total temperature of 1660° R, total pressure of 1270 pounds per square foot absolute, and velocities of 520 (fig. 6(c)) and 565 (fig. 6(d)) feet per second. The rake used for these surveys was located at the circumferential position shown in figure 5(f). The pressure profile was relatively flat over the range of afterburner lengths investigated and over a range of afterburner fuel-air ratios from 0 to 0.059.

Fuel-air-ratio distribution. - As previously mentioned in the section APPARATUS, a fixed-orifice single-manifold fuel system was used for this investigation. As a result, the fuel bars were required to operate over a fuel-flow range of 10:1 with pressure differentials as low as 0.3 pound per square inch. A check on the flow characteristics of the fuel bars indicated a ± 10 percent variation in the fuel-flow rate from the highest to the lowest fuel orifice (located at the top and bottom of the afterburner, respectively), due to gravity, at a mean fuel-bar pressure differential of 2.5 pounds per square inch. Higher pressure differentials would reduce this variation in flow from the top to the bottom of the afterburner, whereas smaller pressure differentials would give larger flow variations. Variations of fuel distribution within the afterburner due to gravity of less than ± 10 percent (average fuel-bar pressure differentials greater than 2.5 lb/sq in.) probably would not have a significant effect on afterburner performance, whereas greater variations may have an effect. However, there were not enough data obtained below a fuel-bar pressure differential of 2.5 pounds per square inch to establish any definite trends. It should be pointed out that the horizontal position of the total-pressure rake located at the nozzle inlet (station 11) may have made the rake insensitive to changes in performance resulting from variations in the fuel-air ratio from the top to the bottom of the afterburner (at extremely low fuel-bar pressure differentials).

Typical fuel-air-ratio profiles at the afterburner inlet for an afterburner fuel-air ratio of 0.050 are presented in figure 7 for two circumferential probe positions (see fig. 5(d)) around the afterburner for a fuel-bar pressure differential of about 2.7 pounds per square inch. The curves indicate that the radial fuel-air distribution was

0317122A1030

nearly uniform for both positions. Similar fuel-air-ratio surveys made at the end of the investigation indicated that there was essentially no change in the fuel-air-ratio distribution.

Typical Variations in Afterburner Parameters

In order to show the variations of the afterburner parameters with fuel-air ratio and to give an indication of the experimental accuracy of the data, typical data plots are presented in figure 8 for several afterburner-inlet velocities at an afterburner-inlet total temperature of 1660° R and a total pressure of 1270 pounds per square foot absolute for an afterburner length of 42 inches.

The plots of the afterburner variables show the accuracy with which afterburner conditions were maintained during a series of runs. For a particular combination of afterburner-inlet conditions, the pressure and temperature were established within ± 1 percent of the desired nominal values, whereas the velocity could not be established closer than ± 6 percent. For this reason, cross plotting the afterburner combustion-efficiency data against velocity was necessary in order to obtain data at comparable velocities. Afterburner combustion efficiency was computed as described in appendix C, and the estimated accuracy of the computation (considering the accuracy of the measurement of total pressure, gas flow, and the effective flow area of the exhaust-nozzle throat) is ± 5 percent.

When the desired afterburner conditions became established, data were obtained over the range of afterburner fuel-air ratios shown in figure 8. The solid symbols in figure 8(c) represent the lean blowout points for these afterburner-inlet conditions. Figure 8(d) indicates the variation of the exhaust-nozzle flow area required to maintain the afterburner-inlet velocity constant as the afterburner fuel-air ratio was varied. The limiting nozzle flow area (shown by the long-dashed line) is the largest area for which the effective nozzle throat remained positioned in the plane of the axis of the exhaust-nozzle butterfly valve (see appendix A). Thus, no performance data are presented for exhaust-nozzle areas greater than this limiting area.

RESULTS AND DISCUSSION

The performance data obtained in this investigation are presented first as typical basic data plots and then in the form of summary figures and cross plots.

DECLASSIFIED

Typical Performance Data

The basic performance data obtained for the same conditions presented in figure 8 are shown in figure 9. The performance figures presented in the remainder of the report are cross plots of data plots similar to those presented here.

A typical plot of the effect of fuel-air ratio on combustion efficiency is presented in figure 9(a). In general, these curves indicate a rapid rise in combustion efficiency as the fuel-air ratio is increased, a leveling off from $(f/a)_{AB,u}$ of about 0.045 to about 0.067, and, finally, another sharp rise at higher-than-stoichiometric fuel-air ratios. In general, the effect of increasing the afterburner fuel-air ratio from 0.045 to 0.067 caused a change of 5 percentage points in combustion efficiency. These trends were essentially the same for the other conditions investigated.

The sharp rise in these curves at higher-than-stoichiometric fuel-air ratios is a characteristic resulting from the definition of combustion efficiency used in this report (see appendix C). For this reason, no additional data at fuel-air ratios above stoichiometric are presented. The decrease in combustion-efficiency level as the afterburner-inlet velocity increased (fig. 9(a)) is typical for all the conditions investigated.

The effect of afterburner fuel-air ratio on combustion temperature is presented in figure 9(b). The dashed curve indicates the ideal combustion temperature which would be attained if the combustion efficiency were 100 percent.

The combustor total-pressure-loss coefficient data are presented in figure 9(c) over a range of afterburner fuel-air ratios for several afterburner-inlet velocities. Nonafterburning or zero-fuel-air-ratio data are included for each velocity where possible. The afterburner pressure-loss coefficient increased almost linearly with fuel-air ratio (increasing combustion temperature) up to stoichiometric. The variation in pressure loss reflects the variation in the afterburner momentum pressure drop with increased combustor temperature. Variations in the pressure loss with the primary variables are presented in the section Effect of Afterburner-Inlet Variables and Afterburner Length on Afterburner Total-Pressure-Loss Coefficient.

Effect of Afterburner-Inlet Variables and Afterburner Length on Combustion Efficiency

In figure 10 constant-velocity surfaces were developed by cross plotting data (similar to that presented in fig. 9(a)) at an afterburner

fuel-air ratio of 0.055. These surfaces summarize the data and illustrate the individual and interrelated qualitative effects of afterburner-inlet total temperature, total pressure, and velocity on combustion efficiency. (A discussion of the quantitative effects will be given for succeeding figures.) The boundaries of the surfaces were defined by the limits of the test program or the combustion limits of the afterburner. As was previously mentioned in the discussion of figure 9(a), changing the fuel-air ratio from 0.045 to 0.067 had little effect on combustion efficiency; thus, only the data for a fuel-air ratio of 0.055 are presented in this manner.

In general, figure 10 indicates that, for the range of variables covered and for a particular afterburner combustion-chamber length and fuel-air ratio, a change in any one of the afterburner-inlet variables produced changes in combustion efficiency, such that increases in temperature and pressure and decreases in velocity resulted in increases in efficiency. The slopes of these curves decreased as the afterburner-inlet conditions became more conducive to efficient combustion, that is, as temperature and pressure increased and velocity decreased. One exception was the effect of afterburner-inlet velocity on combustion efficiency for the 30-inch afterburner (fig. 10(a)). In this case, the change in efficiency for a change in velocity was essentially constant regardless of temperature or pressure.

Increasing the afterburner length generally had a twofold effect on combustion efficiency: The over-all level of efficiency increased, and the slope of the efficiency curves (for changes in temperature or pressure) decreased. The largest increases in efficiency were obtained by increasing the length from 30 to 54 inches. Further increases in afterburner length produced smaller increases in efficiency.

Inlet total temperature. - As previously stated, the magnitude of the change in combustion efficiency produced by a change in afterburner-inlet temperature is dependent on both the inlet pressure and the afterburner length for a particular velocity. A typical cross plot showing these trends is presented in figure 11.

For example, changing the afterburner-inlet total temperature from 1260° to 1860° R with a constant inlet velocity of 400 feet per second increased the efficiency 27 and 23 percentage points when operating the 30-inch afterburner at total pressures of 750 and 1800 pounds per square foot absolute, respectively. When the afterburner length was increased to 66 inches, the same change in inlet temperature at the same value of inlet velocity increased the efficiency 17 and 4 percentage points at pressures of 750 and 1800 pounds per square foot absolute, respectively.

Inlet total pressure. - Similar to the effect with temperature, the magnitude of the change in combustion efficiency with a change in

~~DECLASSIFIED~~

afterburner-inlet total pressure was also found to depend on the level of the afterburner-inlet temperature and the afterburner length for a particular inlet velocity. A typical cross plot showing these trends is presented in figure 12. For example, at an afterburner length of 30 inches and velocity of 400 feet per second, changing the afterburner-inlet total pressure from 750 to 1800 pounds per square foot absolute increased the combustion efficiency 19 and 15 percentage points at total temperatures of 1260° and 1860° R, respectively. When the afterburner length was increased to 66 inches (at a velocity of 400 ft/sec), the same change in pressure increased the efficiency 15 percentage points at a total temperature of 1260° R and 4 percentage points at a total temperature of 1860° R.

Velocity. - The improvement in afterburner performance (fig. 13) with a decrease in afterburner-inlet velocity from 600 to 400 feet per second at an afterburner-inlet total temperature of 1860° R was approximately constant for the 30-inch afterburner. The combustion efficiency increased about 5 percentage points. For the 66-inch afterburner the improvement depended on whether or not the other inlet conditions were conducive to high combustion efficiency. Thus, for a total pressure of 750 pounds per square foot absolute and a total temperature of 1860° R, decreasing the velocity from 600 to 400 feet per second increased the efficiency about 9 percentage points; whereas with more favorable conditions (total temperature, 1860° R; total pressure, 1800 lb/sq ft abs), the same change in velocity increased the efficiency by only about 5 percentage points.

Afterburner length. - The qualitative effects of afterburner length (defined as the axial distance from the trailing edge of the flameholder to the effective nozzle throat (see appendix A)) on combustion efficiency can be seen by comparing the various parts of figure 10. The quantitative effects of length on efficiency are illustrated in figure 14, which presents cross plots showing these effects for particular combinations of inlet conditions for afterburner fuel-air ratios of 0.045, 0.055, and 0.0676. As pointed out previously, the limits of the data presented in figure 14 were determined by either the limits of the test program or the combustion limits of the afterburner, which are discussed in the section Effect of Afterburner-Inlet Variables and Afterburner Length on Lean Blowout Limits. In addition to the effect of afterburner length on efficiency, the effects of afterburner-inlet temperature, pressure, and velocity are also shown. The effects of the parameters on combustion efficiency at fuel-air ratios of 0.045 and 0.0676 were essentially the same as the effects previously presented for a fuel-air ratio of 0.055 (figs. 11 to 13).

In general, it is evident from figure 14 that, as afterburner length increases, the rate of increase in combustion efficiency decreases. Further, it is evident from figure 10 that, as length increases, the effect

of changing temperature and pressure on efficiency decreases, and the level of efficiency increases. For example, increasing the pressure and temperature from the lowest to the highest values investigated at a velocity of 400 feet per second and a fuel-air ratio of 0.055 (figs. 14(d) to (f)) increased the efficiency of the 30-inch afterburner 39 percentage points (from 38 to 77 percent), whereas a similar change in conditions increased the efficiency of the 66-inch afterburner only 21 percentage points (from 78 to 99 percent). Increasing the afterburner combustion-chamber length from 30 to 66 inches produced large increases in combustion efficiency (from a min. increase of 22 percentage points to a max. increase of 42 percentage points). Regardless of afterburner-inlet conditions, increasing the afterburner length from 30 to 54 inches produced the largest part of this increase in combustion efficiency (21 to 37 percentage points). Further increases in afterburner length produced increases in efficiency which, in addition to being somewhat less than those for lengths below 54 inches, were also dependent upon the afterburner-inlet conditions. This effect is illustrated by the fact that, at a constant velocity of 400 feet per second and a fuel-air ratio of 0.055, an increase in afterburner length from 54 to 66 inches increased the combustion efficiency about 11 percentage points at an inlet total pressure and total temperature of 750 pounds per square foot and 1260° R, respectively (fig. 14(d)); whereas the same change in afterburner length increased the efficiency only 1 percentage point at an inlet total pressure and total temperature of 1800 pounds per square foot and 1860° R, respectively (fig. 14(f)).

Effect of Afterburner-Inlet Variables and Afterburner Length on Afterburner Total-Pressure-Loss Coefficient

Cross plots of the effect of afterburner length on afterburner total-pressure-loss coefficient $\frac{P_7 - P_{12}}{P_7 - P_7}$ for afterburner temperature ratios up to 2.8 are shown in figure 15 for afterburner-inlet velocities of 400, 500, 550, and 600 feet per second. Afterburner-inlet total pressure and total temperature had no measurable effect on the afterburner pressure-loss coefficient. Cross plots rather than the original data are presented so that comparisons can be made at the same afterburner temperature ratios.

The cold (nonafterburning) pressure loss at a temperature ratio of 1.0 is probably largely due to the flameholder rather than to the wall friction drag, inasmuch as the loss remained independent of afterburner length over the range of lengths from 30 to 66 inches. This cold pressure loss was also unaffected by changes in velocity from 400 to 600 feet per second. It should be noted, however, that the scatter in the data from which these curves were obtained was about ± 0.3 unit of pressure-loss coefficient.

DECLASSIFIED

With afterburning, the total-pressure-loss coefficient changed considerably with changes in afterburner length and temperature ratio but only slightly with changes in velocity. As would be expected, the loss coefficient increased as the velocity or the temperature ratio was increased because of the accompanying increase in momentum pressure drop. Afterburner length, on the other hand, had an unusual effect such that the pressure-drop coefficient attained a minimum value at an intermediate value of afterburner length. In every case at a temperature ratio of 1.6, the loss coefficient reached a minimum value at an afterburner length of 55 inches. As the temperature ratio and the velocity were increased, however, there was a decrease in the length at which the pressure-loss coefficient reached a minimum, the major effect being that of temperature ratio.

The measured total-pressure loss in the exhaust nozzle $P_{11} - P_{12}$ indicated that the increases in pressure-loss coefficient, as afterburner length is either increased or decreased from the length for minimum-loss coefficient, occurred in the exhaust nozzle. This could possibly mean that burning is occurring in the exhaust nozzle as well as in the combustion chamber. For the shorter afterburners, burning could occur in the exhaust nozzle because there is not sufficient time for complete combustion within the combustion chamber. For the longer afterburners, where the greatest increases in pressure-loss coefficient occur at high temperature ratios (high afterburner fuel-air ratios), there may be regions in the gas mixture which are too rich to burn in the combustion chamber. In longer afterburners, however, these over-rich regions may become sufficiently mixed with air to permit burning of the mixture as it passes through the exhaust nozzle. Since the velocities in the exhaust nozzle are quite high (up to a Mach number of 1 at the throat), any afterburning occurring in the nozzle would result in a higher-than-normal momentum pressure drop.

Computations indicated that the increases in afterburner pressure loss resulting from increases in temperature ratio can be accounted for in terms of increased momentum pressure drop. The symbols in figure 15 at the points of minimum-loss coefficient represent an attempt to check the data with the theory. These points were determined by computing the momentum pressure drop (ref. 12) for each temperature ratio and adding it to the measured cold (nonafterburning) pressure loss. The comparison was made at approximately the minimum-loss-coefficient length, because the method of calculation (ref. 12) does not account for afterburning through the nozzle. However, a reasonably good check between the theory and the data was obtained.

0317122A1030
[REDACTED]

Effect of Afterburner-Inlet Variables and Afterburner Length on Lean Blowout Limits

Regions of afterburner operation are presented in figure 16 in terms of afterburner-inlet velocity and afterburner fuel-air ratio for afterburner lengths of 30, 42, 54, and 66 inches over a range of afterburner-inlet total temperatures and total pressures. The solid symbols represent the lean blowout limits of operation; and the tailed symbols indicate the conditions limited by the maximum exhaust-nozzle area, which was reached before rich blowout occurred. The conditions limited by minimum-exhaust-nozzle-area limits and rich blowout points are labeled on this figure. For conditions where rich blowout or maximum-nozzle-area limits were not encountered, data were obtained up to an afterburner fuel-air ratio of 0.08. This fuel-air-ratio limit is marked by open symbols.

Total temperature. - In general, higher afterburner-inlet temperatures reduced the lean blowout fuel-air ratio, with the greatest reduction occurring at low afterburner-inlet pressures. For instance, increasing the afterburner-inlet temperature from 1260° to 1860° R reduced the lean blowout fuel-air ratio as much as 0.017 (from 0.051 to 0.034) for a low afterburner-inlet pressure (750 lb/sq ft abs) and an afterburner length of 42 inches at a velocity of 500 feet per second (fig. 16(b)). For the same velocity and increase in temperature, the lean blowout fuel-air ratio changed as little as 0.008 (from 0.035 to 0.027) at a high pressure (1800 lb/sq ft abs) and an afterburner length of 42 inches (fig. 16(b)). These trends are similar for all lengths and afterburner conditions investigated.

Total pressure. - Similar to the effect of increasing the temperature, increasing the afterburner-inlet pressure for the conditions investigated tended to decrease the lean blowout fuel-air ratio. (One exception occurred at a total temperature of 1860° R for the 66-in. afterburner.) A typical change in lean blowout fuel-air ratio (from 0.033 to 0.026) occurred for the 30-inch afterburner when the pressure was changed from 750 to 1270 pounds per square foot absolute at an afterburner-inlet total temperature of 1860° R and a velocity of 500 feet per second (fig. 16(a)). A further increase in total pressure from 1270 to 1800 pounds per square foot absolute had practically no effect on lean blowout fuel-air ratio for these conditions.

Velocity. - The effect of changing the inlet velocity on the lean blowout fuel-air ratio was found to be dependent on the initial level of velocity for most afterburner-inlet conditions. For example, changing the velocity from 400 to 500 feet per second increased the lean blowout fuel-air ratio as little as 0.002 (from 0.031 to 0.033) for a typical condition (fig. 16(d)). Further increases in velocity (from 500 to 600

~~DECCLASSIFIED~~

ft/sec), however, increased the lean blowout fuel-air ratio as much as 0.004 (from 0.033 to 0.037) at the same afterburner-inlet pressure and temperature. For some afterburner-inlet conditions, the effect of afterburner-inlet velocity on lean blowout fuel-air ratio was greater than in the example just given, while for other conditions the effect was negligible.

Afterburner length. - The lean blowout data presented in figure 16 are cross-plotted in figure 17 to show the effect of afterburner length on lean blowout limits. For most cases, the lean blowout fuel-air ratio tended to increase as the afterburner length was increased; this effect is greatest at a temperature of 1260° R and a pressure of 1270 pounds per square foot absolute. For the other inlet conditions investigated, only small increases in lean blowout fuel-air ratio occurred as the afterburner length was increased.

Effect of Afterburner-Inlet Variables and Afterburner Length on Combustion Instabilities

Regions of combustion instabilities are presented in figure 18 in terms of afterburner-inlet velocity and afterburner fuel-air ratio for afterburner lengths of 30, 42, 54, and 66 inches over a range of afterburner-inlet total temperatures and total pressures.

Two types of combustion instabilities were encountered: (1) low-frequency combustion instabilities (defined as frequencies from 10 to 300 cps), and (2) high-frequency combustion instabilities (defined as frequencies from 800 to 3000 cps). The high-frequency combustion instabilities (commonly called screech) were characterized by high-frequency pressure oscillations in the combustion zone and were detected by the special instrumentation described in the section APPARATUS (fig. 5(e)). As mentioned previously, the very-low-frequency combustion instabilities (including buzz and rumble) were detected visually by the fluctuations in the afterburner combustion-chamber pressures as evidenced on the manometer boards and audibly by the facility operator.

Inasmuch as no inner liner or screech suppressor was used in this program, combustion instabilities were encountered more frequently with this afterburner than with an afterburner having a screech-suppressing liner.

The open symbols in figure 18 represent low-frequency combustion instabilities, while the solid symbols indicate high-frequency combustion instabilities. The tailed symbols indicate lean blowout. Horizontal lines connecting the data points indicate that the instability was encountered over the range of fuel-air ratios covered by the line.

Low-frequency combustion instabilities occurred more frequently as the afterburner-inlet total pressure was increased and the afterburner length was decreased; no low-frequency instabilities were encountered with the 66-inch afterburner. Generally, the regions of low-frequency instabilities occurred at extremely rich fuel-air ratios and at fuel-air ratios near lean blowout.

For high afterburner-inlet total pressures a transition occurred from low-frequency to high-frequency combustion instabilities as the afterburner length was increased. High-frequency combustion instabilities were encountered more frequently as the afterburner combustion-chamber length and afterburner-inlet pressure were increased and were absent entirely with an afterburner combustion-chamber length of 30 inches. As previously noted for low-frequency instabilities, the high-frequency instabilities also were encountered at high afterburner fuel-air ratios and at fuel-air ratios near lean blowout. The transition from stable to unstable combustion was very gradual inasmuch as the afterburner fuel-flow rate was usually changed quite slowly. The general observation was made that, in unstable regions and at high afterburner fuel-air ratios, the severity of the instability increased as the fuel-air ratio increased.

High-frequency instabilities, in general, did not greatly affect efficiency. This was probably due to the fact that, under most conditions (i.e., afterburner lengths above 42 in. and afterburner-inlet total pressures above 1270 lb/sq ft abs) where these high-frequency instabilities were encountered, the afterburner was already operating at a high efficiency level. A negligible effect of high-frequency combustion instabilities on efficiency is also observed in reference 11.

SUMMARY OF RESULTS

A typical present-day full-scale high-performance afterburner was investigated in a duct test rig to determine the effects of afterburner-inlet total temperature, total pressure, velocity, and fuel-air ratio, and afterburner combustion-chamber length on combustion efficiency, afterburner total-pressure-loss coefficient, combustion instabilities, and lean blowout limits.

In general, for a given afterburner combustion-chamber length, fuel-air ratio, and for the range of variables covered, a change in any one of the afterburner-inlet parameters produced a corresponding change in combustion efficiency. The magnitude of the change in efficiency decreased as the afterburner-inlet conditions became more favorable to efficient combustion (i.e., high temperature, high pressure, and low velocity). One exception to this was the effect of afterburner-inlet velocity on the performance of the 30-inch-long combustion chamber.

DECLASSIFIED

For this case, the change in combustion efficiency for a change in afterburner-inlet velocity was essentially the same regardless of temperature or pressure.

Changing the afterburner-inlet total temperature from 1260° to 1860° R increased the efficiency as little as 4 and as much as 27 percentage points. The variation in efficiency produced by changing pressure and velocity was somewhat less than that for changes in temperature but still significant for the range of conditions investigated.

Increasing the afterburner combustion-chamber length had a twofold effect on combustion efficiency: (1) The over-all level of combustion efficiency increased, and (2) the slopes of the efficiency curves (for changes in temperature or pressure) decreased. Increasing the afterburner combustion-chamber length from 30 to 66 inches produced large increases in combustion efficiency (from a min. increase of 22 percentage points to a max. increase of 42 percentage points). The greatest part of this increase was obtained by increasing the combustion-chamber length from 30 to 54 inches; further increases produced relatively small increases in efficiency.

At the higher fuel-air ratios, performance was relatively insensitive to fuel-air ratio. In general, the effect of increasing the afterburner fuel-air ratio from 0.045 to 0.067 caused a change of 5 percentage points in combustion efficiency.

At an afterburner temperature ratio of 1.6, the afterburner total-pressure-loss coefficient reached a minimum at an afterburner combustion-chamber length of 55 inches. As the temperature ratio and velocity were increased, there was a decrease in the length at which the pressure-loss coefficient reached a minimum, the major effect being that of temperature ratio. Afterburner-inlet total temperature and total pressure had no measurable effect on the pressure-loss coefficient. Good agreement between experimental minimum-loss coefficient and calculated momentum pressure losses was obtained.

Increasing the afterburner-inlet total temperature from 1260° to 1860° R reduced the lean blowout fuel-air ratio 0.017 (from 0.051 to 0.034) at a total pressure of 750 pounds per square foot absolute. On the other hand, at a total pressure of 1800 pounds per square foot absolute, this change in temperature changed the lean blowout fuel-air ratio only about 0.008 (from 0.037 to 0.027).

Similar to the effect of increasing the temperature, increasing the afterburner-inlet total pressure tended to decrease the lean blowout fuel-air ratio. (One exception occurred at a total temperature of 1860° R for an afterburner combustion-chamber length of 66 in.) Increasing the afterburner-inlet velocity or the afterburner length increased the lean blowout fuel-air ratio for most conditions investigated.

0313122A1230
[REDACTED]

High-frequency combustion instabilities were encountered more frequently as the afterburner combustion-chamber length and afterburner-inlet pressure were increased and were absent entirely with an afterburner combustion-chamber length of 30 inches. Low-frequency combustion instabilities occurred more frequently as afterburner-inlet total pressure was increased and the length was decreased and were absent entirely with an afterburner combustion-chamber length of 66 inches.

Lewis Flight Propulsion Laboratory
National Advisory Committee for Aeronautics
Cleveland, Ohio, March 12, 1957

[REDACTED]

~~DECLASSIFIED~~

APPENDIX A

VARIABLE-AREA EXHAUST NOZZLE

The variable-area nozzle used in this investigation was a water-cooled butterfly valve installed in the end of a cylindrical afterburner. By rotating the valve, the flow area of the exhaust-nozzle throat could be varied from approximately 1.77 to 3.32 square feet. A calibration of nozzle effective flow area was obtained from the measured total temperature, total pressure, and gas flow over a range of nozzle pressure ratios up to 3.5 and gas total temperatures from 1260° to 1860° R. For the range of temperatures covered, there was no change in the effective flow area of the exhaust-nozzle throat with temperature. For temperatures above 1860° R, it was assumed that the flow area was independent of temperature. This flow calibration was used in the computation of the afterburning combustion temperature.

The position of the nozzle throat, determined from measurements of wall static pressures along the nozzle spool piece, varied with increasing nozzle area from the positions shown successively in figure 19. The condition shown in figure 19(a) existed for the fully closed butterfly valve to an intermediate open position. Further opening of the valve caused the effective nozzle throat to assume the position indicated in figure 19(b). Full opening caused the effective nozzle throat to move to the downstream position shown in figure 19(c).

In order to maintain the condition shown in figure 19(a), it was necessary to limit the effective exhaust-nozzle-throat area to about 3.05 square feet. Data are presented herein only for the case in which the effective throat area is located as shown in figure 19(a). For this condition, the average position of the throat was assumed to be at the shaft. For cases where burning occurred between stations 11 and 12, the pressure loss due to the burning was determined by the difference in pressure between the single water-cooled total-pressure probe installed at station 12 and a probe on the rake at station 11 at the same immersion depth:

$$P_{12,av} = P_{11,av} \left(\frac{P_{12} \text{ (single probe)}}{P_{11} \text{ (single probe)}} \right)$$

When there was no burning in the nozzle, there was no measurable pressure difference between the individual pressure probes at stations 11 and 12.

APPENDIX B

SYMBOLS

A	exhaust-nozzle-throat area, sq ft
f/a	fuel-air ratio
g	acceleration due to gravity, 32.17 ft/sec ²
m	mass flow, slugs/sec
P	total pressure, lb/sq ft abs
p	static pressure, lb/sq ft abs
R	gas constant, 53.35 ft-lb/(lb)(°R)
T	total temperature, °R
V	velocity, ft/sec
w	weight flow, lb/sec
η	combustion efficiency

Subscripts:

AB	afterburner
a	air
av	average
eff	effective
f	fuel
g	gas
id	ideal
o	over all
p	preheater
st	stoichiometric

DECLASSIFIED

NACA RM E57C07

21

- u available air
- 3 upstream of airflow measuring screen, mixing-chamber outlet
- 4 diffuser inlet
- 5 spray-bar inlet
- 6 fuel injection
- 7 afterburner inlet, diffuser exit
- 8 downstream of flameholder
- 11 exhaust-nozzle inlet, afterburner exit
- 12 effective exhaust-nozzle exit

APPENDIX C

METHODS OF CALCULATION

Air Flow

The air flow was determined from the measured pressure drop across the diffuser-inlet screen calibrated against a series of fixed-area exhaust nozzles of known flow coefficient.

Gas Flow

The afterburner gas flow is the sum of the measured air and fuel flows:

$$w_g = w_a + w_{f,p} + w_{f,AB}$$

Afterburner-Inlet Velocity

The velocity at the diffuser exit (afterburner inlet) was computed from measured total and static pressures and the total temperature by use of the one-dimensional-flow parameters, which are a function of total- to static-pressure ratio, of reference 13:

$$V_7 = \left(\frac{V}{\sqrt{gRT}} \right)_7 \sqrt{gRT_5}$$

For this calculation it was assumed that $T_5 = T_7$.

Fuel-Air Ratio

The method employed for computing fuel-air ratio is similar to the method of reference 5. The fuel-air ratios used are defined as follows:

$$\text{Preheater fuel-air ratio } (f/a)_p = \frac{w_{f,p}}{w_a}$$

$$\text{Afterburner total fuel-air ratio } (f/a)_{AB} = \frac{w_{f,AB}}{w_a}$$

DECLASSIFIED

$$\text{Over-all fuel-air ratio } (f/a)_o = \frac{w_{f,p} + w_{f,h}}{w_a}$$

$$\begin{aligned}\text{Afterburner available air } (f/a)_{AB,u} &= \frac{\text{Total unburned fuel to afterburner}}{\text{Total available air}} \\ &= \frac{w_{f,AB} + (w_{f,p} - w_{f,p,id})}{w_a - \frac{w_{f,p,id}}{(f/a)_{st}}}\end{aligned}$$

where $(w_{f,p} - w_{f,p,id})$ is the fuel not burned in the preheater and charged to the afterburner, and $\frac{w_{f,p,id}}{(f/a)_{st}}$ is the air reacted in the pre-heater. Dividing the numerator and denominator of the previous equation by w_a gives

$$(f/a)_{AB,u} = \frac{(f/a)_{AB} + (f/a)_p - (f/a)_{p,id}}{1 - \frac{(f/a)_{p,id}}{0.0676}}$$

where 0.0676 is the stoichiometric fuel-air ratio for the fuel used. But, since

$$(f/a)_{AB} + (f/a)_p = (f/a)_o$$

then

$$(f/a)_{AB,u} = \frac{(f/a)_o - (f/a)_{p,id}}{1 - \frac{(f/a)_{p,id}}{0.0676}}$$

The ideal preheater fuel-air ratio $(f/a)_{p,id}$ is obtained from reference 14.

Combustion Temperature

The total temperature of the exhaust gas was computed from the effective area of the exhaust-nozzle throat, measured nozzle-exit total pressure, measured gas flow, and the fact that the exhaust nozzle was choked:

$$T_{12} = \frac{g}{R} \left[\left(\frac{m\sqrt{gRT}}{PA} \right)_{12} \left(\frac{P_{12}A_{eff}}{w_g} \right) \right]^2$$

where $\left(\frac{m\sqrt{gRT}}{PA} \right)_{12}$ is the dimensionless total-pressure parameter for critical flow at the exhaust nozzle (ref. 13).

Afterburner Combustion Efficiency

The afterburner combustion efficiency was defined as the ratio of the actual afterburner temperature rise to the theoretical afterburner temperature rise:

$$\eta_{AB} = \frac{T_{12} - T_5}{T_{12,id} - T_5}$$

Values of $T_{12,id}$ were obtained by the method of reference 14. For afterburner fuel-air ratios below stoichiometric, the efficiency computed using this definition agrees favorably with the efficiency computed using other definitions of combustion efficiency currently in use. For afterburner fuel-air ratios higher than stoichiometric, this definition may give efficiencies approaching 100 percent or greater, because the ideal temperature decreases for afterburner fuel-air ratios higher than stoichiometric while the actual afterburner temperature may continue to increase (see fig. 9(b)).

REFERENCES

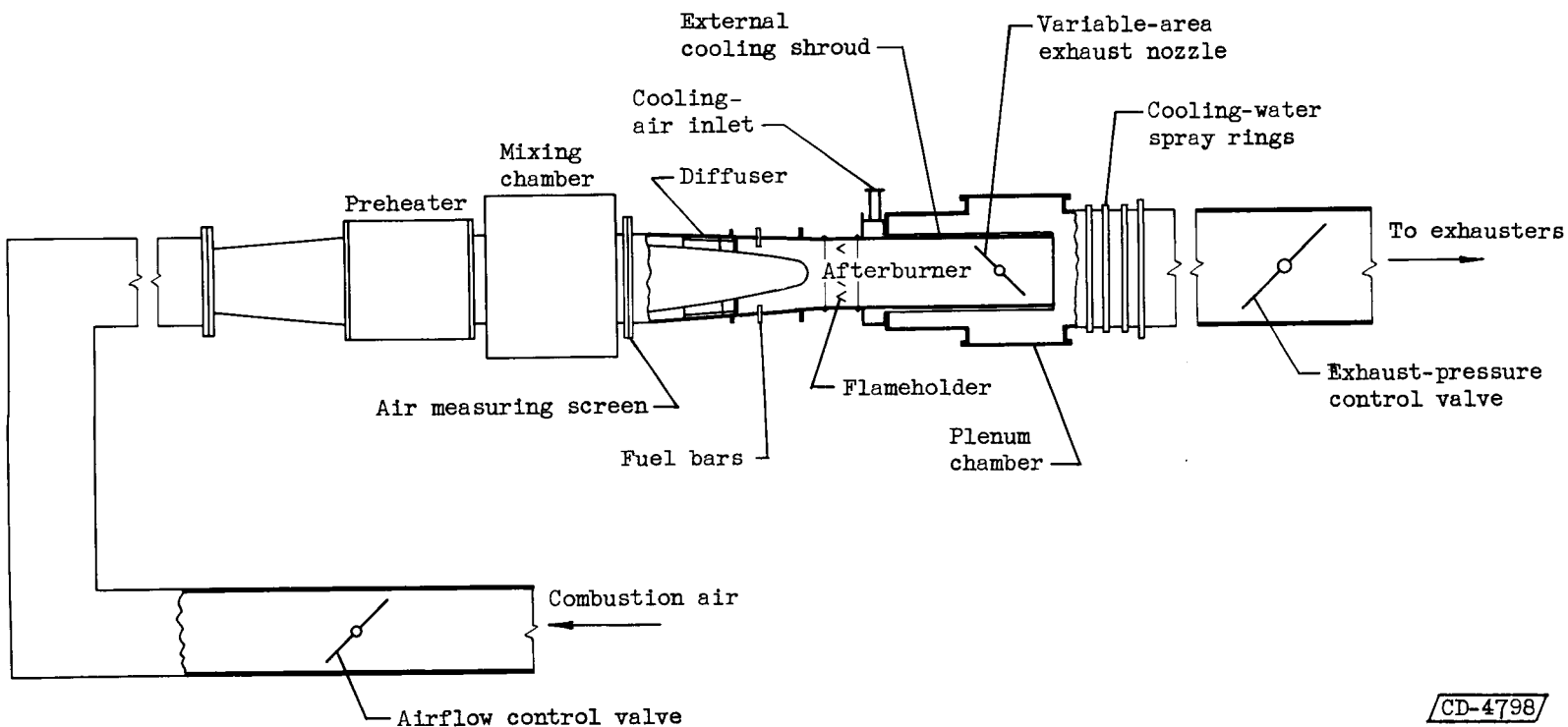
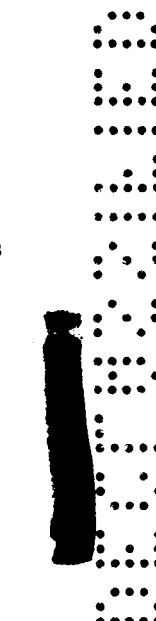
1. Lundin, Bruce T., Gabriel, David S., and Fleming, William A.: Summary of NACA Research on Afterburners for Turbojet Engines. NACA RM E55L12, 1956.
2. Useller, James W., Braithwaite, Willis M., and Rudey, Carl J.: Influence of Combustion-Chamber Length on Afterburner Performance. NACA RM E54E06, 1954.
3. Ciepluch, Carl C., Velie, Wallace W., and Burley, Richard R.: Afterburner Performance with Combustion-Chamber Lengths from 10 to 62 Inches at Several Afterburner-Inlet Temperatures. NACA RM E55K09, 1956.
4. Prince, William R., Velie, Wallace W., and Braithwaite, Willis M.: Full-Scale Evaluation of Some Flameholder Design Concepts for High-Inlet-Velocity Afterburners. NACA RM E56D10, 1956.

~~DECLASSIFIED~~

NACA RM E57C07

25

5. Nakanishi, S., Velie, W. W., and Bryant, L.: An Investigation of Effects of Flame-Holder Gutter Shape on Afterburner Performance. NACA RM E53J14, 1954.
6. Henzel, James G., Jr., and Wentworth, Carl B.: Free-Jet Investigation of 20-Inch Ram-Jet Combustor Utilizing High-Heat-Release Pilot Burner. NACA RM E53H14, 1953.
7. Henzel, James G., Jr., and Bryant, Lively: Investigation of Effect of Number and Width of Annular Flame-Holder Gutters on Afterburner Performance. NACA RM E54C30, 1954.
8. Braithwaite, Willis M., Renas, Paul E., and Jansen, Emmert T.: Altitude Investigation of Three Flame-Holder and Fuel-Systems Configurations in a Short Converging Afterburner on a Turbojet Engine. NACA RM E52G29, 1952.
9. Fleming, W. A., Conrad, E. William, and Young, A. W.: Experimental Investigation of Tail-Pipe-Burner Design Variables. NACA RM E50K22, 1951.
10. Jansen, Emmert T., Velie, Wallace W., and Wilsted, H. Dean: Experimental Investigation of the Effect of Fuel-Injection-System Design Variables on Afterburner Performance. NACA RM E53K16, 1954.
11. Trout, Arthur M., Koffel, William K., and Smolak, George R.: Investigation of Afterburner Combustion Screech and Method of Its Control at High Combustor Pressure Levels. NACA RM E55K25, 1956.
12. Pinkel, I. Irving, and Shames, Harold: Analysis of Jet-Propulsion-Engine Combustion-Chamber Pressure Losses. NACA Rep 880, 1947. (Supersedes NACA TN 1180.)
13. Turner, L. Richard, Addie, Albert N., and Zimmerman, Richard H.: Charts for the Analysis of One-Dimensional Steady Compressible Flow. NACA TN 1419, 1948.
14. Huntley, S. C.: Ideal Temperature Rise Due to Constant-Pressure Combustion of a JP-4 Fuel. NACA RM E55G27a, 1955.

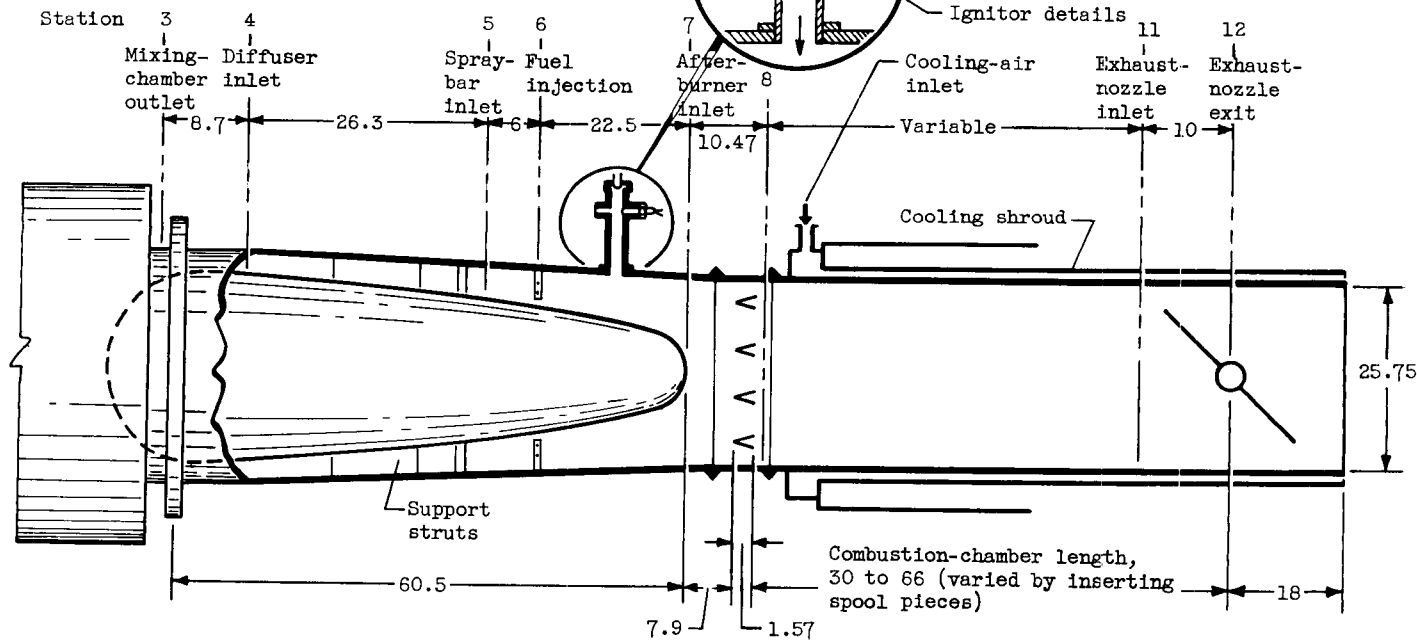


(a) Test rig.

Figure 1. - Schematic diagram of simulated afterburner test rig and afterburner.

Station	Instrumentation			
	Total-pressure tubes	Static-pressure tubes	Wall static taps	Thermo-couples
3	4			
4	18	6	6	
5				25
7	26	4	8	
8			6	
11	12		4	
12	1			8 Skin

^aDifferential pressure orifices for screech detection



(b) Afterburner. (All dimensions in inches.)

Figure 1. - Concluded. Schematic diagram of simulated afterburner test rig and afterburner.

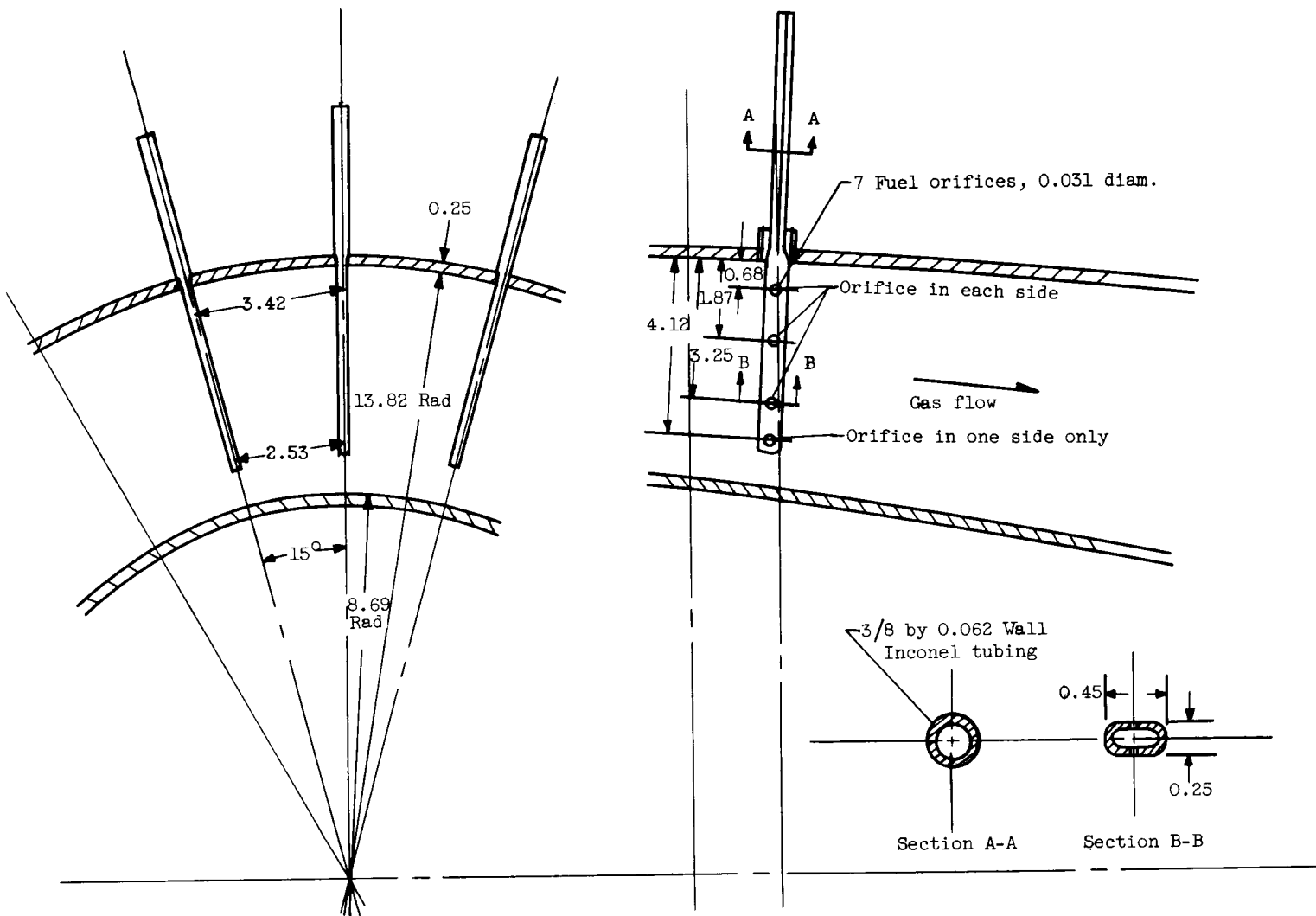


Figure 2. - Afterburner fuel-injection system. (All dimensions in inches except where noted.)

1
2
3
4
5
6
7
8
9
10
11
12
13
14
15
16
17
18
19
20
21
22
23
24
25
26
27
28
29
30
31
32
33
34
35
36
37
38
39
40
41
42
43
44
45
46
47
48
49
50
51
52
53
54
55
56
57
58
59
60
61
62
63
64
65
66
67
68
69
70
71
72
73
74
75
76
77
78
79
80
81
82
83
84
85
86
87
88
89
90
91
92
93
94
95
96
97
98
99
100

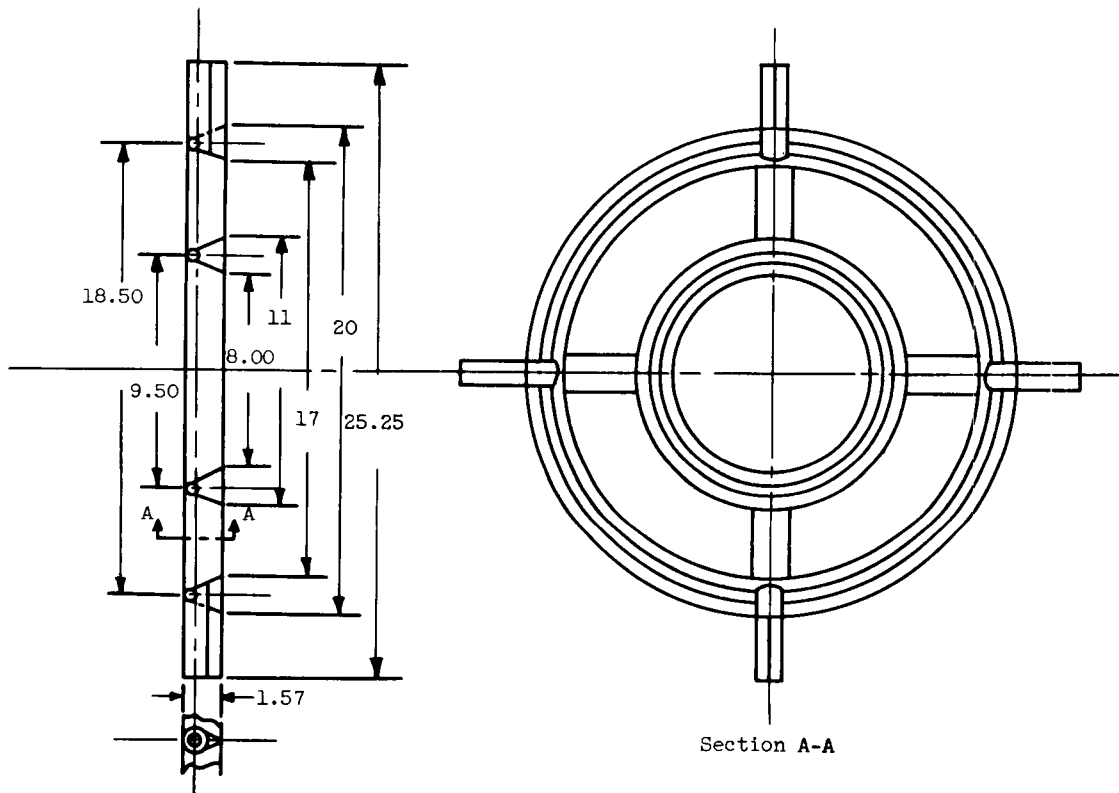
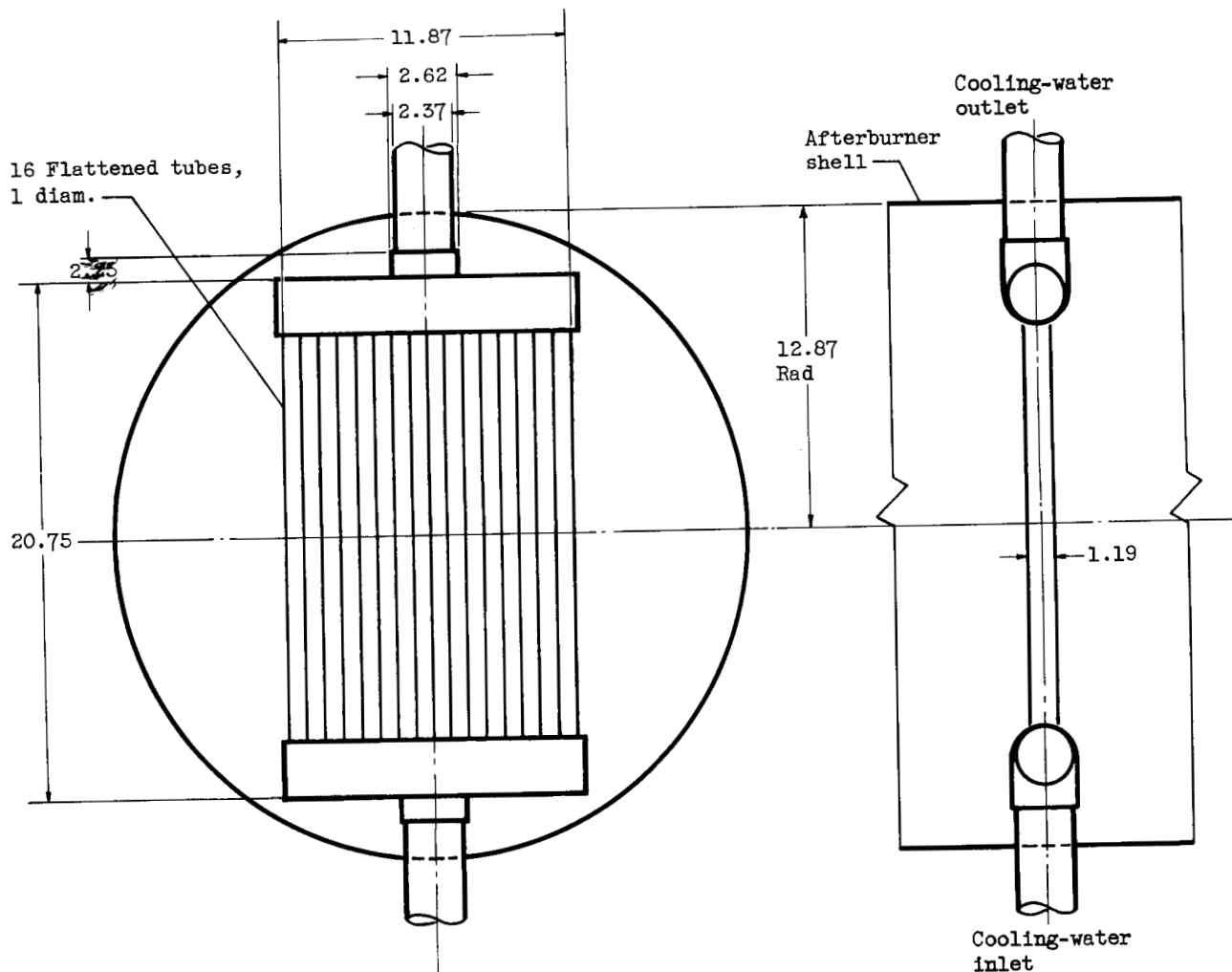


Figure 3. - Flameholder. (All dimensions in inches.)

Schematic



(a) Schematic diagram. (All dimensions in inches.)

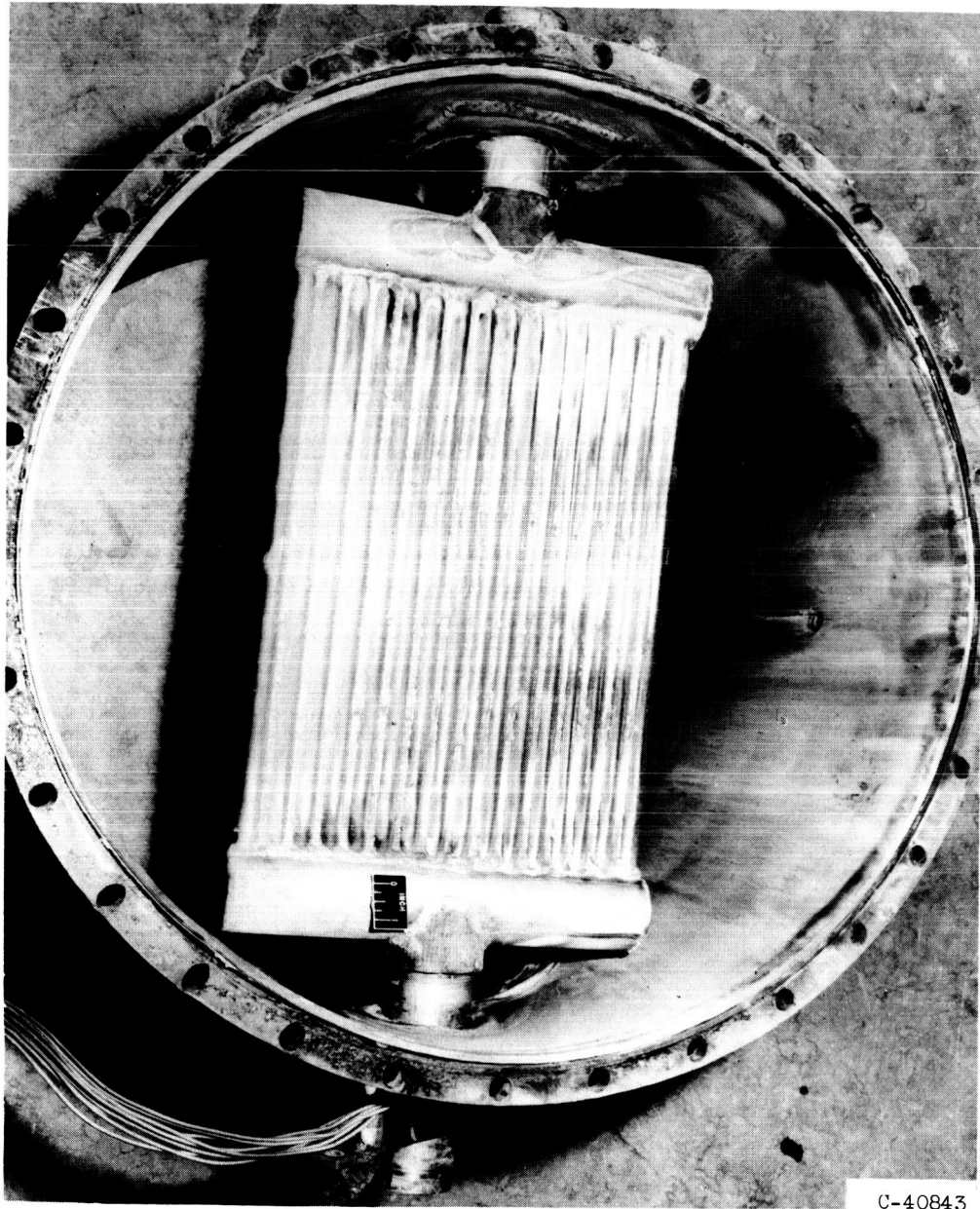
CD-4796

Figure 4. - Variable-area exhaust nozzle.

DECLASSIFIED

NACA RM E57C07

31



C-40843

(b) Photograph looking downstream.

Figure 4. - Concluded. Variable-area exhaust nozzle.

031912301030

32

NACA RM E57C07

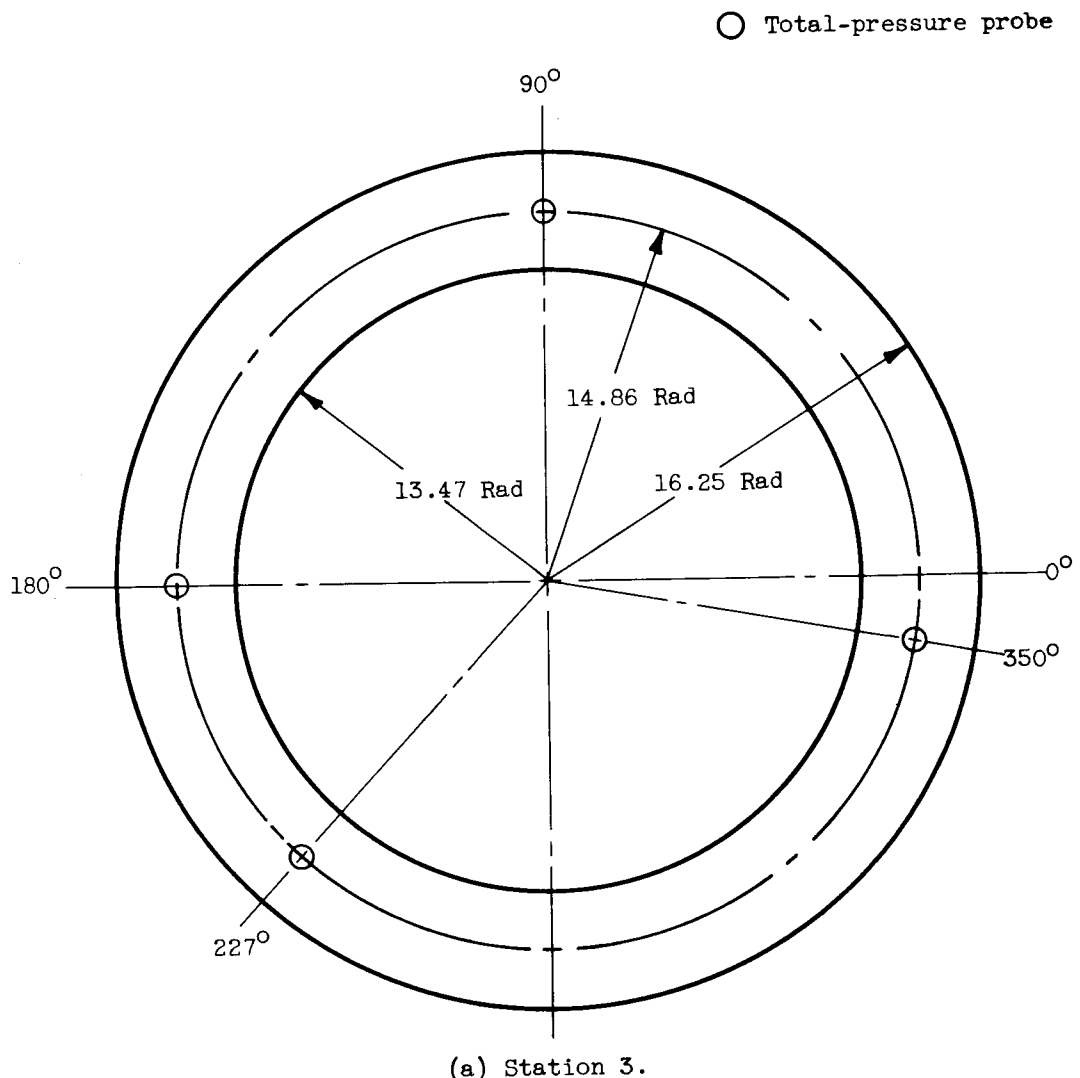


Figure 5. - Schematic diagrams of instrumentation stations viewed looking downstream. (All dimensions in inches except where noted.)

DECLASSIFIED

NACA RM E57C07

33

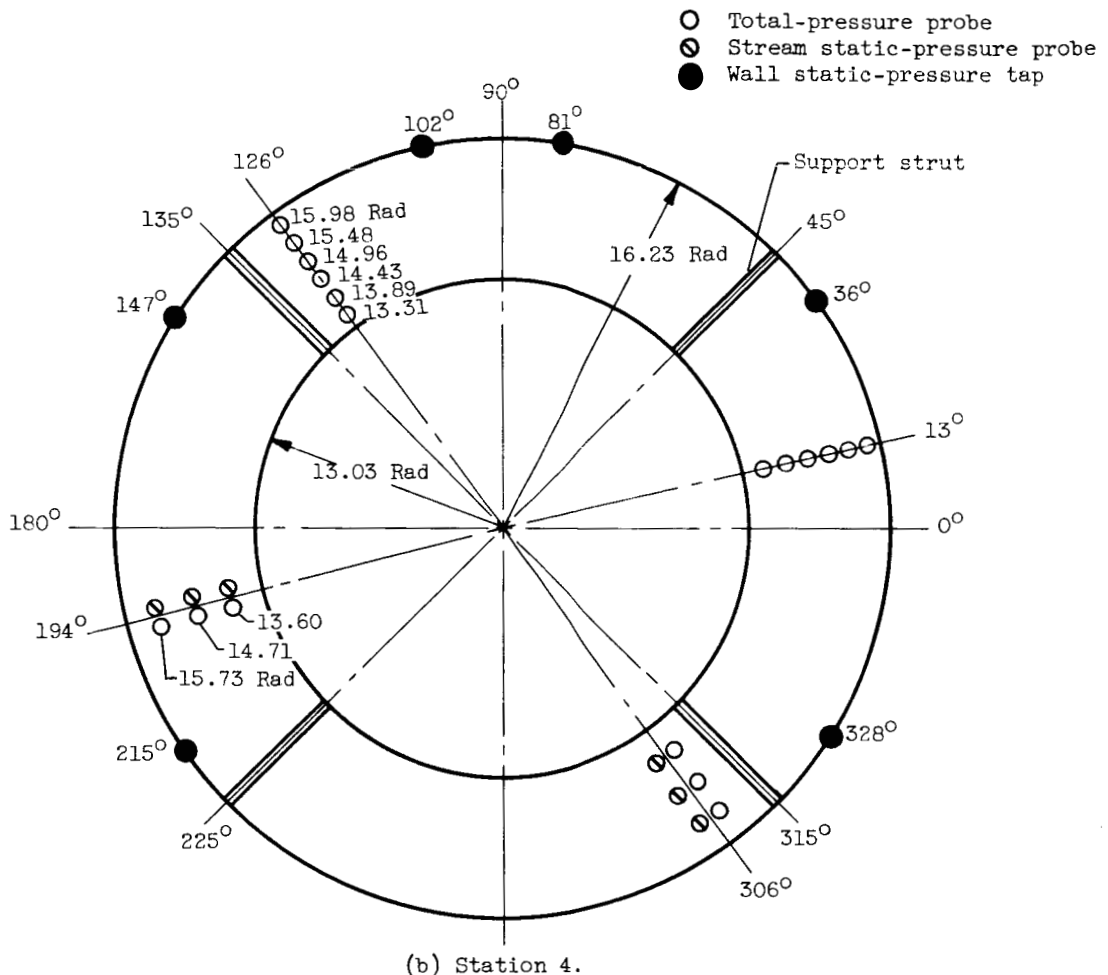


Figure 5. - Continued. Schematic diagrams of instrumentation stations viewed looking downstream. (All dimensions in inches except where noted.)

031712201030

34

NACA RM E57C07

⊗ Thermocouple

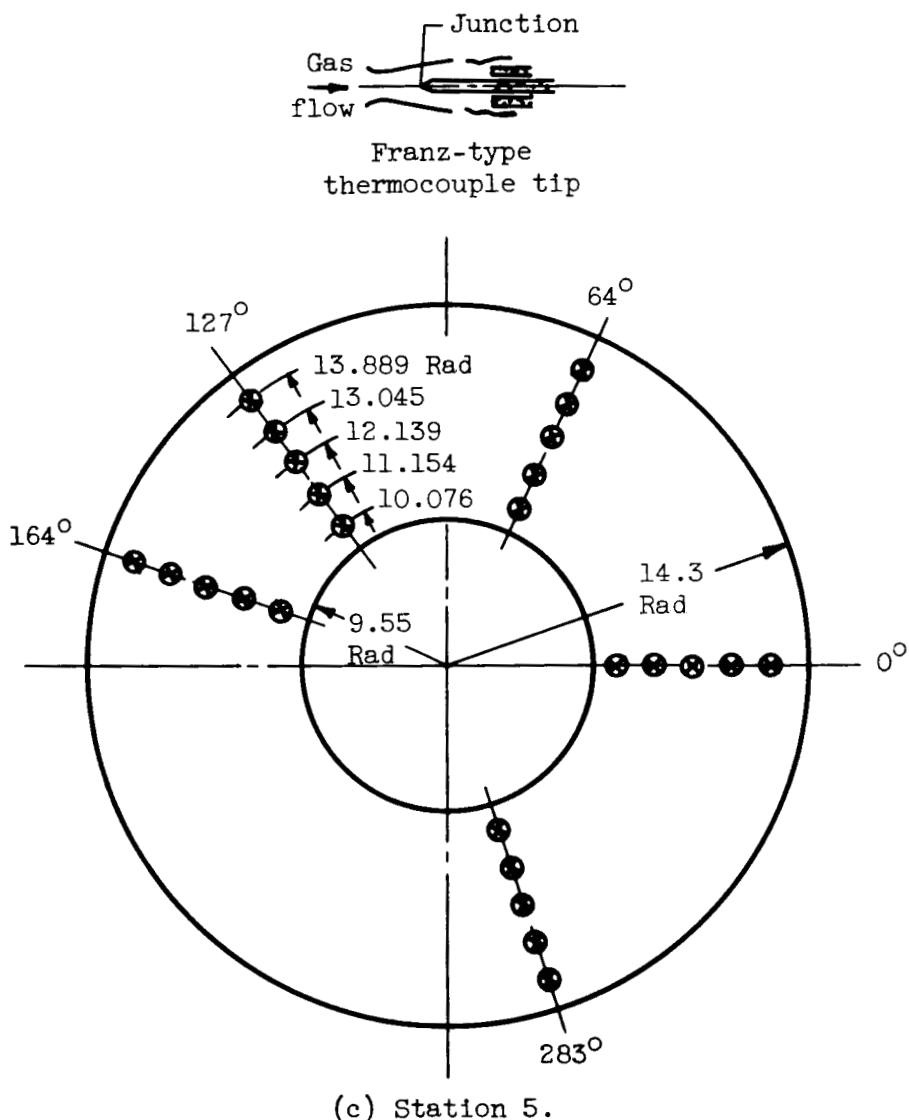


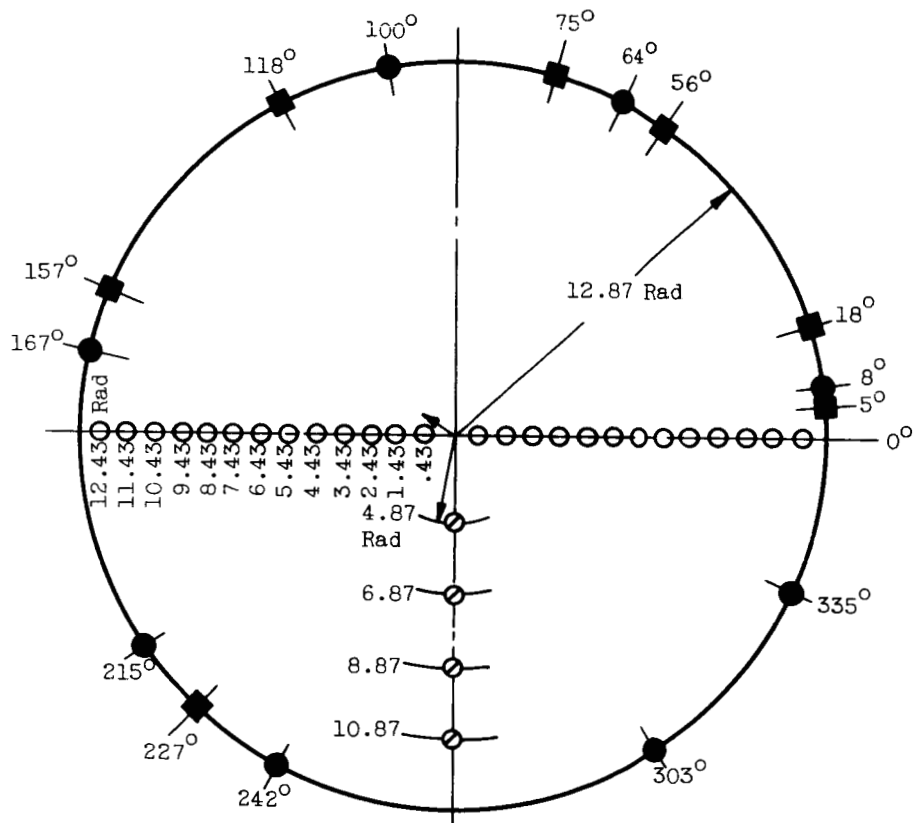
Figure 5. - Continued. Schematic diagrams of instrumentation stations viewed looking downstream. (All dimensions in inches except where noted.)

DECLASSIFIED

NACA RM E57C07

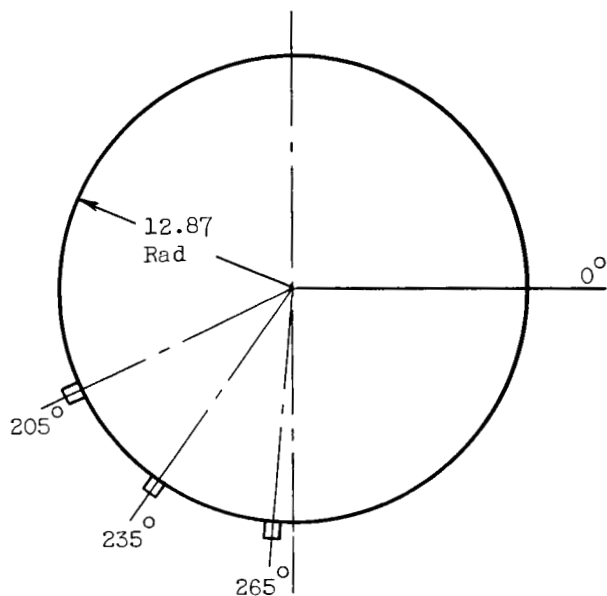
35

- Total-pressure probe
- ◐ Stream static-pressure probe
- Wall static-pressure tap
- Fuel-air-ratio probe

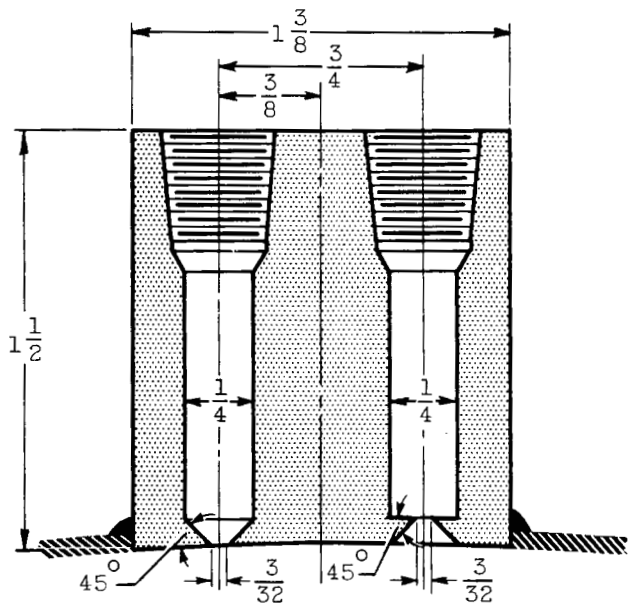


(d) Station 7.

Figure 5. - Continued. Schematic diagrams of instrumentation stations viewed looking downstream. (All dimensions in inches except where noted.)



Circumferential locations of orifice pairs



Cross section showing one pair of differential pressure orifices. CD-4761

(e) Station 8.

Figure 5. - Continued. Schematic diagrams of instrumentation stations viewed looking downstream. (All dimensions in inches except where noted.)

DECLASSIFIED

NACA RM E57C07

37

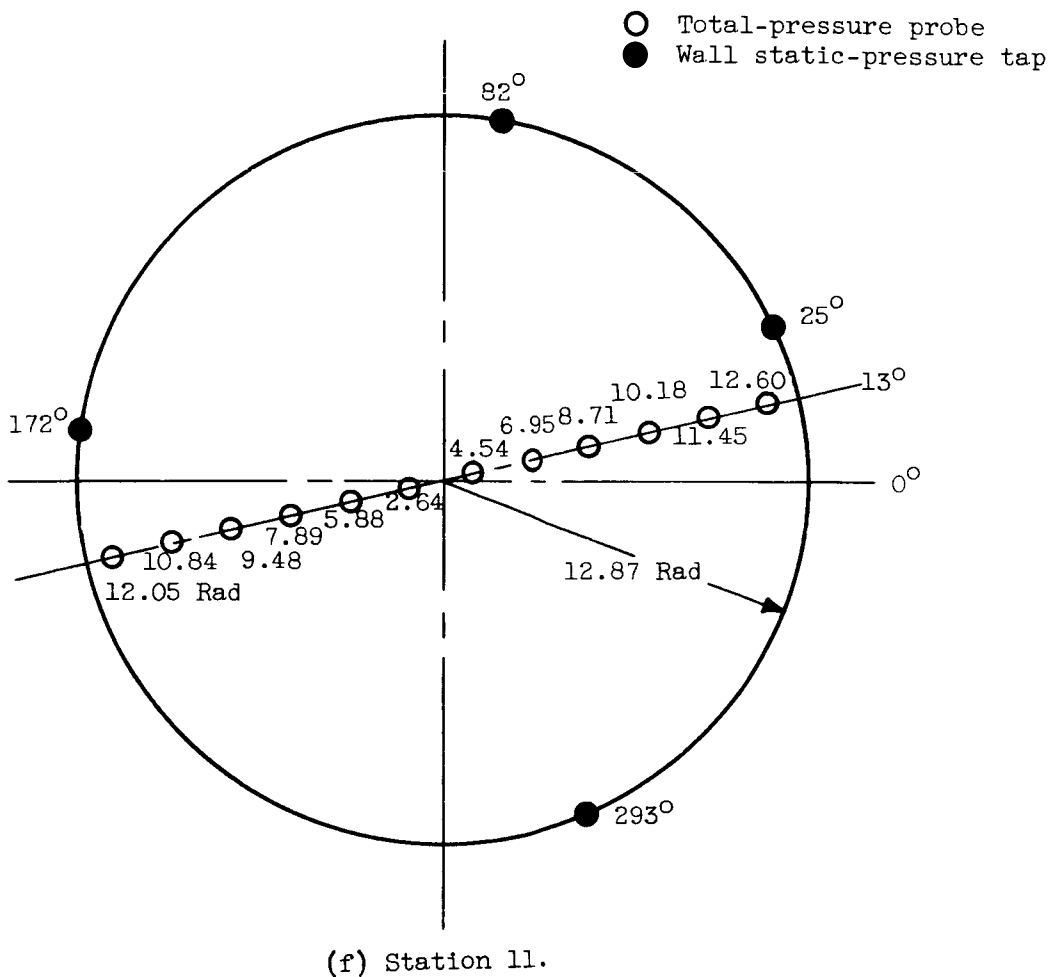
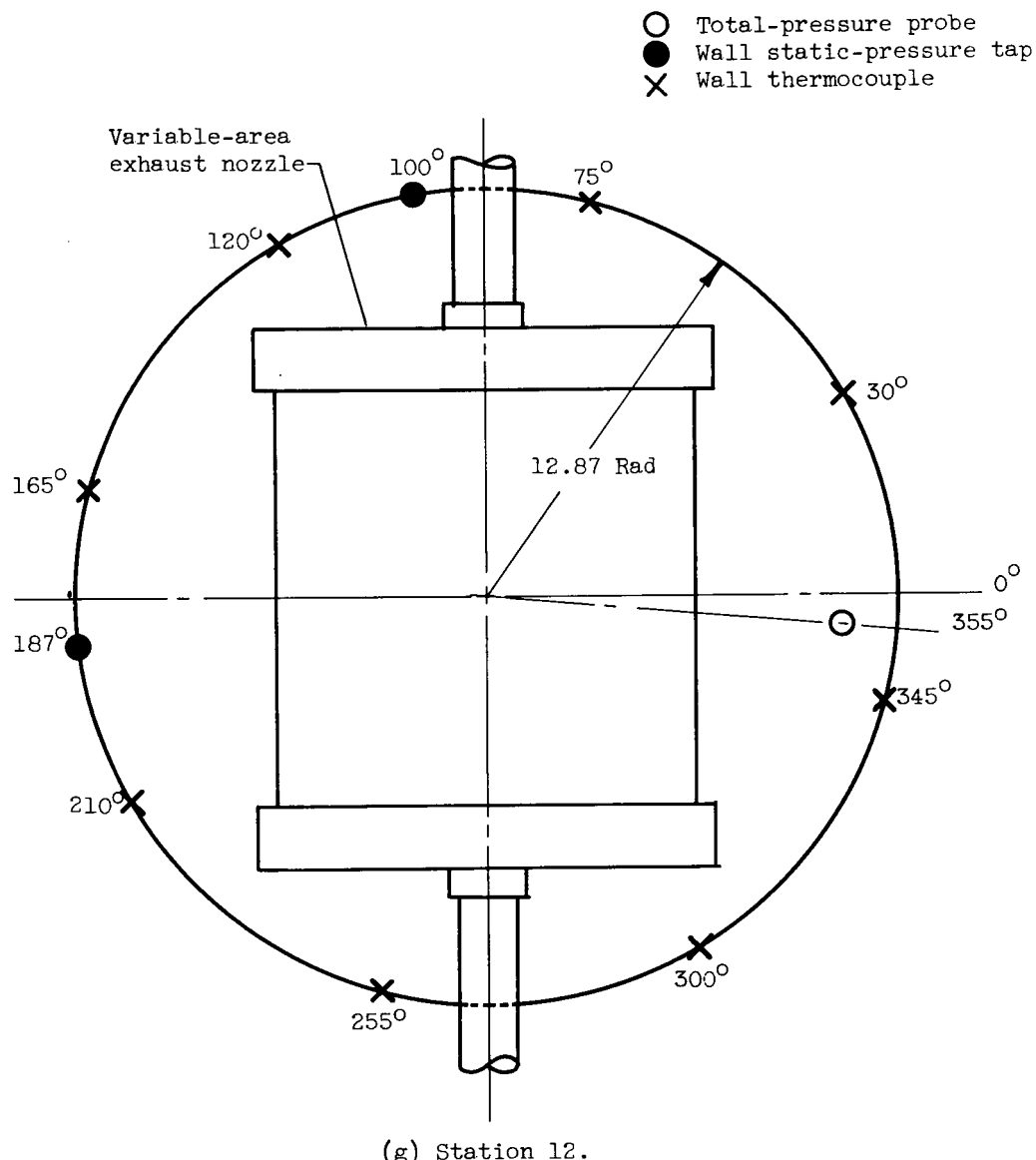


Figure 5. - Continued. Schematic diagrams of instrumentation stations viewed looking downstream. (All dimensions in inches except where noted.)

03171220J030

38

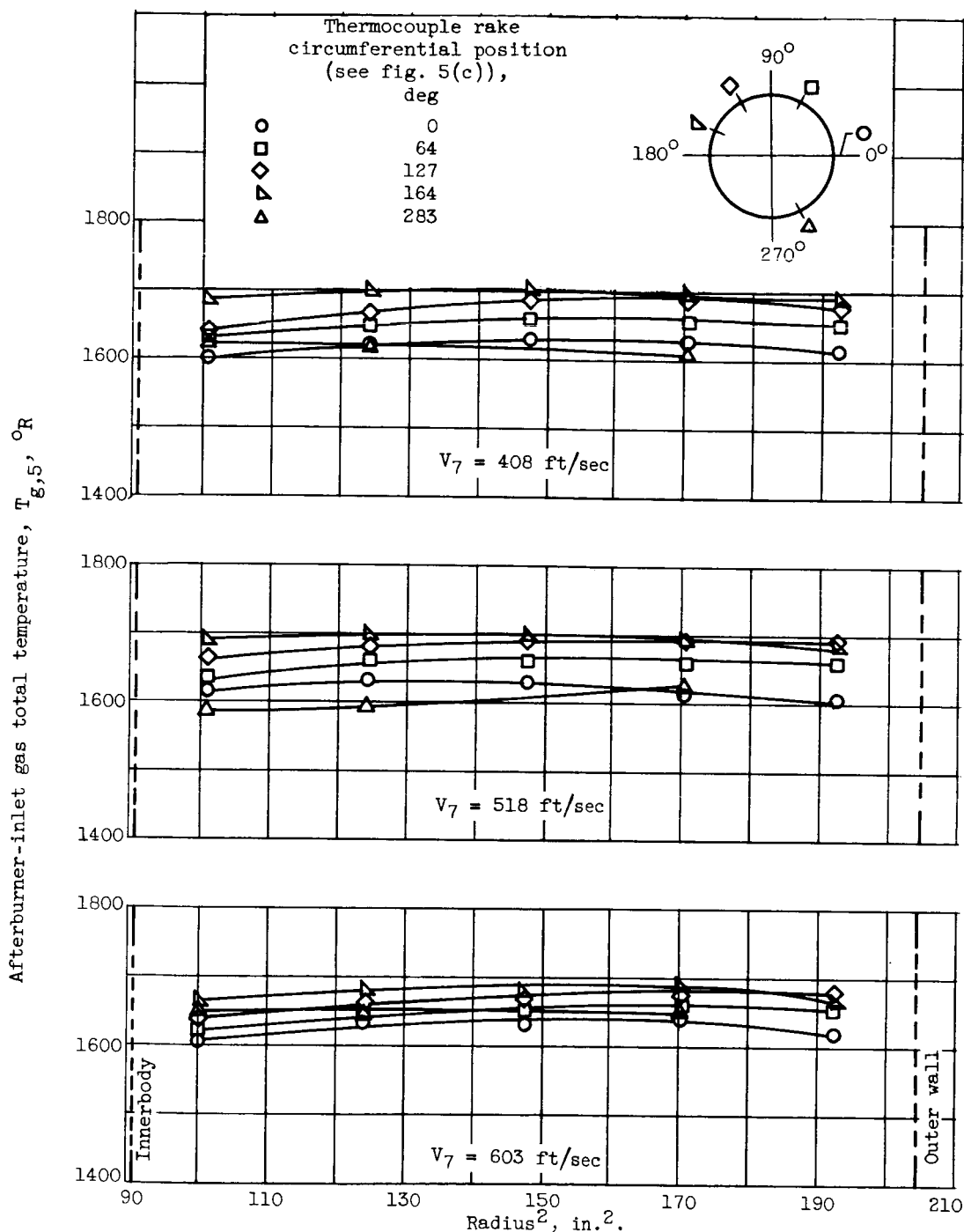
NACA RM E57C07



(g) Station 12.

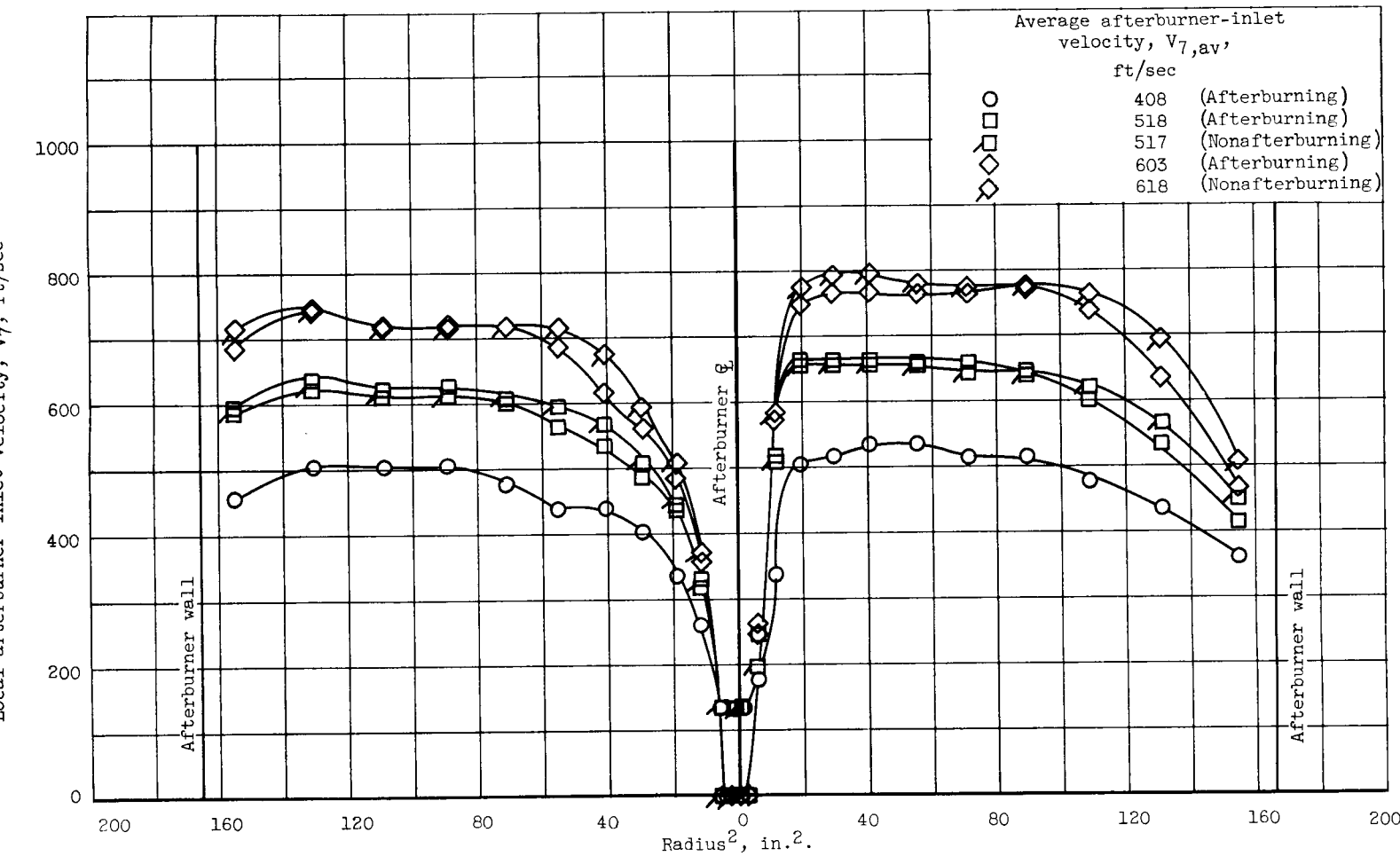
Figure 5. - Concluded. Schematic diagrams of instrumentation stations viewed looking downstream. (All dimensions in inches except where noted.)

DECLASSIFIED



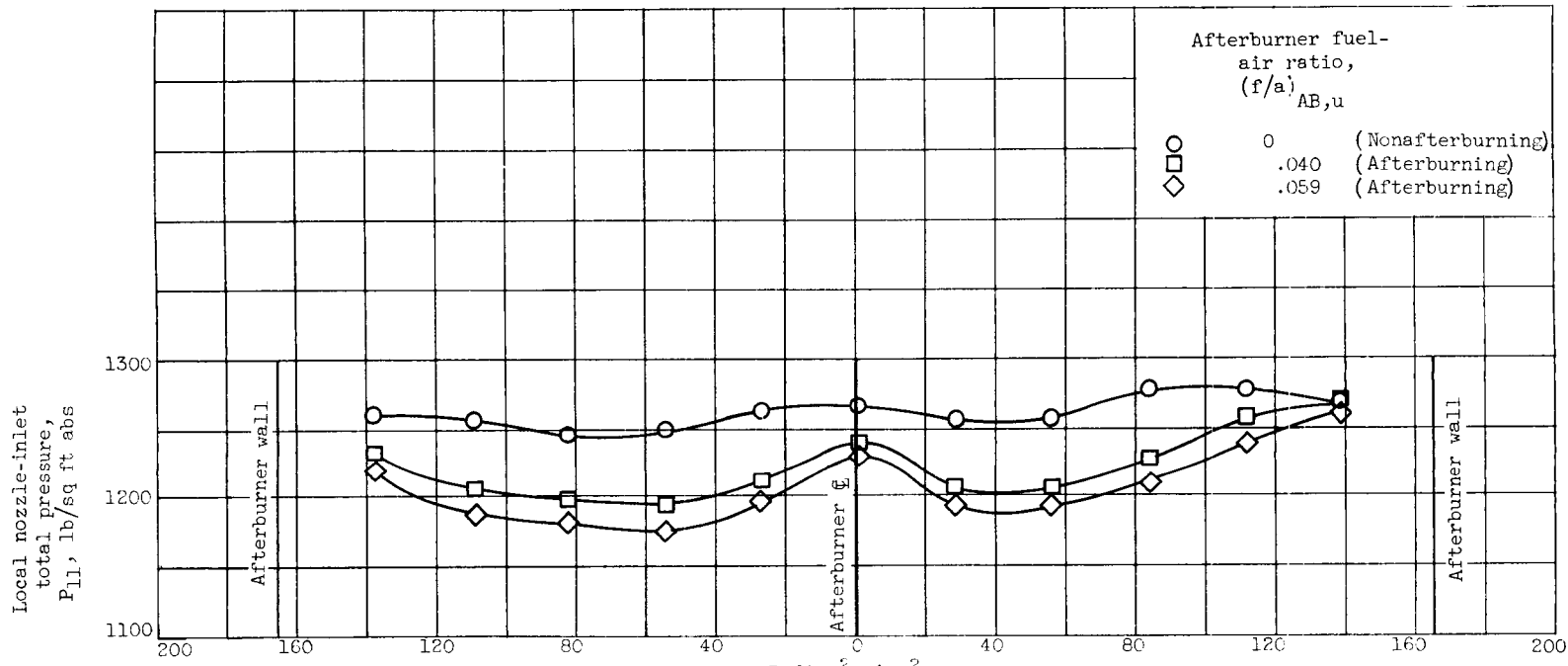
(a) Gas temperature at station 5 for several afterburner-inlet velocities; V_7 , afterburner-inlet velocity.

Figure 6. - Typical profiles for nominal afterburner-inlet pressure of 1270 pounds per square foot absolute and temperature of 1660° R.



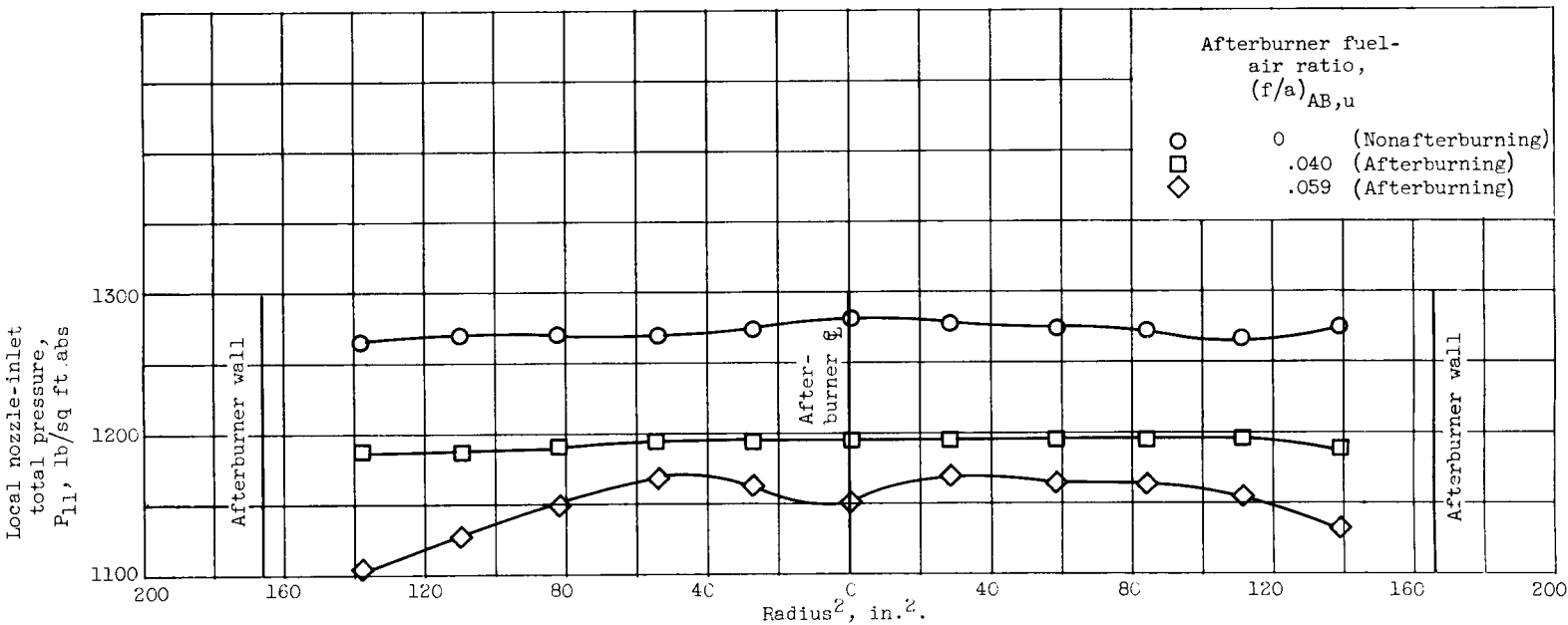
(b) Afterburner-inlet velocity.

Figure 6. - Continued. Typical profiles for nominal afterburner-inlet pressure of 1270 pounds per square foot absolute and temperature of 1660° R.



(c) Nozzle-inlet total pressure; afterburner-inlet velocity, 520 feet per second; afterburner combustion-chamber length, 30 inches.

Figure 6. - Continued. Typical profiles for nominal afterburner-inlet pressure of 1270 pounds per square foot absolute and temperature of 1660° R.



(d) Nozzle-inlet total pressure; afterburner-inlet velocity, 565 feet per second; afterburner combustion-chamber length, 66 inches.

Figure 6. - Concluded. Typical profiles for nominal afterburner-inlet pressure of 1270 pounds per square foot absolute and temperature of 1660° R.

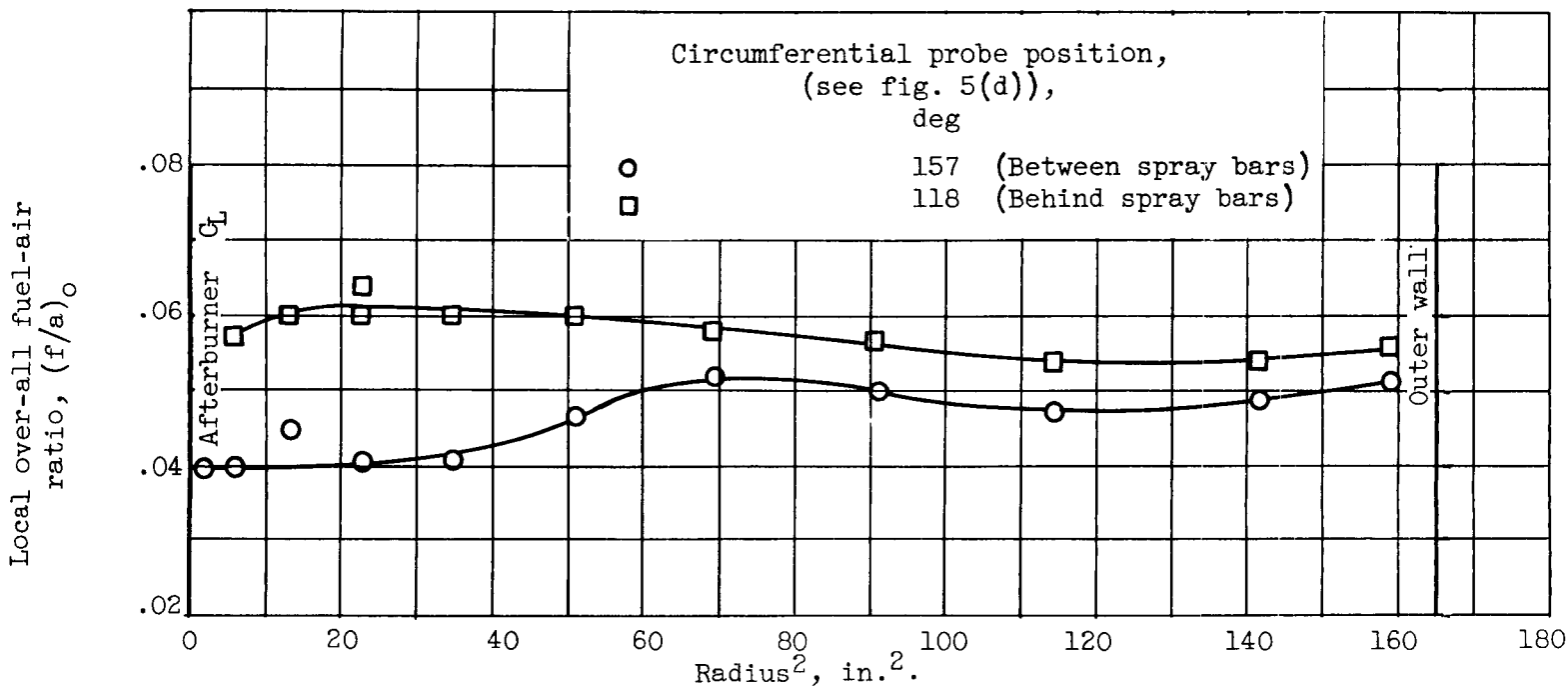
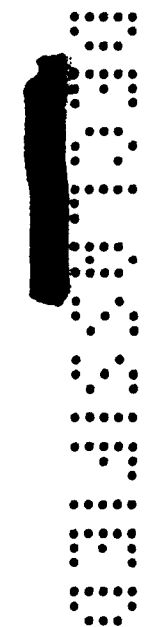


Figure 7. Typical radial fuel-air-ratio profiles for two circumferential probe positions at afterburner inlet. Afterburner fuel-air ratio, 0.050; afterburner-inlet total temperature, 1710°R ; afterburner-inlet total pressure, 1430 pounds per square foot absolute; afterburner-inlet velocity, 550 feet per second.

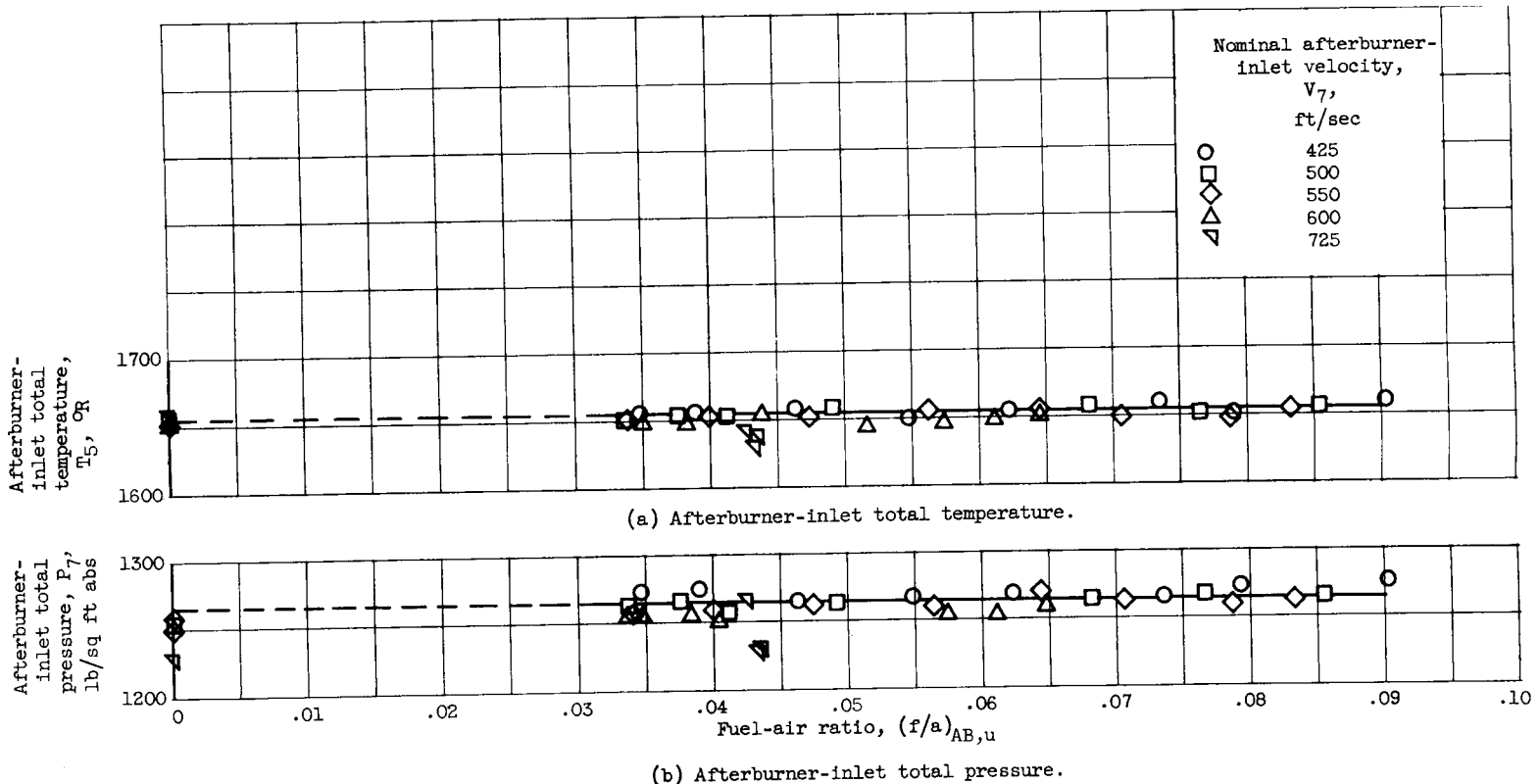
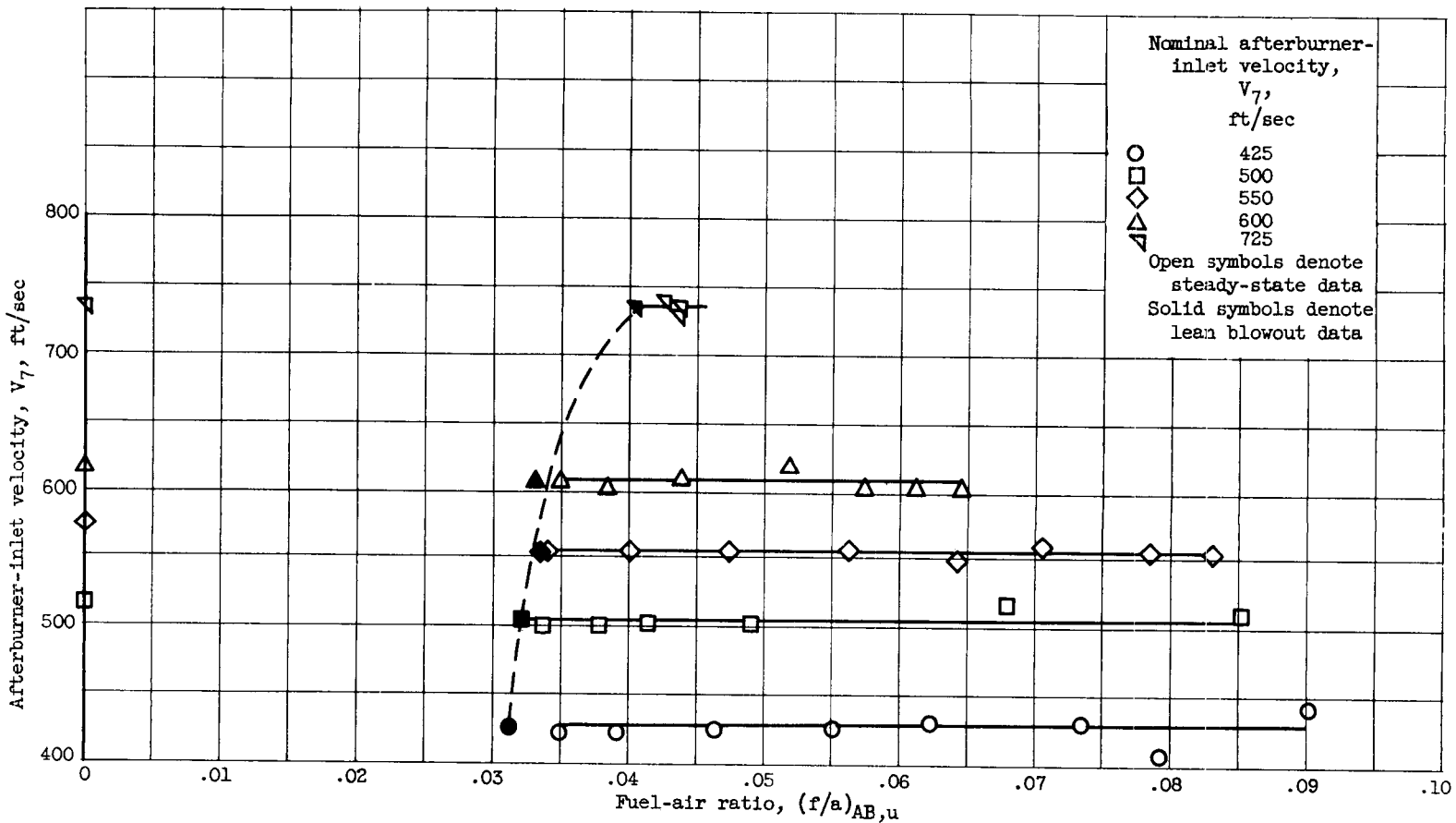


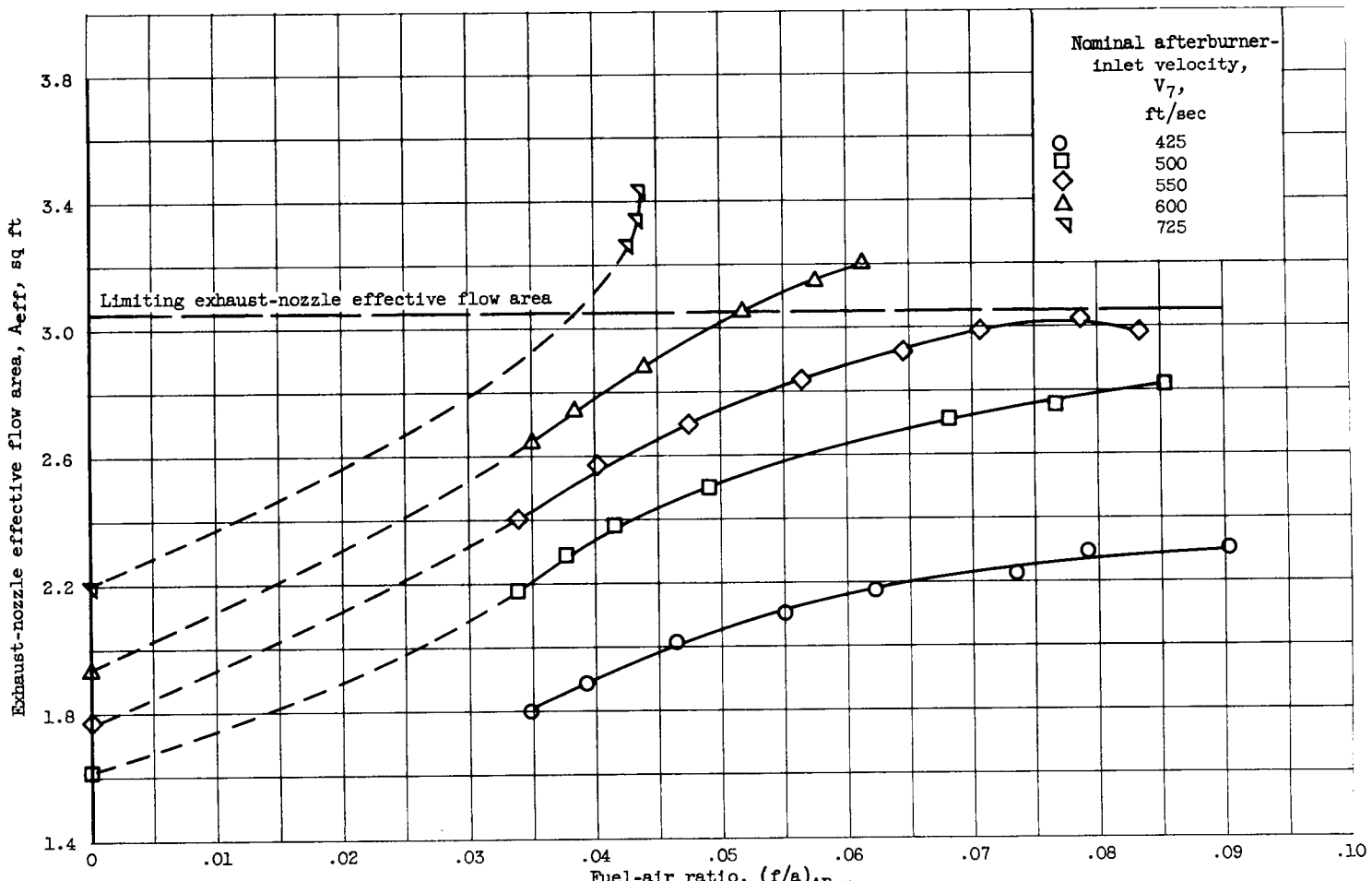
Figure 8. - Typical variations of afterburner conditions in 42-inch-long afterburner for range of velocities. Afterburner-inlet total temperature, 1660°R ; afterburner-inlet total pressure, 1270 pounds per square foot absolute.



(c) Afterburner-inlet velocity and lean blowouts.

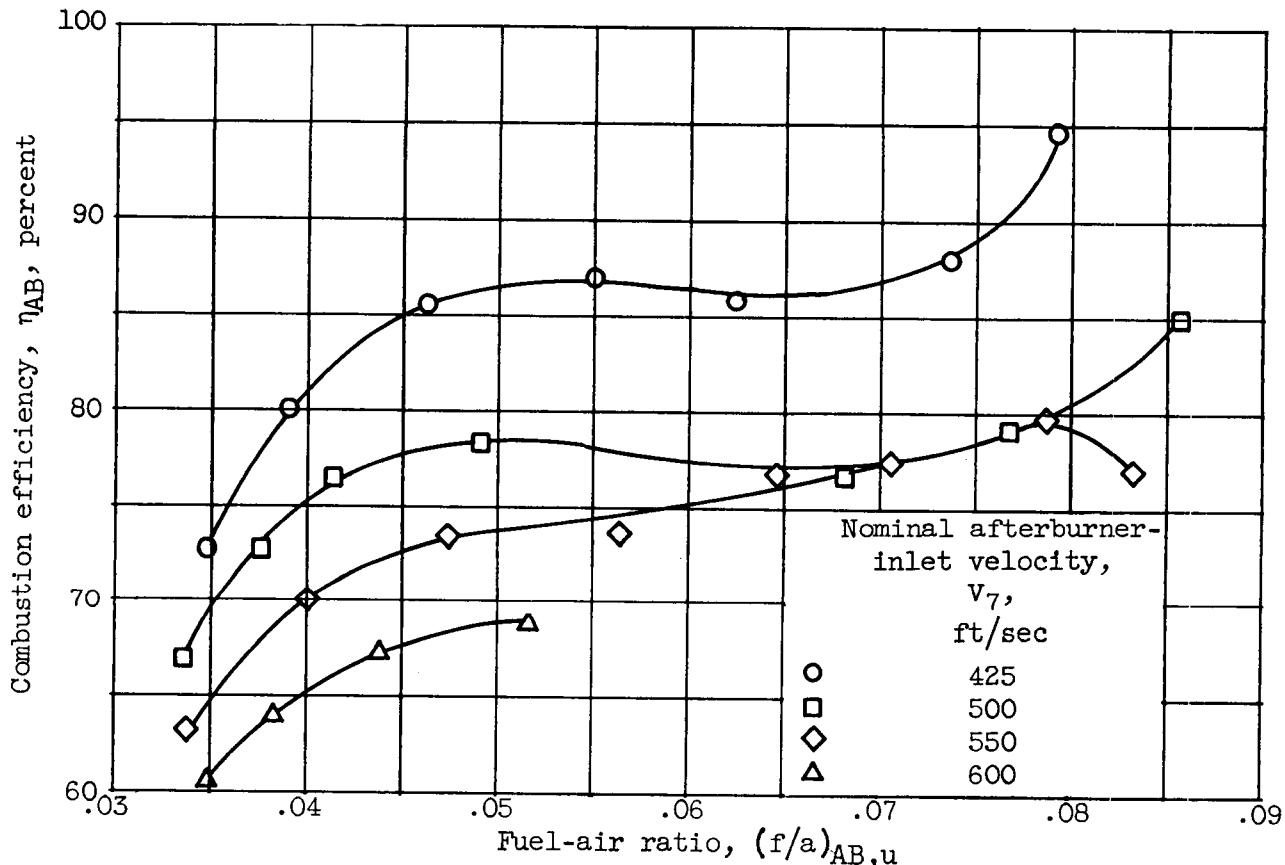
Figure 8. - Continued. Typical variations of afterburner conditions in 42-inch-long afterburner for range of velocities. Afterburner-inlet total temperature, 1660° R; afterburner-inlet total pressure, 1270 pounds per square foot absolute.

NACA RM E57C07



(d) Exhaust-nozzle effective flow area.

Figure 8. - Concluded. Typical variations of afterburner conditions in 42-inch-long afterburner for range of velocities. Afterburner-inlet total temperature, 1660° R; afterburner-inlet total pressure, 1270 pounds per square foot absolute.



(a) Combustion efficiency.

Figure 9. - Typical performance characteristics of 42-inch-long afterburner. Afterburner-inlet total temperature, 1660° R; afterburner-inlet total pressure, 1270 pounds per square foot absolute.

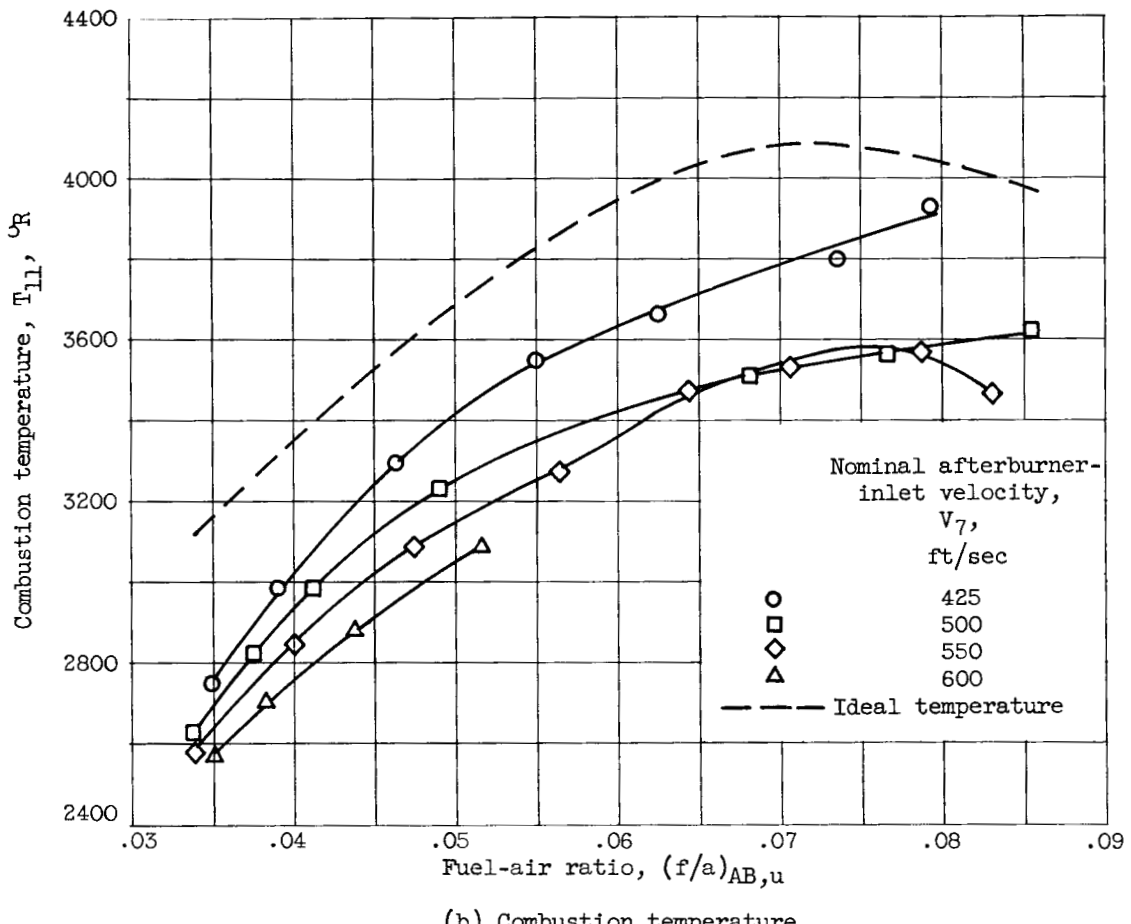
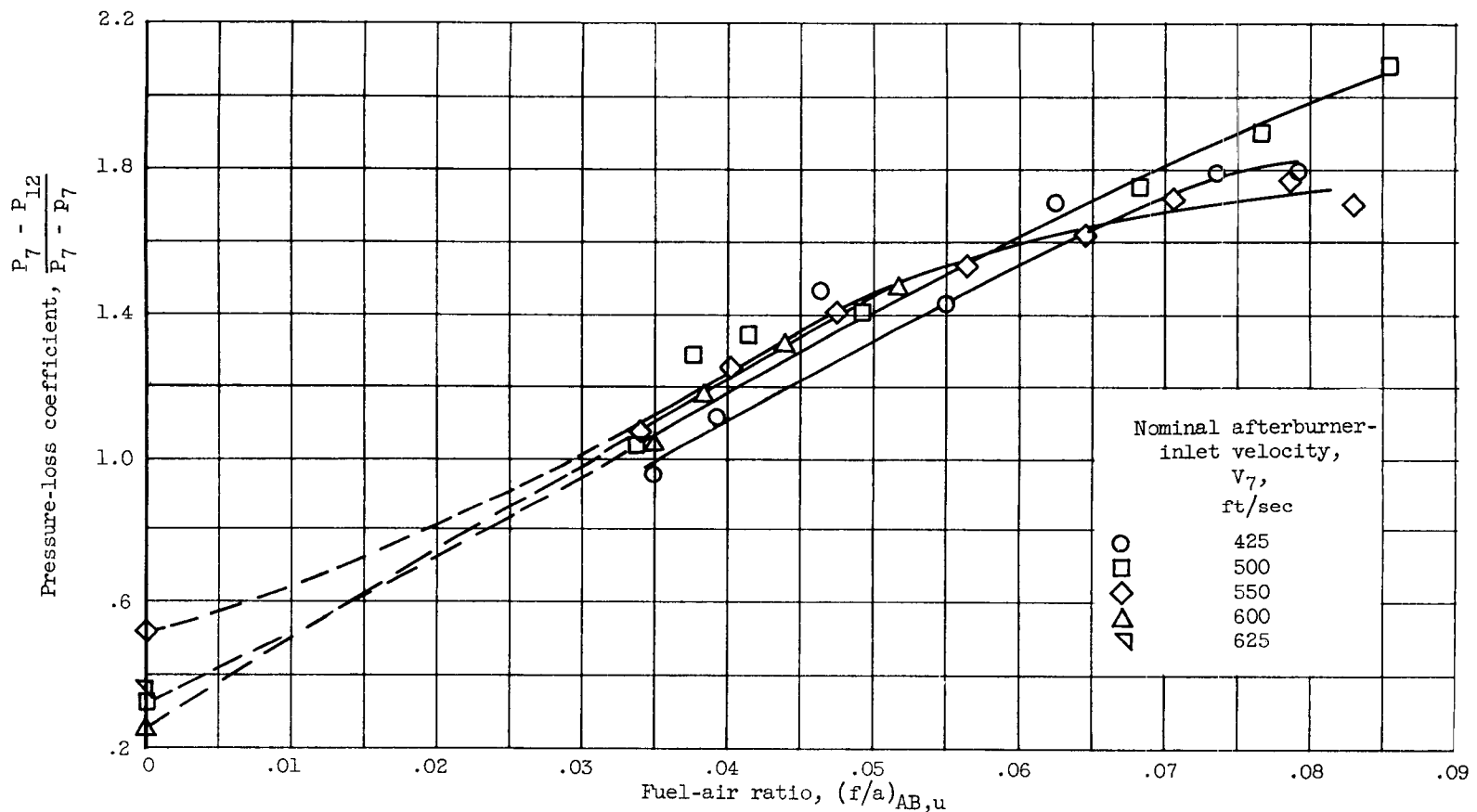


Figure 9. - Continued. Typical performance characteristics of 42-inch-long afterburner. Afterburner-inlet total temperature, 1660° R; afterburner-inlet total pressure, 1270 pounds per square foot absolute.



(c) Pressure-loss coefficient.

Figure 9. - Concluded. Typical performance characteristics of 42-inch-long afterburner. Afterburner-inlet total temperature, 1660° R; afterburner-inlet total pressure, 1270 pounds per square foot absolute.

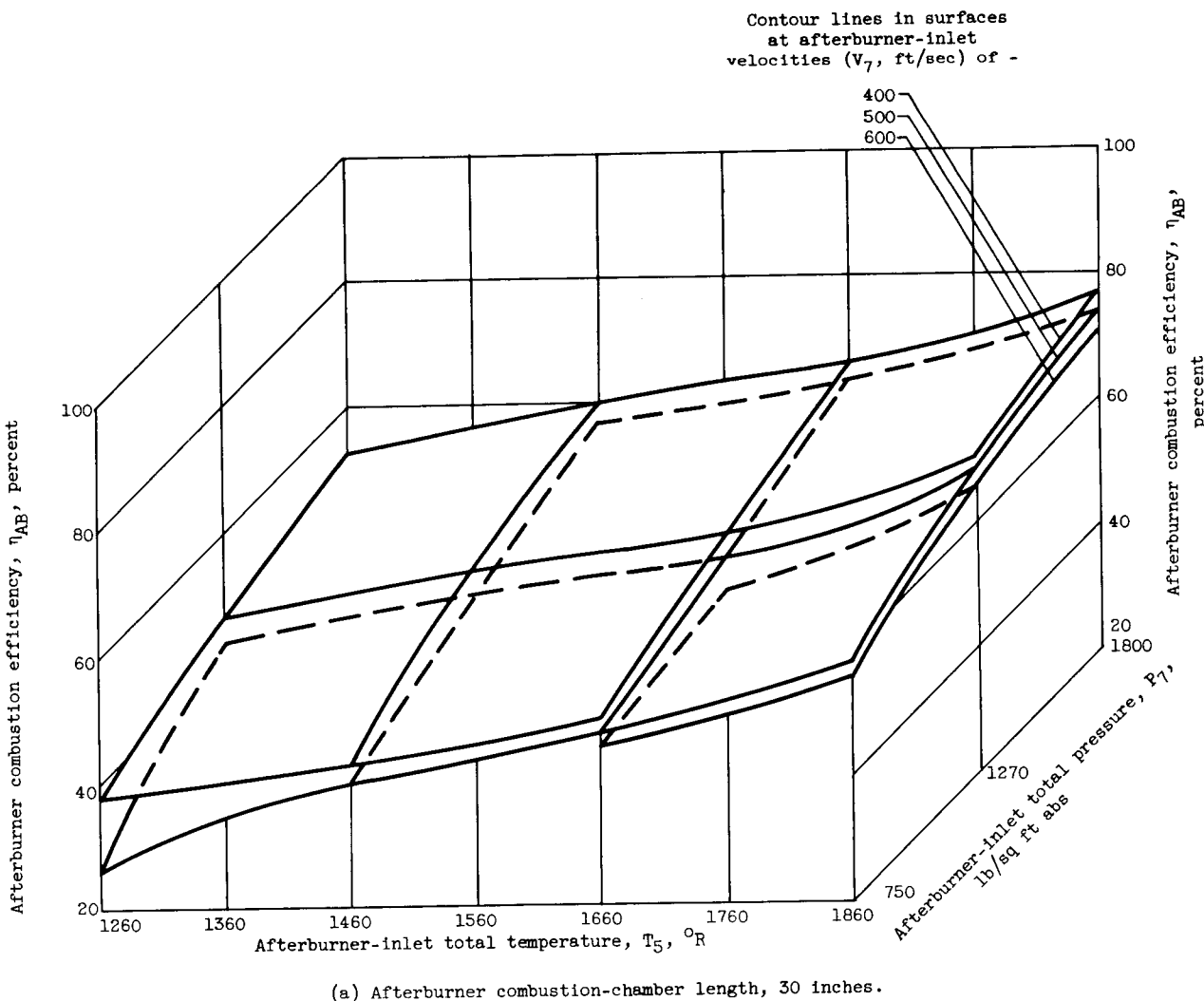


Figure 10. - Isometric figures showing combined effects of afterburner-inlet variables on combustion efficiency. Afterburner fuel-air ratio, 0.055.

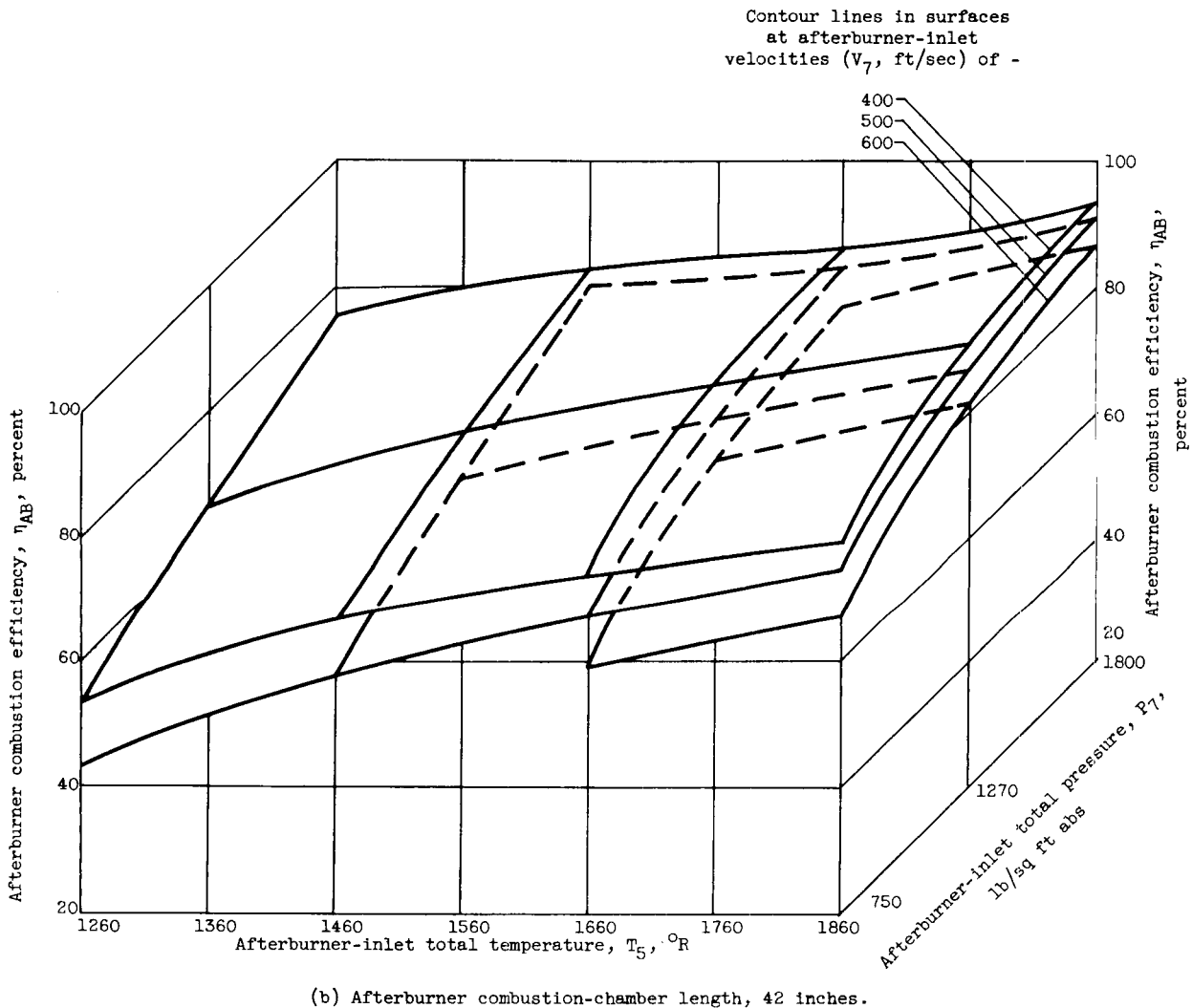
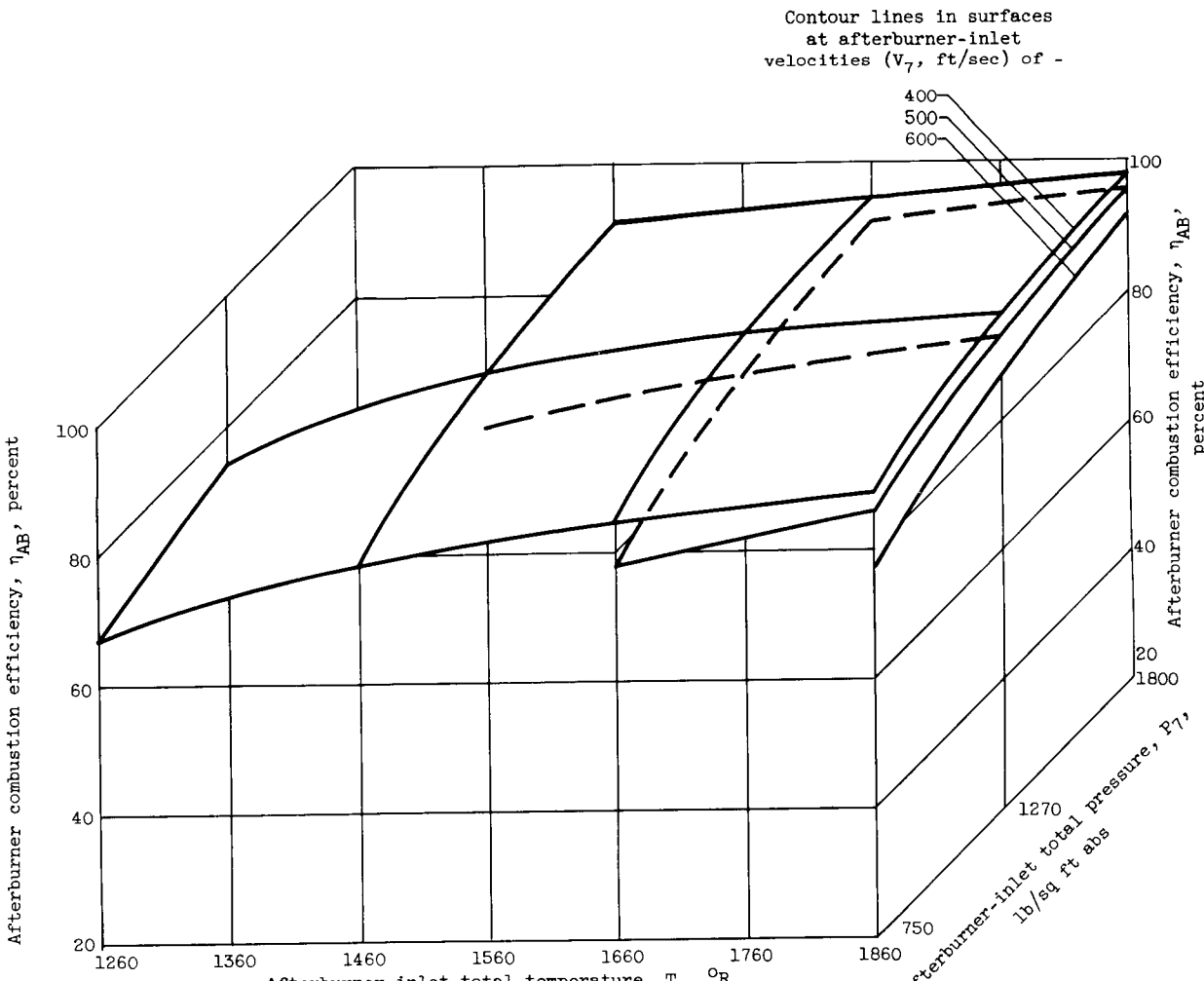


Figure 10. - Continued. Isometric figures showing combined effects of afterburner-inlet variables on combustion efficiency. Afterburner fuel-air ratio, 0.055.



(c) Afterburner combustion-chamber length, 54 inches.

Figure 10. - Continued. Isometric figures showing combined effects of afterburner-inlet variables on combustion efficiency. Afterburner fuel-air ratio, 0.055.

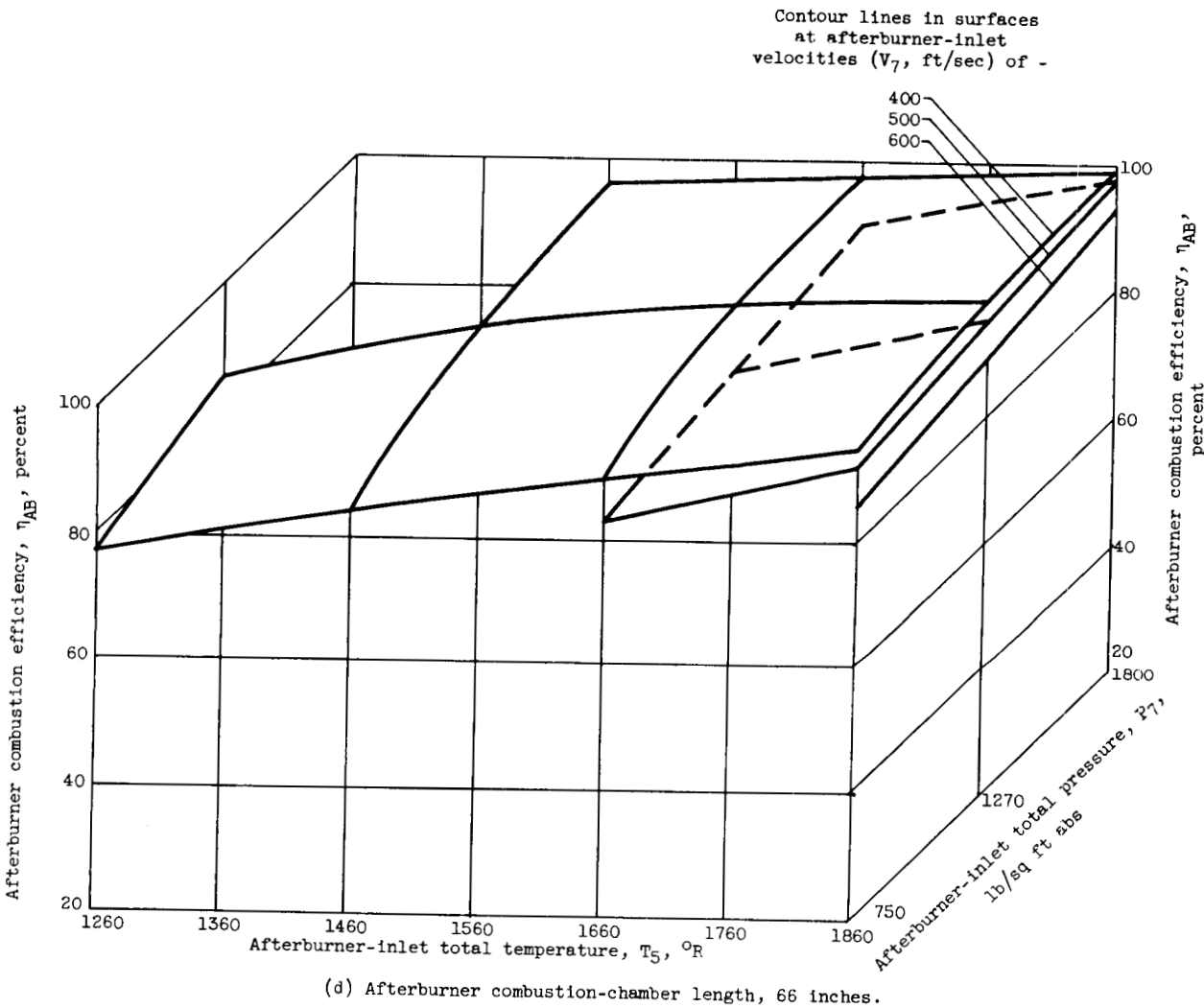


Figure 10. - Concluded. Isometric figures showing combined effects of afterburner-inlet variables on combustion efficiency. Afterburner fuel-air ratio, 0.055.

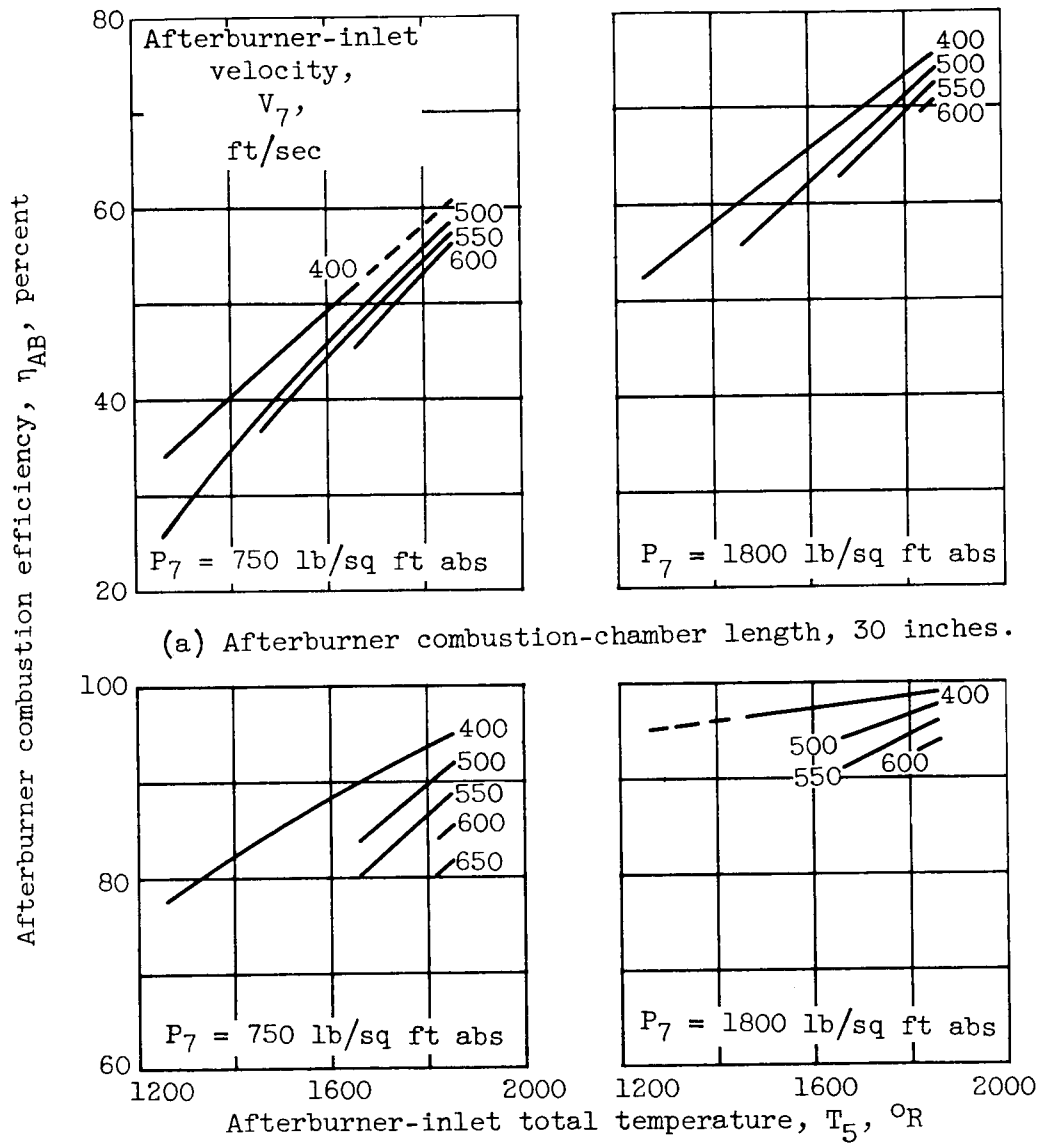


Figure 11. - Effect of afterburner-inlet total temperature on combustion efficiency for extreme values of afterburner-inlet total pressure, afterburner-inlet velocity, and afterburner length. Afterburner fuel-air ratio, 0.055; P_7 , afterburner-inlet total pressure.

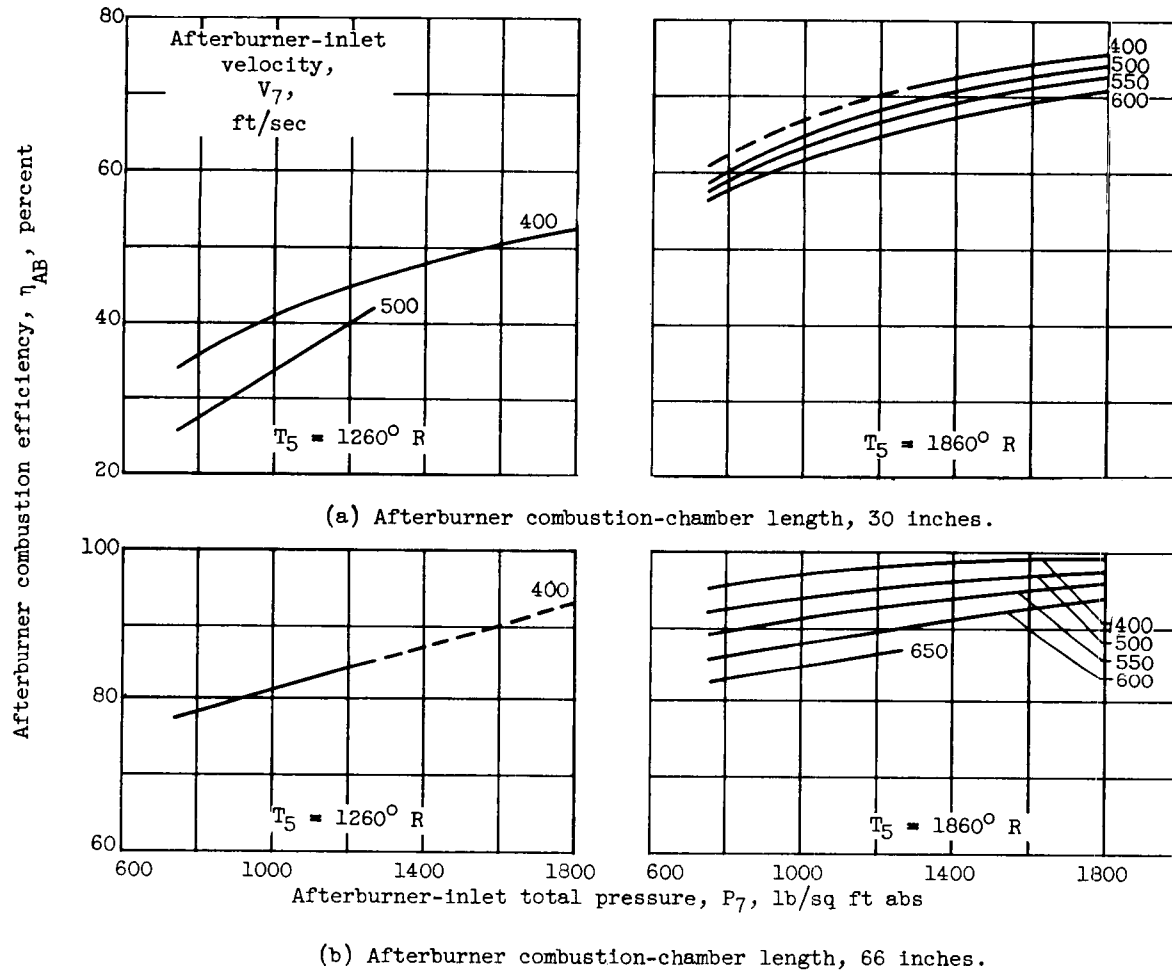


Figure 12. - Effect of afterburner-inlet total pressure on combustion efficiency for extreme values of afterburner-inlet total temperature, afterburner-inlet velocity, and afterburner length. Afterburner fuel-air ratio, 0.055; T_5 , afterburner-inlet total temperature.

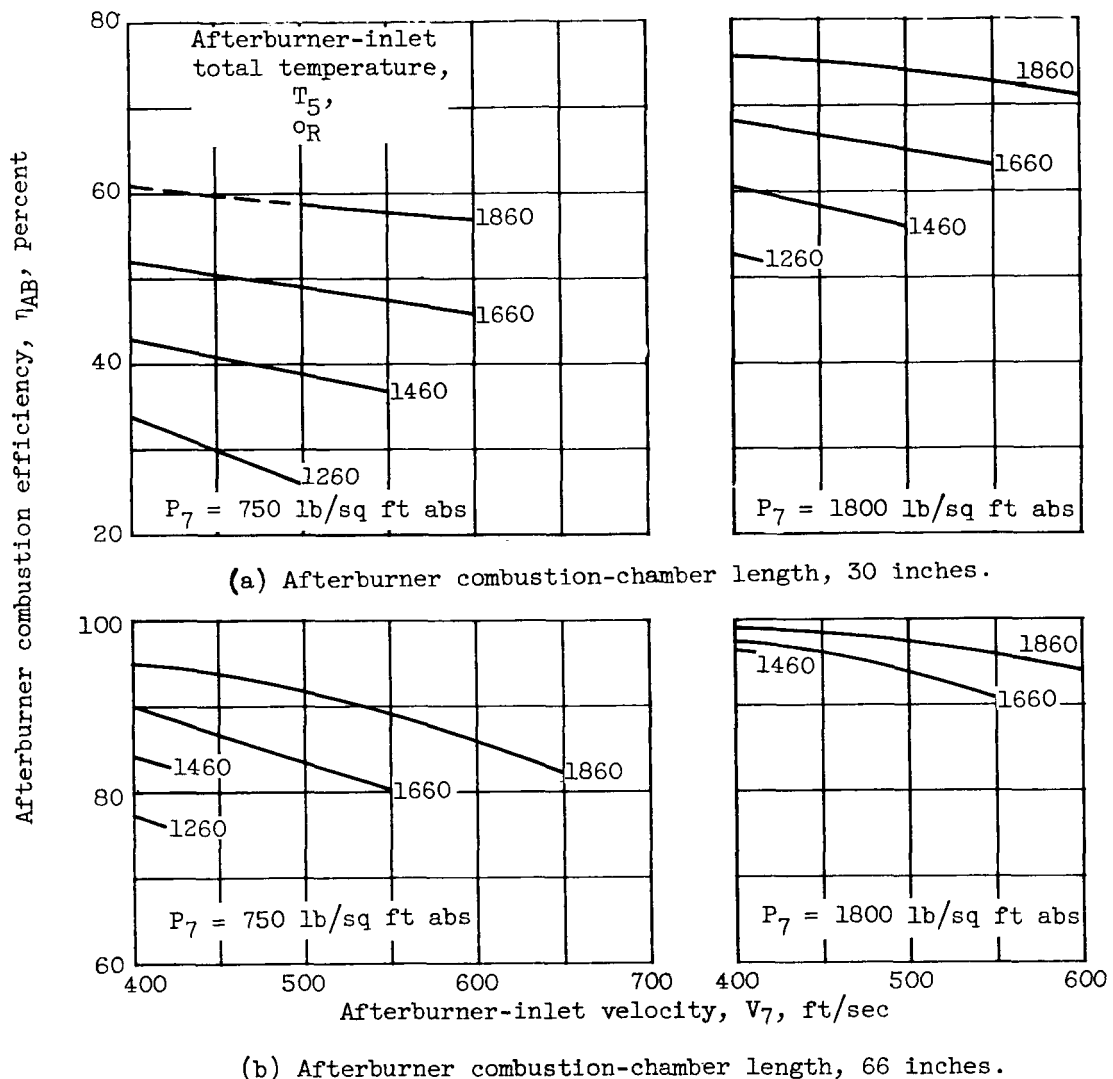
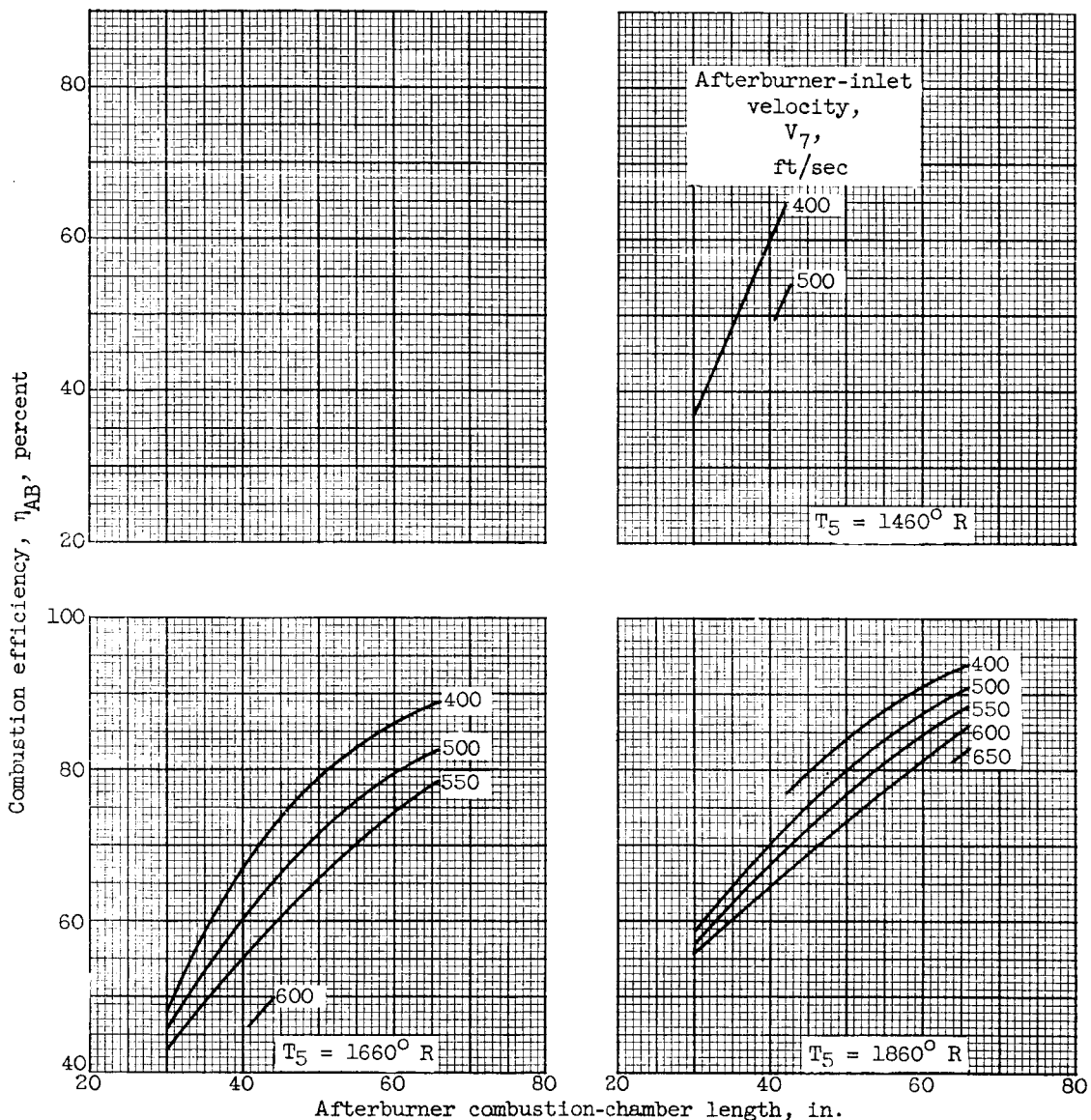


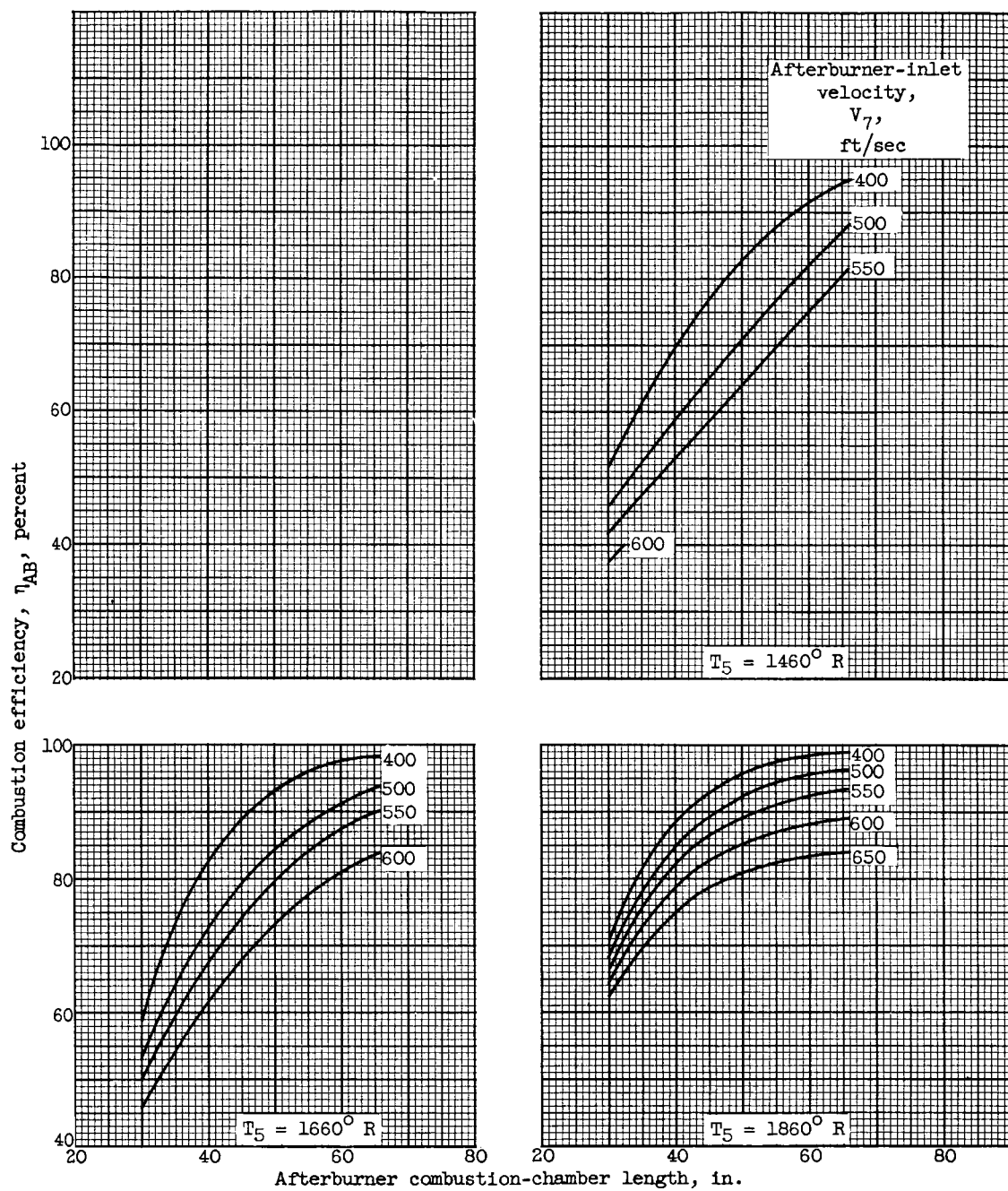
Figure 13. - Effect of afterburner-inlet velocity on combustion efficiency for extreme values of afterburner-inlet total temperature, afterburner-inlet total pressure, and afterburner length. Afterburner fuel-air ratio, 0.055; P_7 , afterburner-inlet total pressure.

REF ID: A6792
REF ID: A6793
REF ID: A6794
REF ID: A6795
REF ID: A6796
REF ID: A6797
REF ID: A6798
REF ID: A6799
REF ID: A6800
REF ID: A6801
REF ID: A6802
REF ID: A6803
REF ID: A6804
REF ID: A6805
REF ID: A6806
REF ID: A6807
REF ID: A6808
REF ID: A6809
REF ID: A6810
REF ID: A6811
REF ID: A6812
REF ID: A6813
REF ID: A6814
REF ID: A6815
REF ID: A6816
REF ID: A6817
REF ID: A6818
REF ID: A6819
REF ID: A6820
REF ID: A6821
REF ID: A6822
REF ID: A6823
REF ID: A6824
REF ID: A6825
REF ID: A6826
REF ID: A6827
REF ID: A6828
REF ID: A6829
REF ID: A6830
REF ID: A6831
REF ID: A6832
REF ID: A6833
REF ID: A6834
REF ID: A6835
REF ID: A6836
REF ID: A6837
REF ID: A6838
REF ID: A6839
REF ID: A6840
REF ID: A6841
REF ID: A6842
REF ID: A6843
REF ID: A6844
REF ID: A6845
REF ID: A6846
REF ID: A6847
REF ID: A6848
REF ID: A6849
REF ID: A6850
REF ID: A6851
REF ID: A6852
REF ID: A6853
REF ID: A6854
REF ID: A6855
REF ID: A6856
REF ID: A6857
REF ID: A6858
REF ID: A6859
REF ID: A6860
REF ID: A6861
REF ID: A6862
REF ID: A6863
REF ID: A6864
REF ID: A6865
REF ID: A6866
REF ID: A6867
REF ID: A6868
REF ID: A6869
REF ID: A6870
REF ID: A6871
REF ID: A6872
REF ID: A6873
REF ID: A6874
REF ID: A6875
REF ID: A6876
REF ID: A6877
REF ID: A6878
REF ID: A6879
REF ID: A6880
REF ID: A6881
REF ID: A6882
REF ID: A6883
REF ID: A6884
REF ID: A6885
REF ID: A6886
REF ID: A6887
REF ID: A6888
REF ID: A6889
REF ID: A6890
REF ID: A6891
REF ID: A6892
REF ID: A6893
REF ID: A6894
REF ID: A6895
REF ID: A6896
REF ID: A6897
REF ID: A6898
REF ID: A6899
REF ID: A6900
REF ID: A6901
REF ID: A6902
REF ID: A6903
REF ID: A6904
REF ID: A6905
REF ID: A6906
REF ID: A6907
REF ID: A6908
REF ID: A6909
REF ID: A6910
REF ID: A6911
REF ID: A6912
REF ID: A6913
REF ID: A6914
REF ID: A6915
REF ID: A6916
REF ID: A6917
REF ID: A6918
REF ID: A6919
REF ID: A6920
REF ID: A6921
REF ID: A6922
REF ID: A6923
REF ID: A6924
REF ID: A6925
REF ID: A6926
REF ID: A6927
REF ID: A6928
REF ID: A6929
REF ID: A6930
REF ID: A6931
REF ID: A6932
REF ID: A6933
REF ID: A6934
REF ID: A6935
REF ID: A6936
REF ID: A6937
REF ID: A6938
REF ID: A6939
REF ID: A6940
REF ID: A6941
REF ID: A6942
REF ID: A6943
REF ID: A6944
REF ID: A6945
REF ID: A6946
REF ID: A6947
REF ID: A6948
REF ID: A6949
REF ID: A6950
REF ID: A6951
REF ID: A6952
REF ID: A6953
REF ID: A6954
REF ID: A6955
REF ID: A6956
REF ID: A6957
REF ID: A6958
REF ID: A6959
REF ID: A6960
REF ID: A6961
REF ID: A6962
REF ID: A6963
REF ID: A6964
REF ID: A6965
REF ID: A6966
REF ID: A6967
REF ID: A6968
REF ID: A6969
REF ID: A6970
REF ID: A6971
REF ID: A6972
REF ID: A6973
REF ID: A6974
REF ID: A6975
REF ID: A6976
REF ID: A6977
REF ID: A6978
REF ID: A6979
REF ID: A6980
REF ID: A6981
REF ID: A6982
REF ID: A6983
REF ID: A6984
REF ID: A6985
REF ID: A6986
REF ID: A6987
REF ID: A6988
REF ID: A6989
REF ID: A6990
REF ID: A6991
REF ID: A6992
REF ID: A6993
REF ID: A6994
REF ID: A6995
REF ID: A6996
REF ID: A6997
REF ID: A6998
REF ID: A6999
REF ID: A6999



(a) Afterburner fuel-air ratio, 0.045; afterburner-inlet total pressure, 750 pounds per square foot absolute.

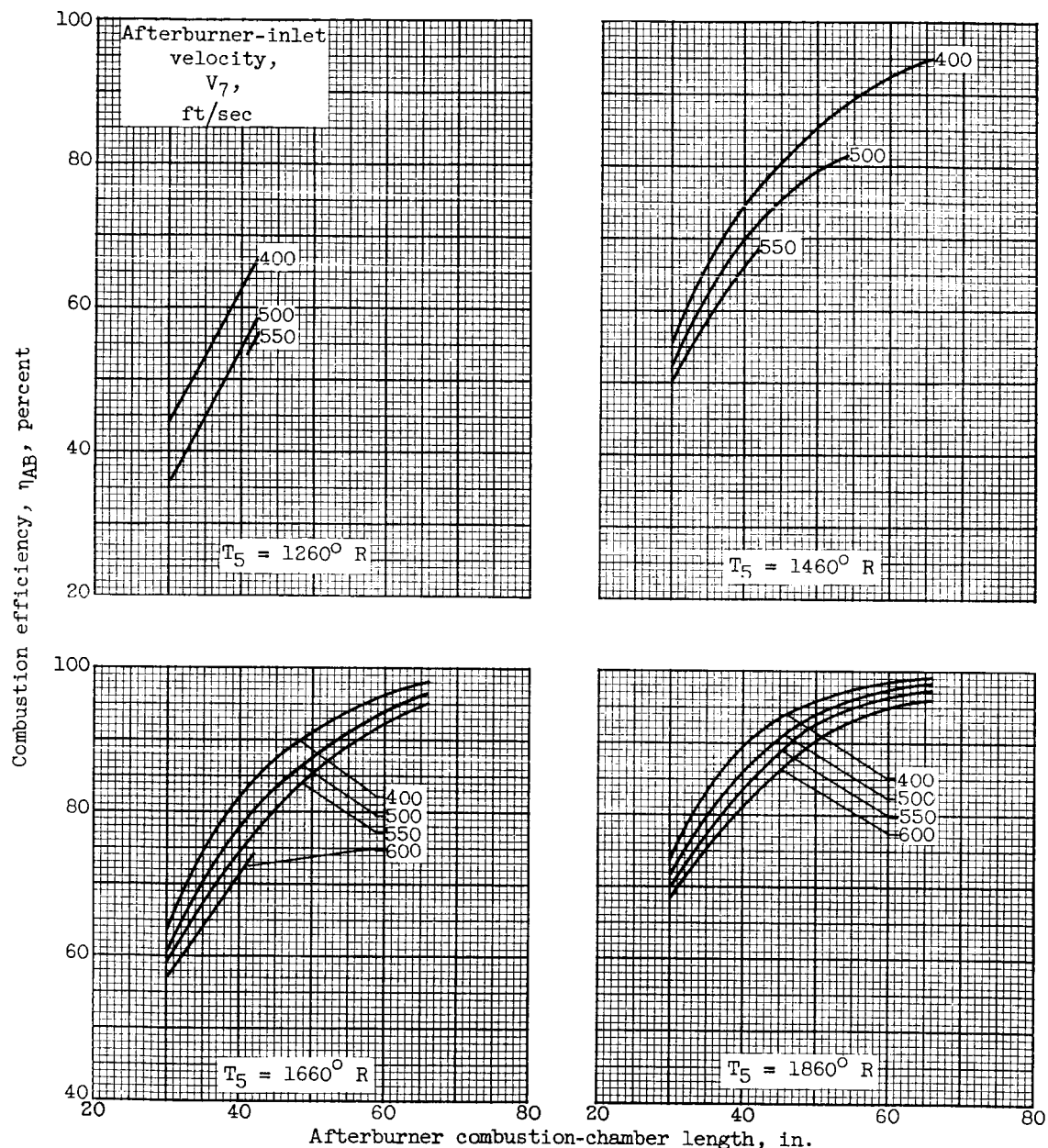
Figure 14. - Effect of afterburner combustion-chamber length on combustion efficiency for several afterburner-inlet velocities. T_5 , afterburner-inlet total temperature.



(b) Afterburner fuel-air ratio, 0.045; afterburner-inlet total pressure, 1270 pounds per square foot absolute.

Figure 14. - Continued. Effect of afterburner combustion-chamber length on combustion efficiency for several afterburner-inlet velocities. T_5 , afterburner-inlet total temperature.

DECLASSIFIED



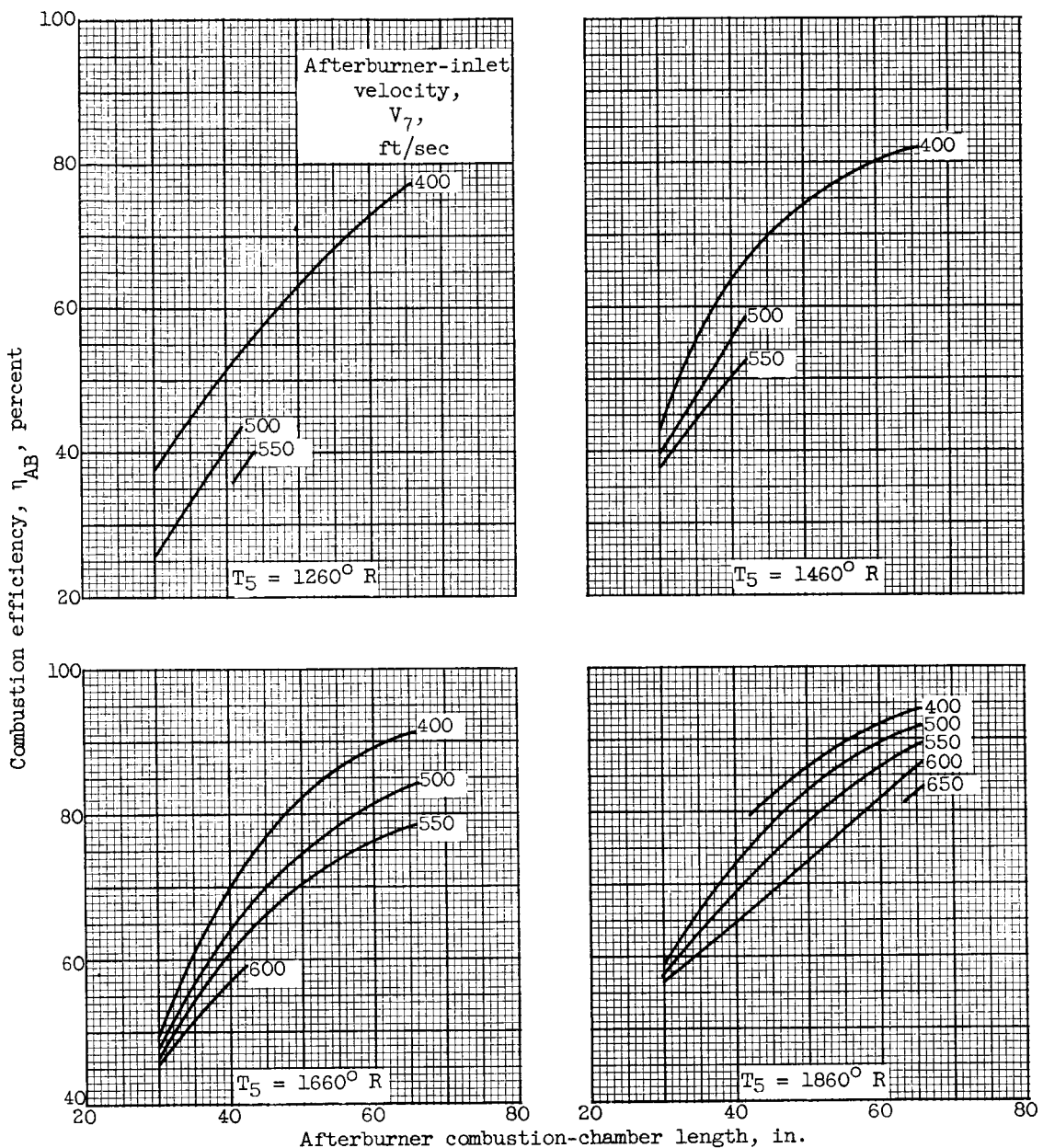
(c) Afterburner fuel-air ratio, 0.045; afterburner-inlet total pressure, 1800 pounds per square foot absolute.

Figure 14. - Continued. Effect of afterburner combustion-chamber length on combustion efficiency for several afterburner-inlet velocities. T_5 , afterburner-inlet total temperature.

0317022A1030

60

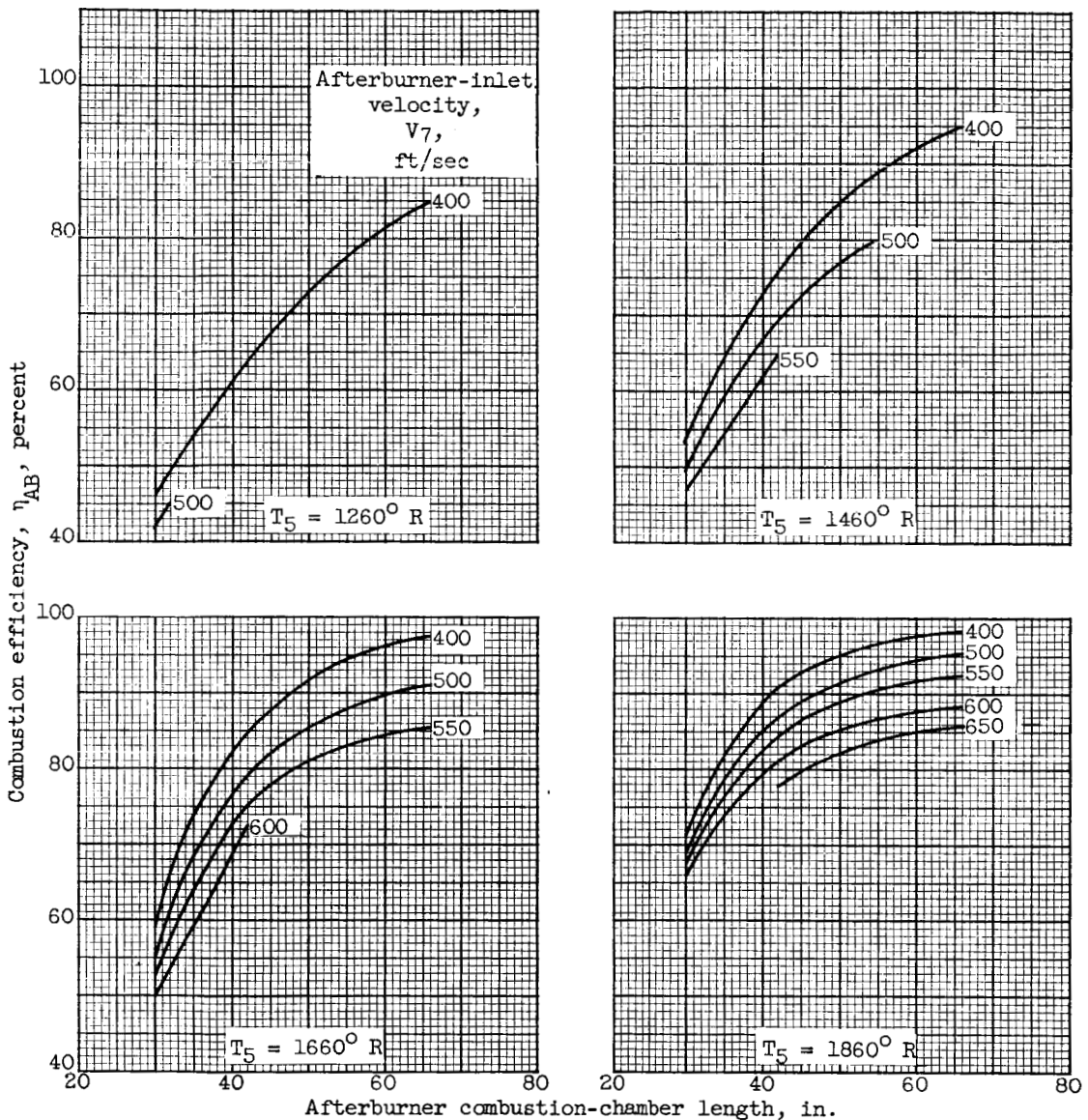
NACA RM E57C07



(d) Afterburner fuel-air ratio, 0.055; afterburner-inlet total pressure, 750 pounds per square foot absolute.

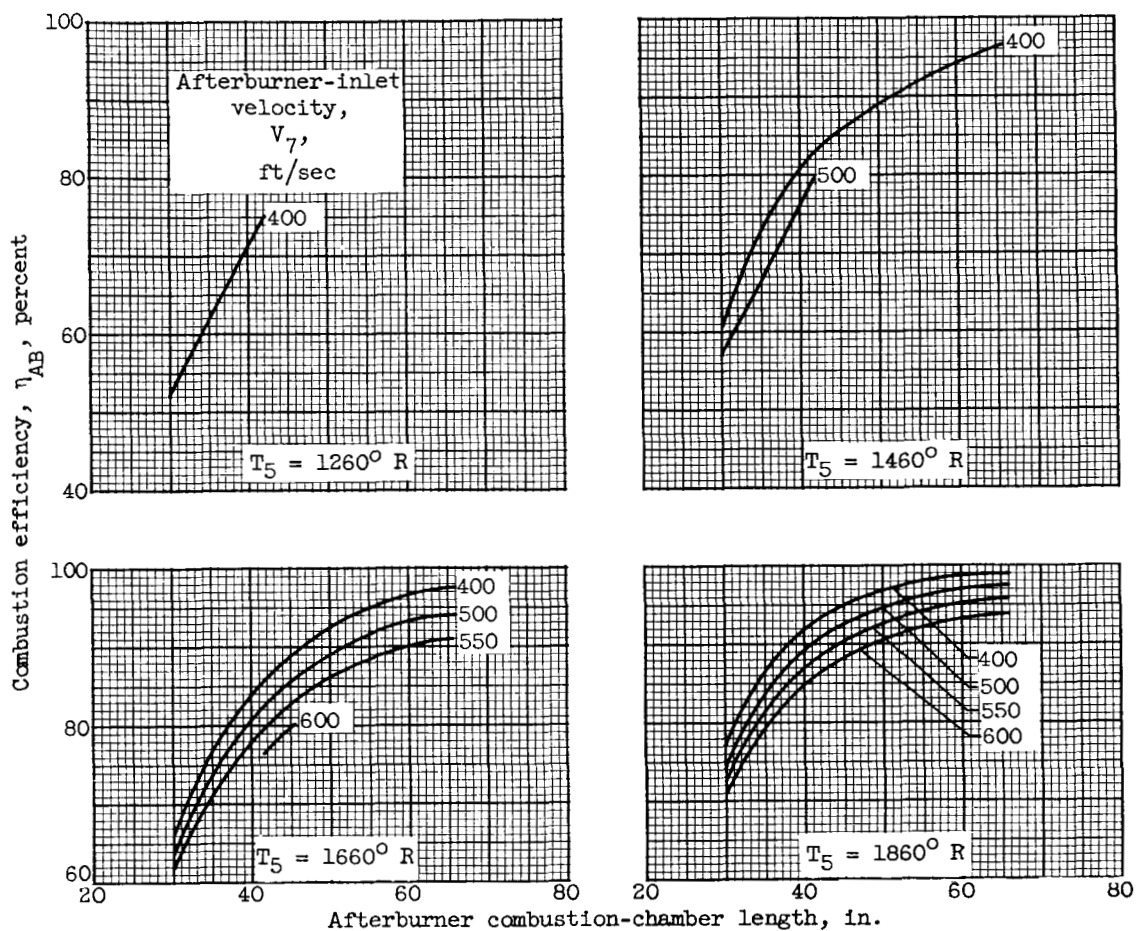
Figure 14. - Continued. Effect of afterburner combustion-chamber length on combustion efficiency for several afterburner-inlet velocities. T_5 , afterburner-inlet total temperature.

DECLASSIFIED



(e) Afterburner fuel-air ratio, 0.055; afterburner-inlet total pressure, 1270 pounds per square foot absolute.

Figure 14. - Continued. Effect of afterburner combustion-chamber length on combustion efficiency for several afterburner-inlet velocities. T_5 , afterburner-inlet total temperature.



(f) Afterburner fuel-air ratio, 0.055; afterburner-inlet total pressure, 1800 pounds per square foot absolute.

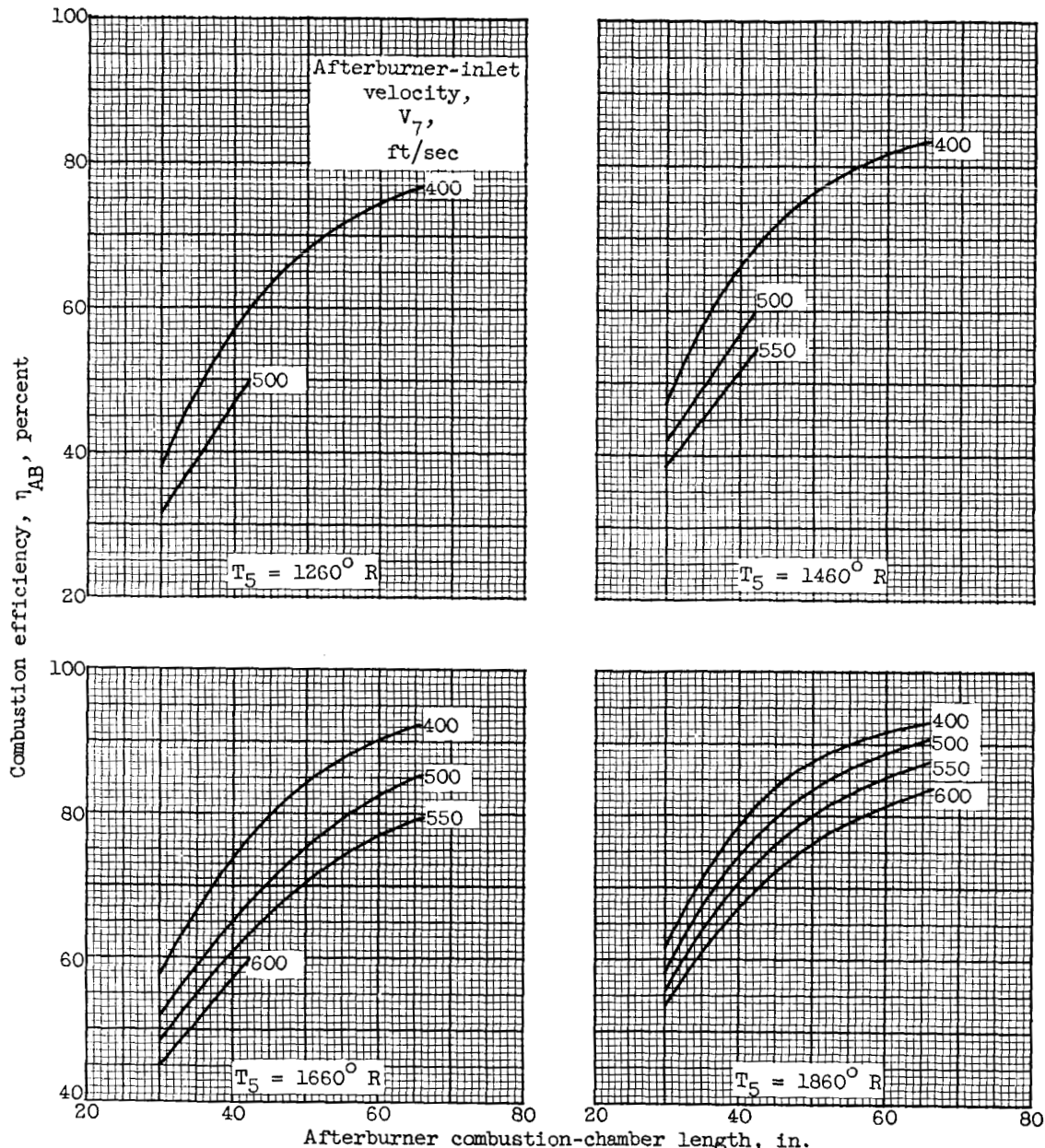
Figure 14. - Continued. Effect of afterburner combustion-chamber length on combustion efficiency for several afterburner-inlet velocities. T_5 , afterburner-inlet total temperature.

DECLASSIFIED

NACA RM E57C07

[REDACTED]

63



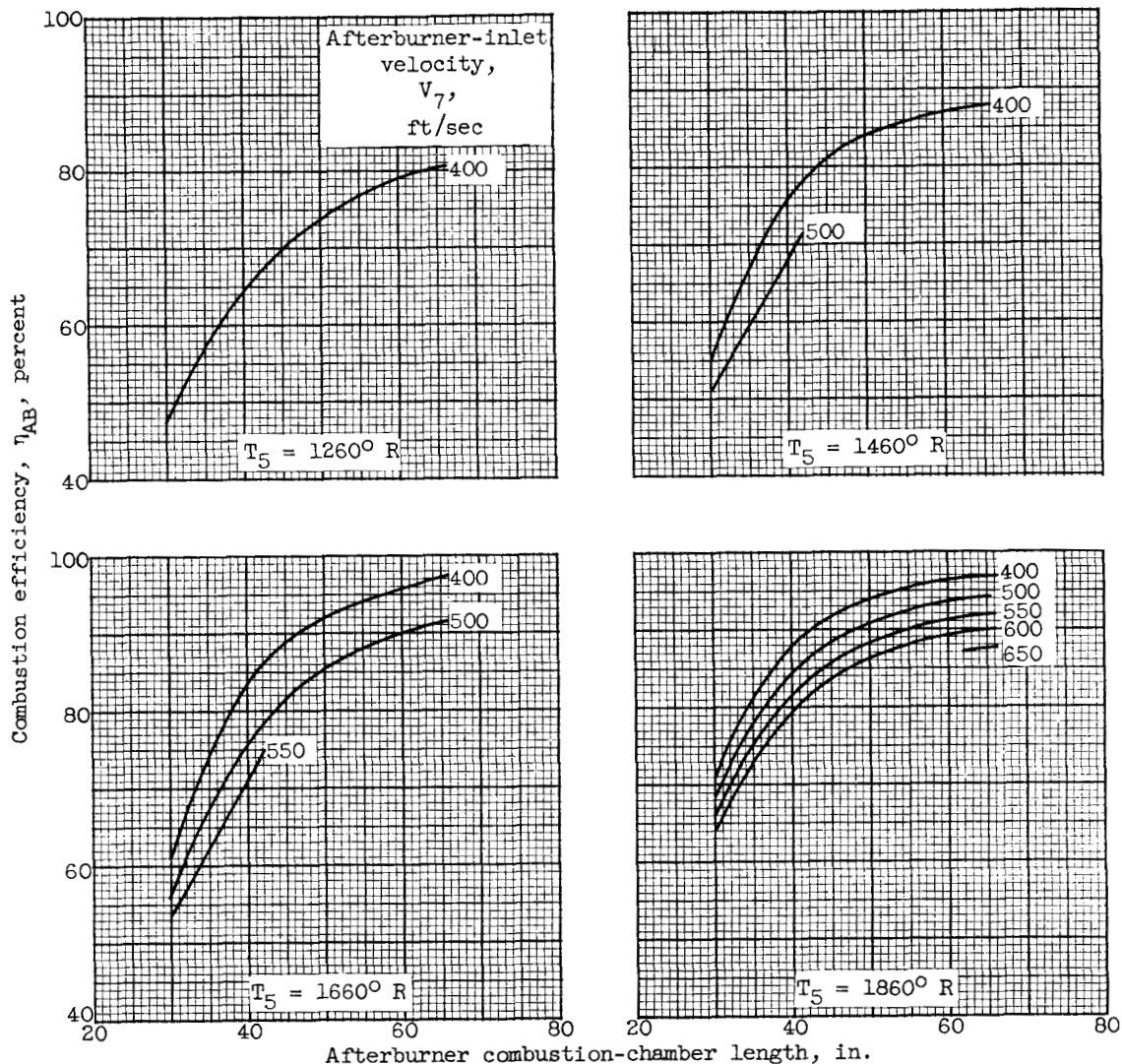
(g) Afterburner fuel-air ratio, 0.0676; afterburner-inlet total pressure, 750 pounds per square foot absolute.

Figure 14. - Continued. Effect of afterburner combustion-chamber length on combustion efficiency for several afterburner-inlet velocities. T_5 , afterburner-inlet total temperature.

031712201030

64

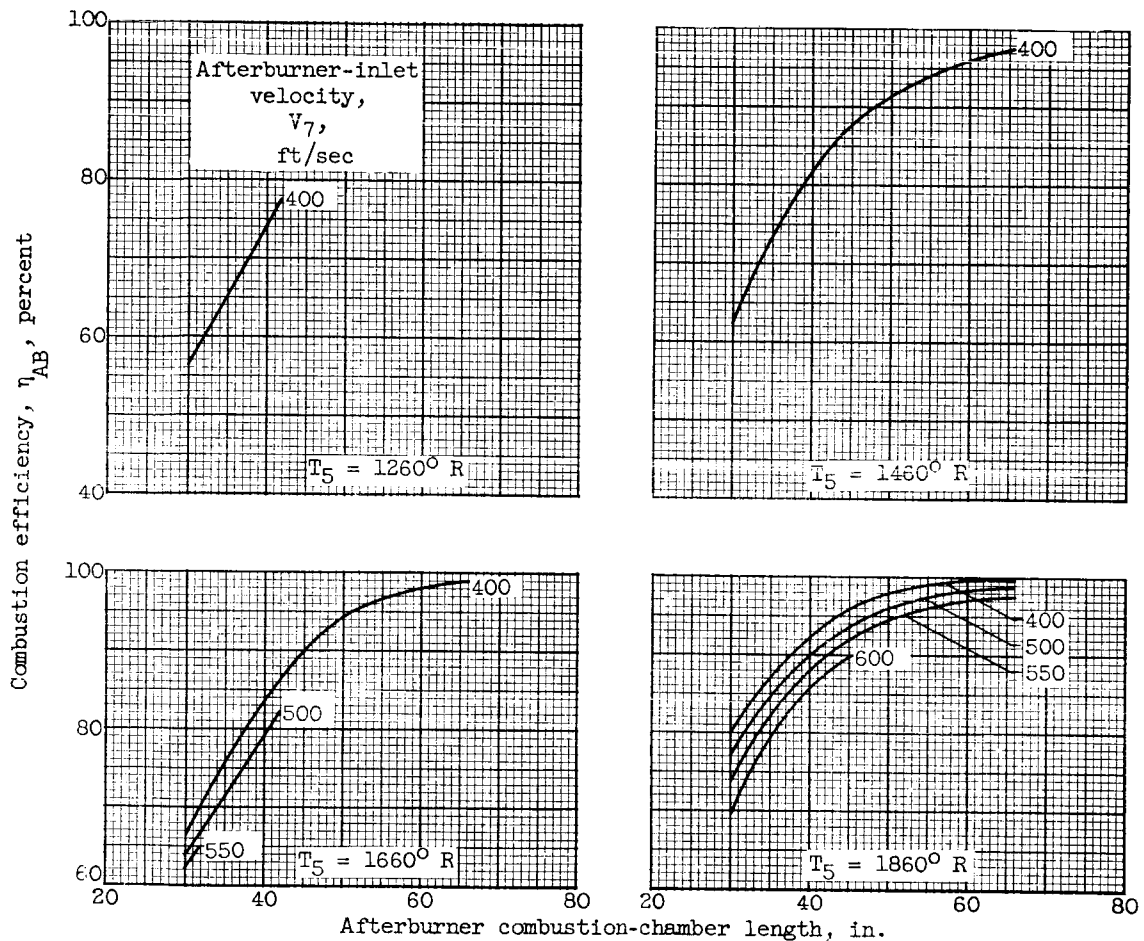
NACA RM E57C07



(h) Afterburner fuel-air ratio, 0.0676; afterburner-inlet total pressure, 1270 pounds per square foot absolute.

Figure 14. - Continued. Effect of afterburner combustion-chamber length on combustion efficiency for several afterburner-inlet velocities. T_5 , afterburner-inlet total temperature.

DECLASSIFIED



(i) Afterburner fuel-air ratio, 0.0676; afterburner-inlet total pressure, 1800 pounds per square foot absolute.

Figure 14. - Concluded. Effect of afterburner combustion-chamber length on combustion efficiency for several afterburner-inlet velocities. T_5 , afterburner-inlet total temperature.

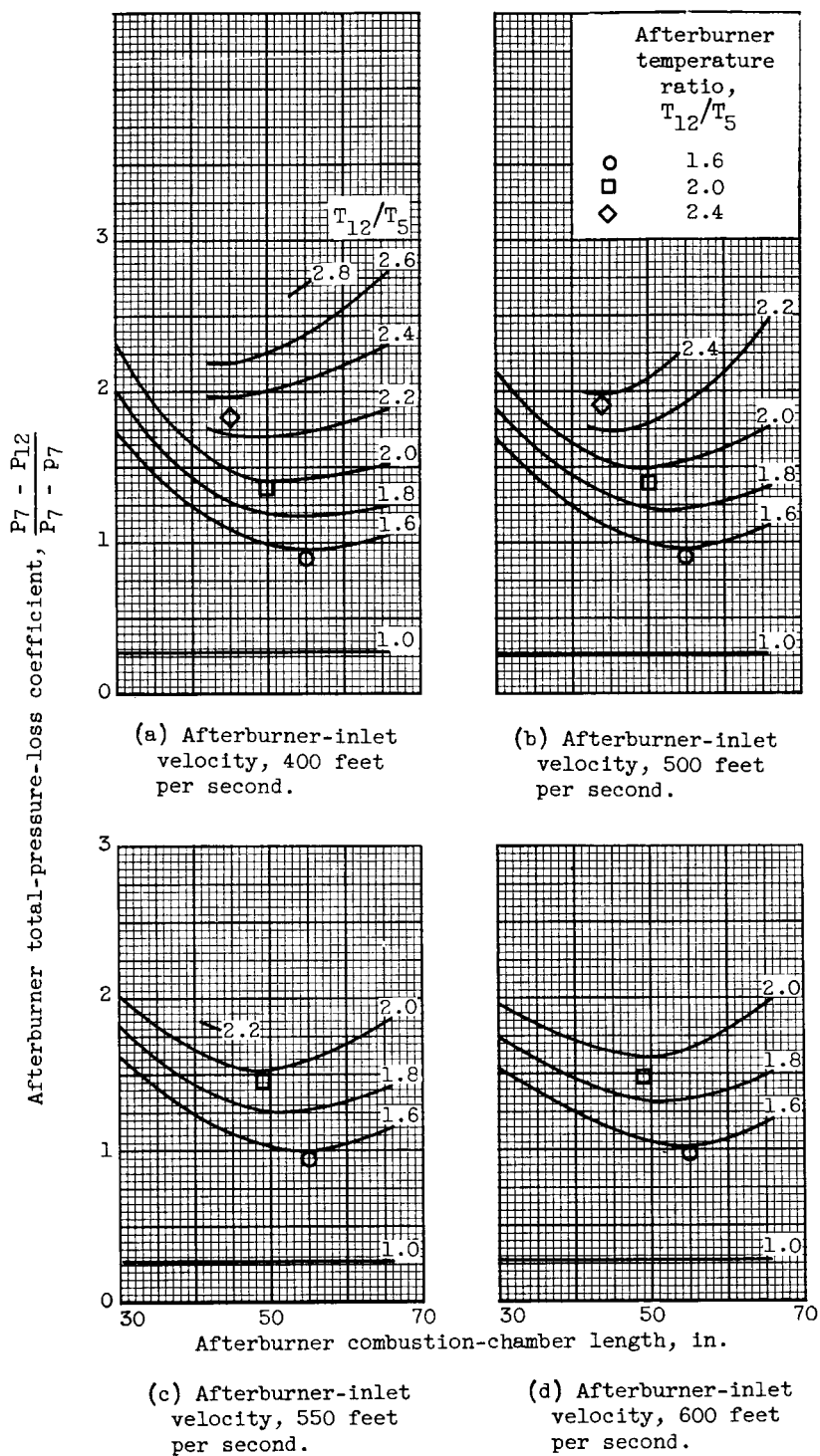
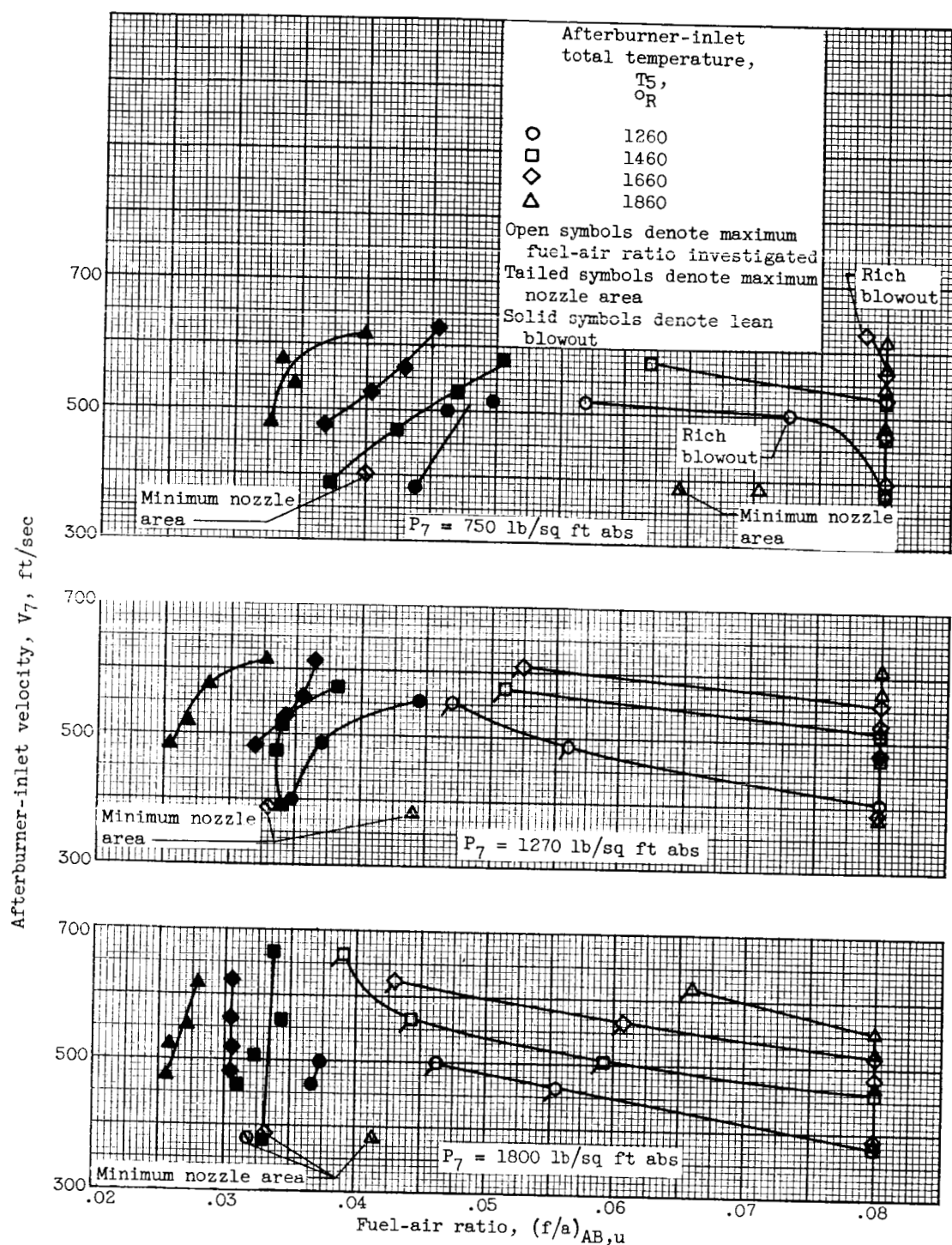


Figure 15. - Effect of afterburner combustion-chamber length on afterburner pressure-loss coefficient for several values of afterburner-inlet velocity and temperature ratio.

DECLASSIFIED

NACA RM E57C07

67



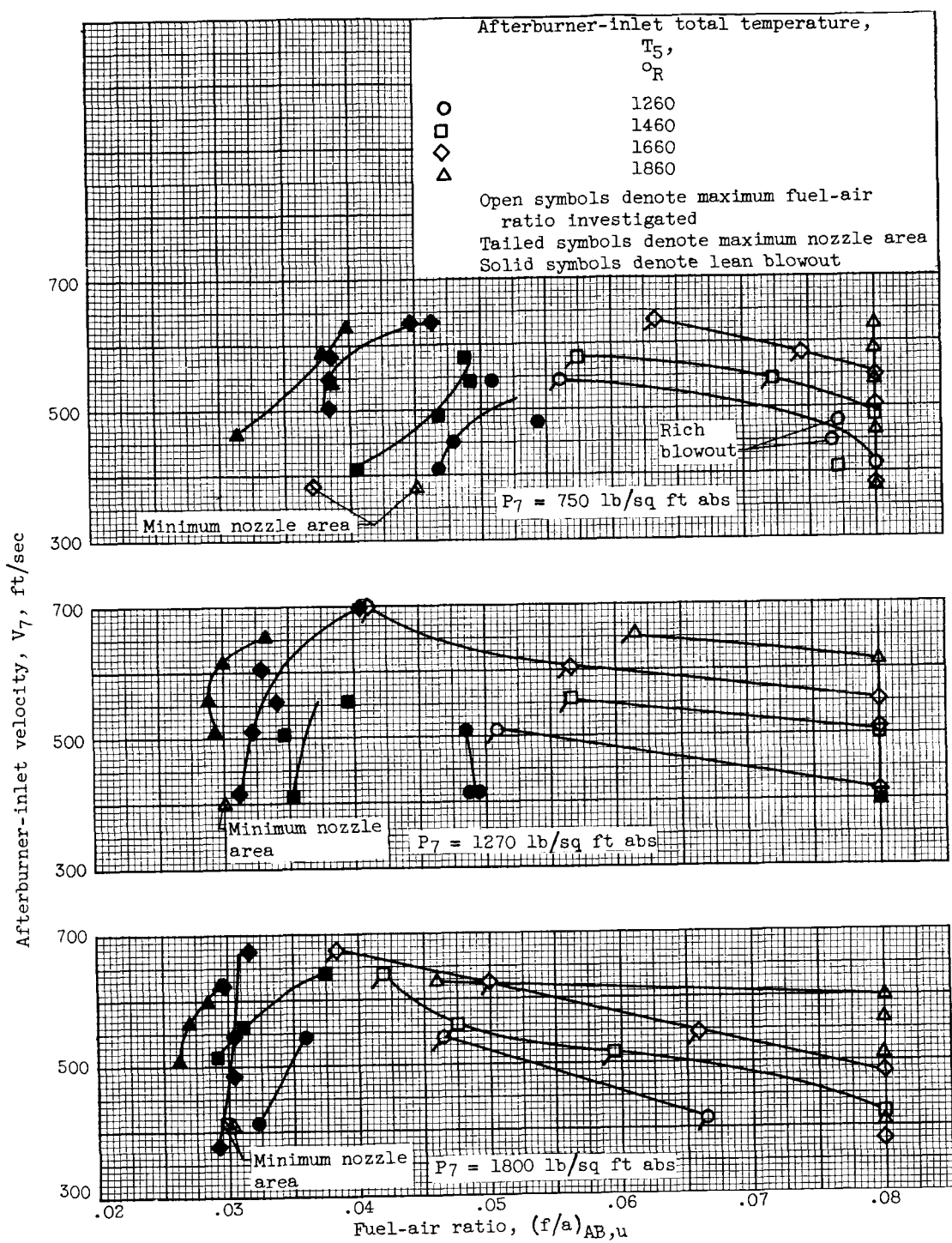
(a) Afterburner combustion-chamber length, 30 inches.

Figure 16. - Regions of afterburner operation at several afterburner-inlet total temperatures and total pressures for afterburners of various lengths. P_7 , afterburner-inlet total pressure.

031912201030

NACA RM E57C07

68



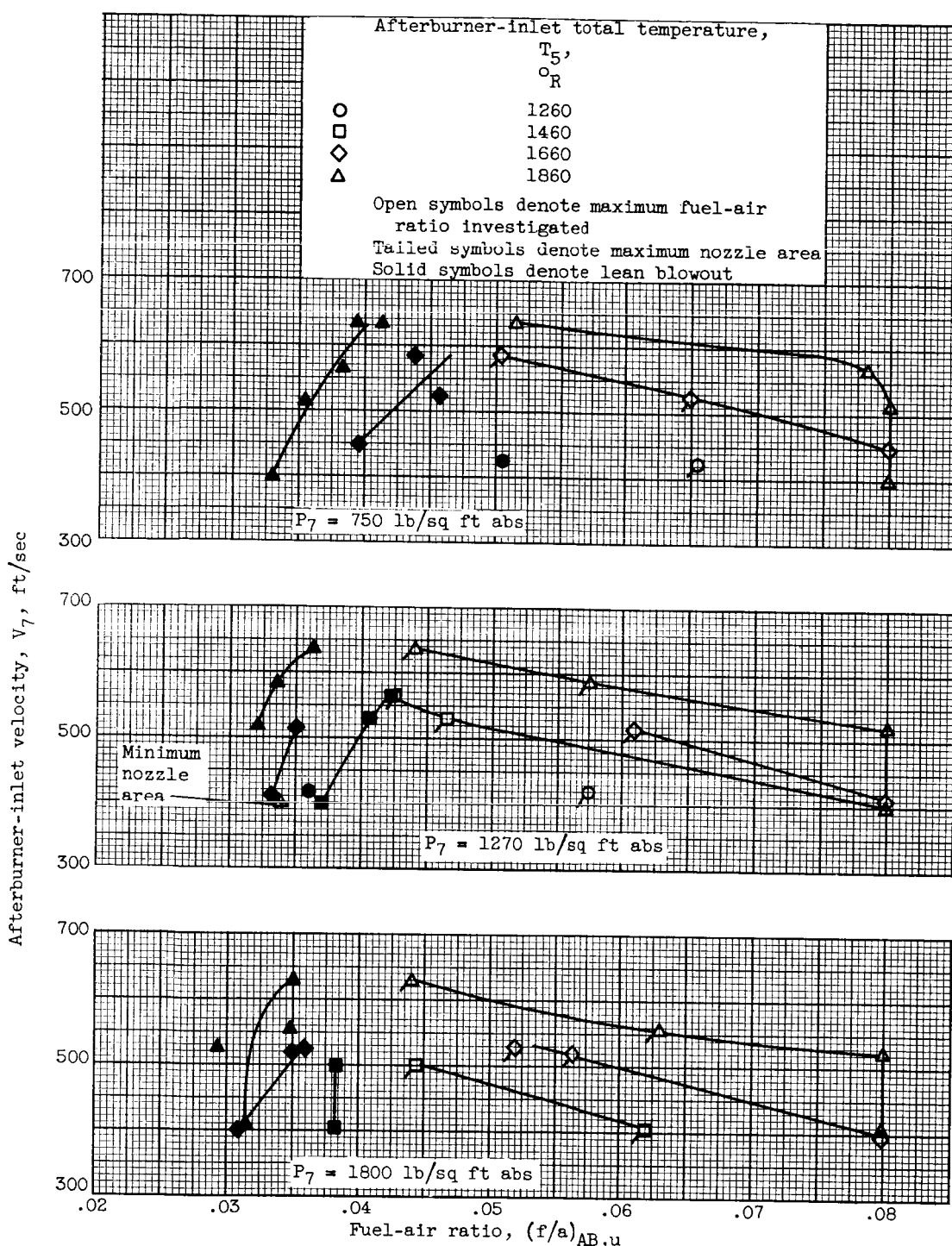
(b) Afterburner combustion-chamber length, 42 inches.

Figure 16. - Continued. Regions of afterburner operation at several afterburner-inlet total temperatures and total pressures for afterburners of various lengths. P_7 , afterburner-inlet total pressure.

DECLASSIFIED

NACA RM E57C07

69



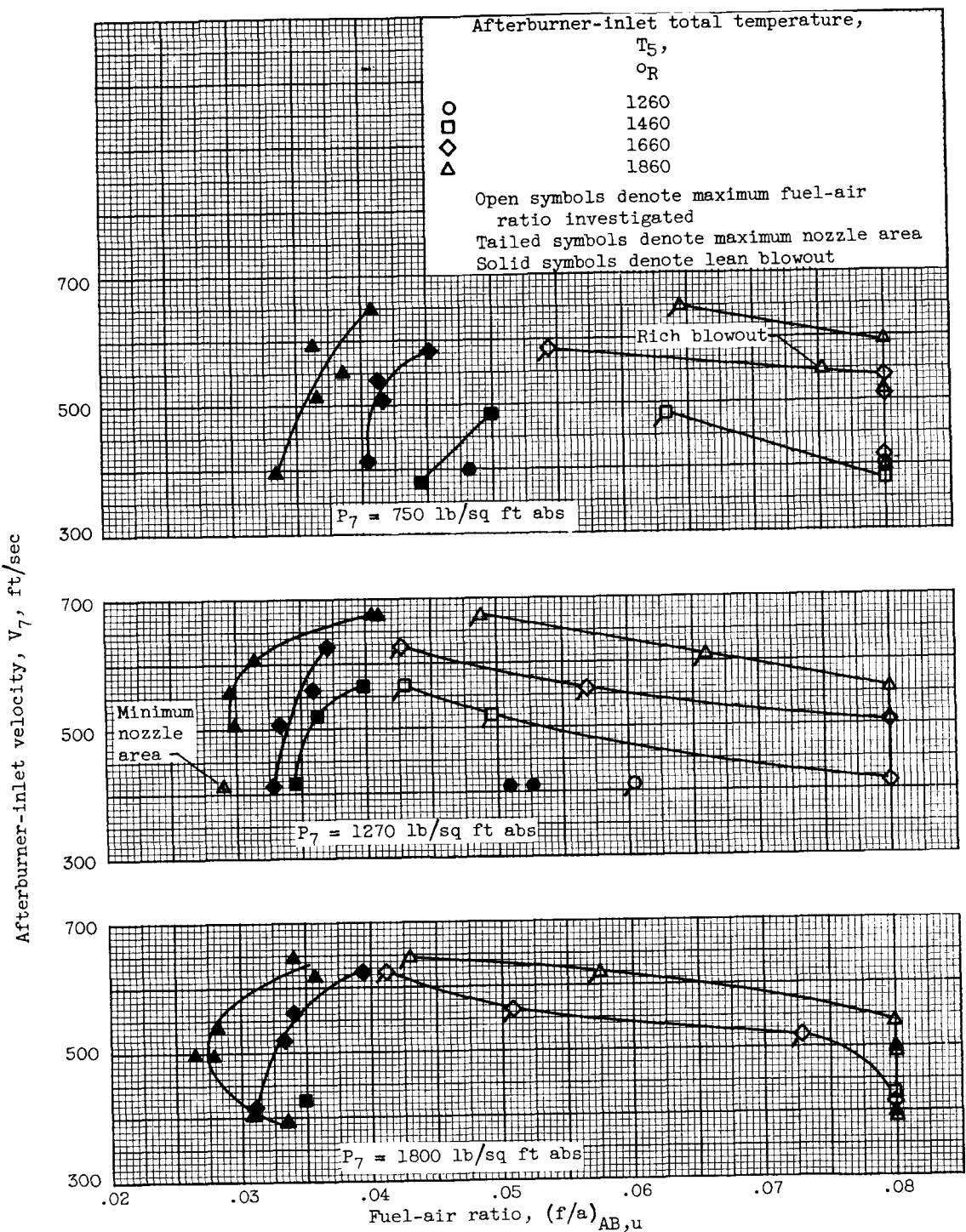
(c) Afterburner combustion-chamber length, 54 inches.

Figure 16. - Continued. Regions of afterburner operation at several afterburner-inlet total temperatures and total pressures for afterburners of various lengths. P_7 , afterburner-inlet total pressure.

0319122A1000

70

NACA RM E57C07



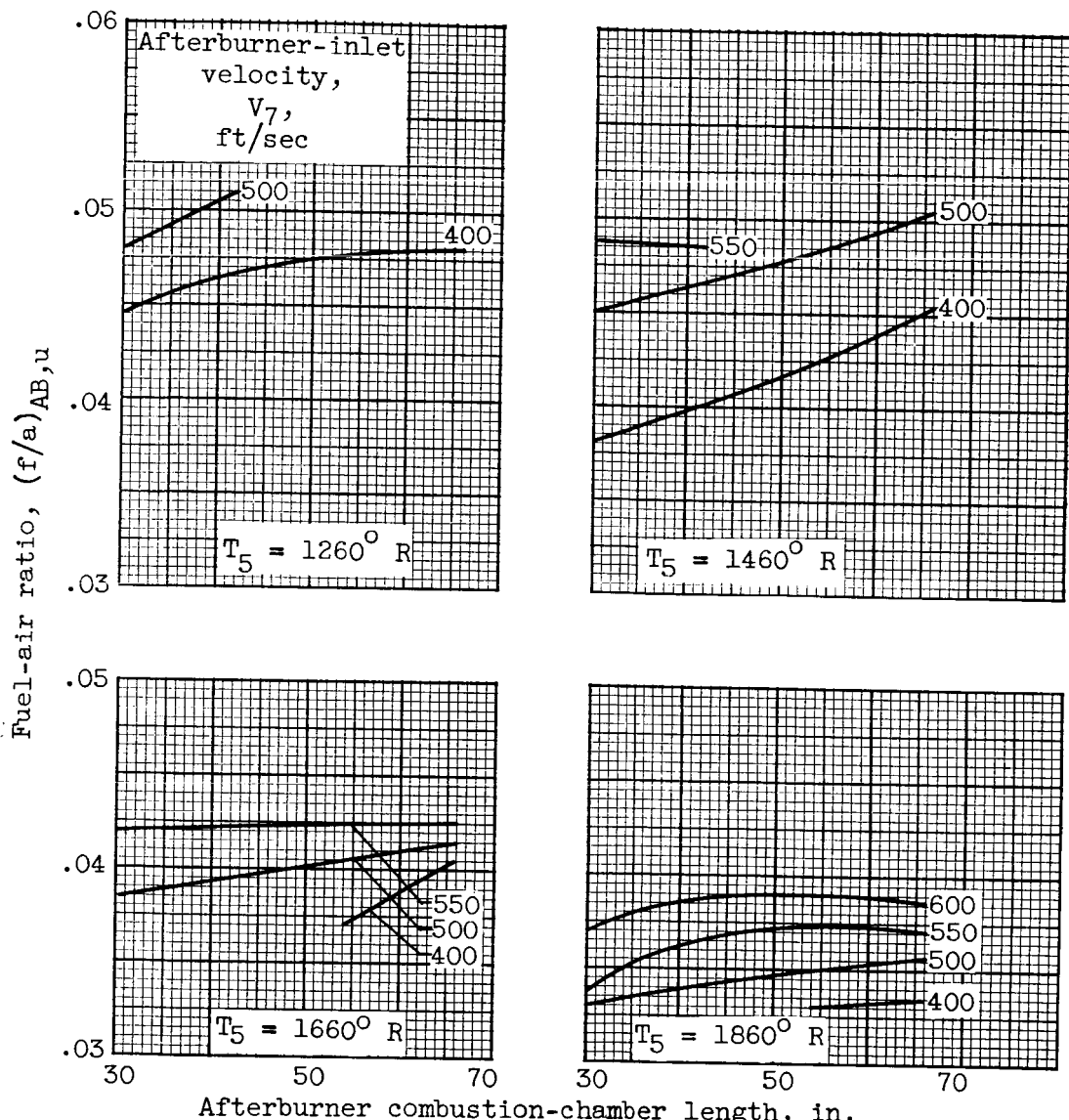
(d) Afterburner combustion-chamber length, 66 inches.

Figure 16. - Concluded. Regions of afterburner operation at several afterburner-inlet total temperatures and total pressures for afterburners of various lengths. P_7 , afterburner-inlet total pressure.

DECLASSIFIED

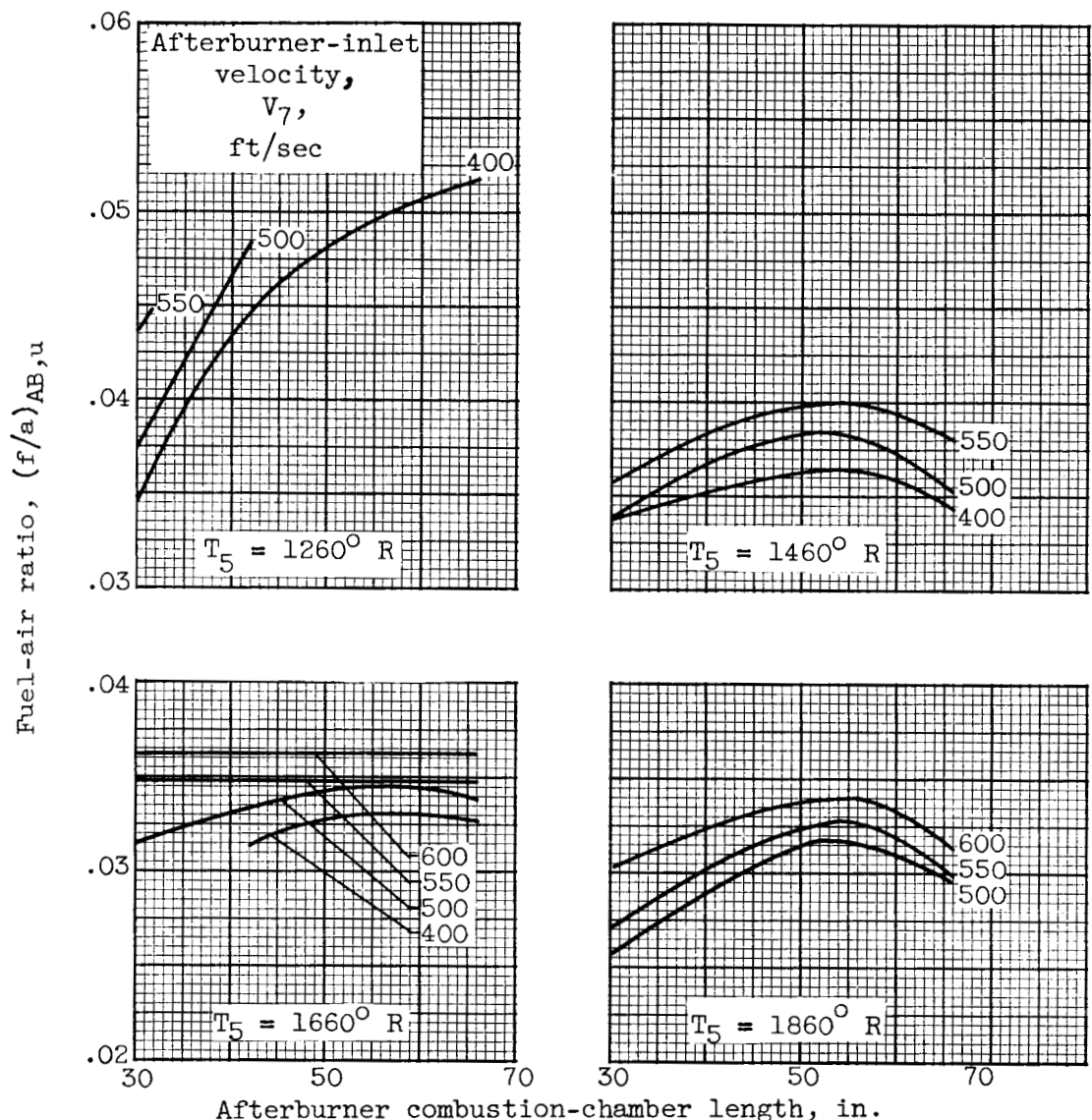
NACA RM E57C07

71



- (a) Afterburner-inlet total pressure, 750 pounds per square foot absolute.

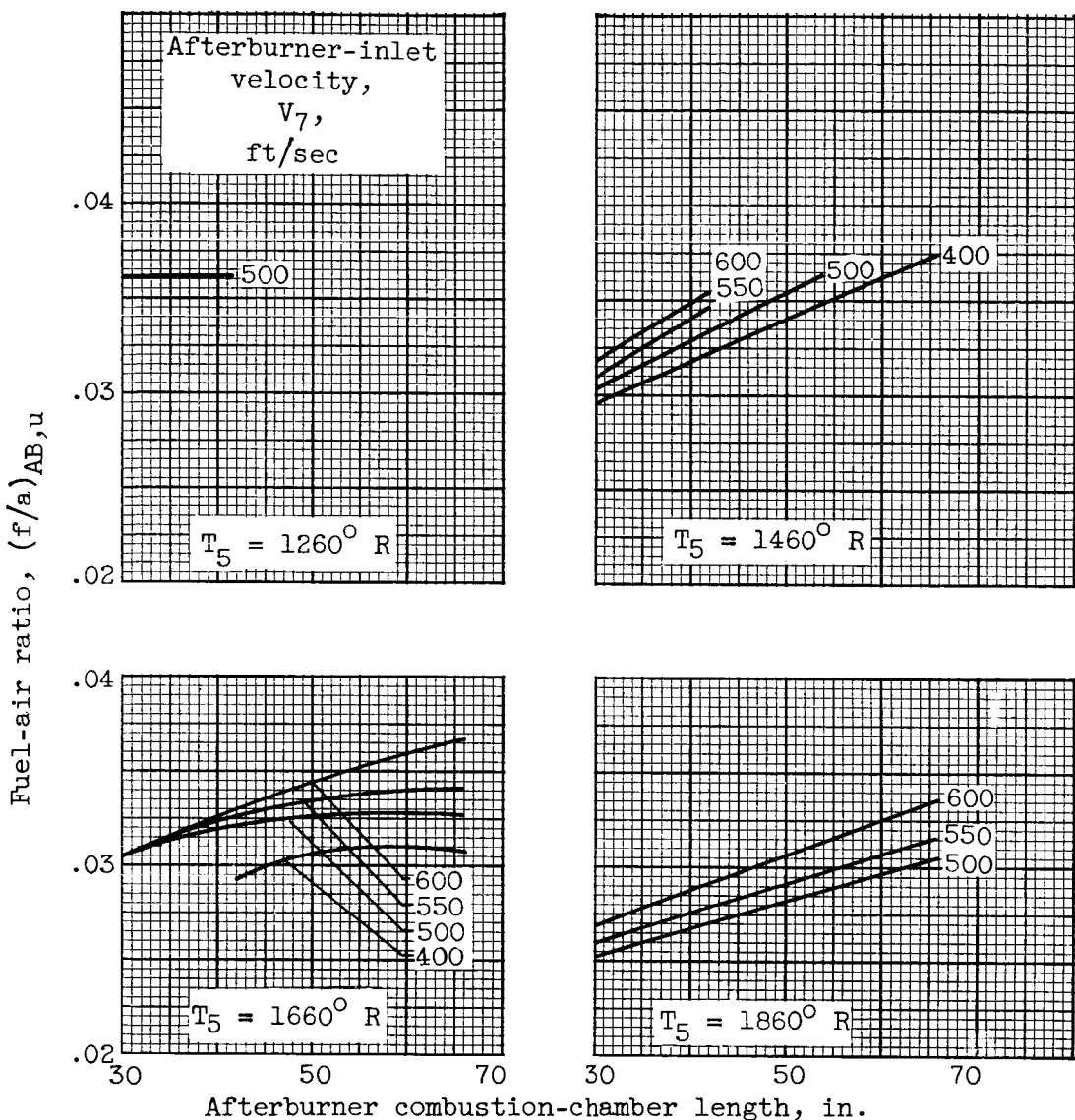
Figure 17. - Effect of afterburner combustion-chamber length on lean blowout limits. T_5 , afterburner-inlet total temperature.



(b) Afterburner-inlet total pressure, 1270 pounds per square foot absolute.

Figure 17. - Continued. Effect of afterburner combustion-chamber length on lean blowout limits. T_5 , afterburner-inlet total temperature.

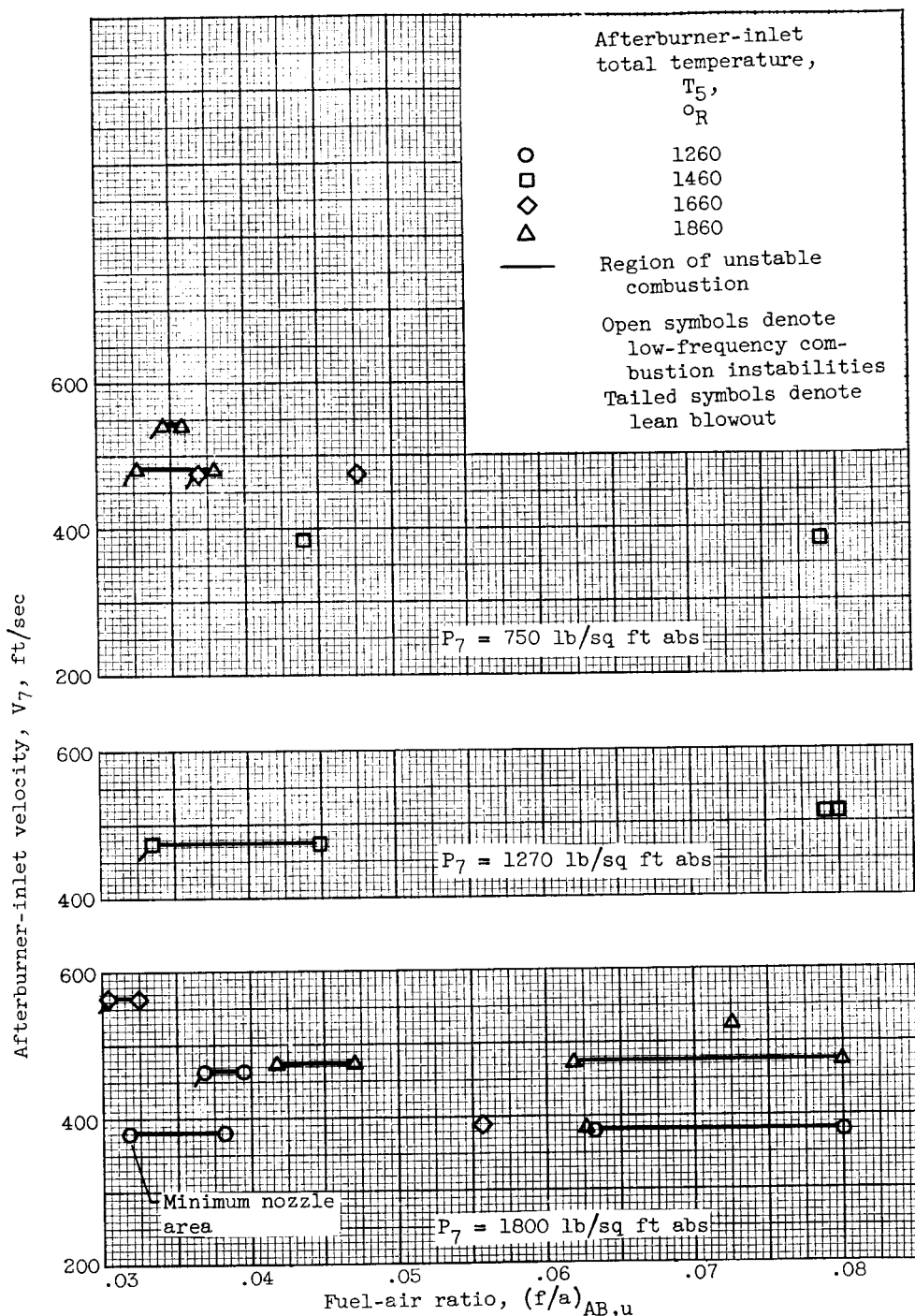
DECLASSIFIED



(c) Afterburner-inlet total pressure, 1800 pounds per square foot absolute.

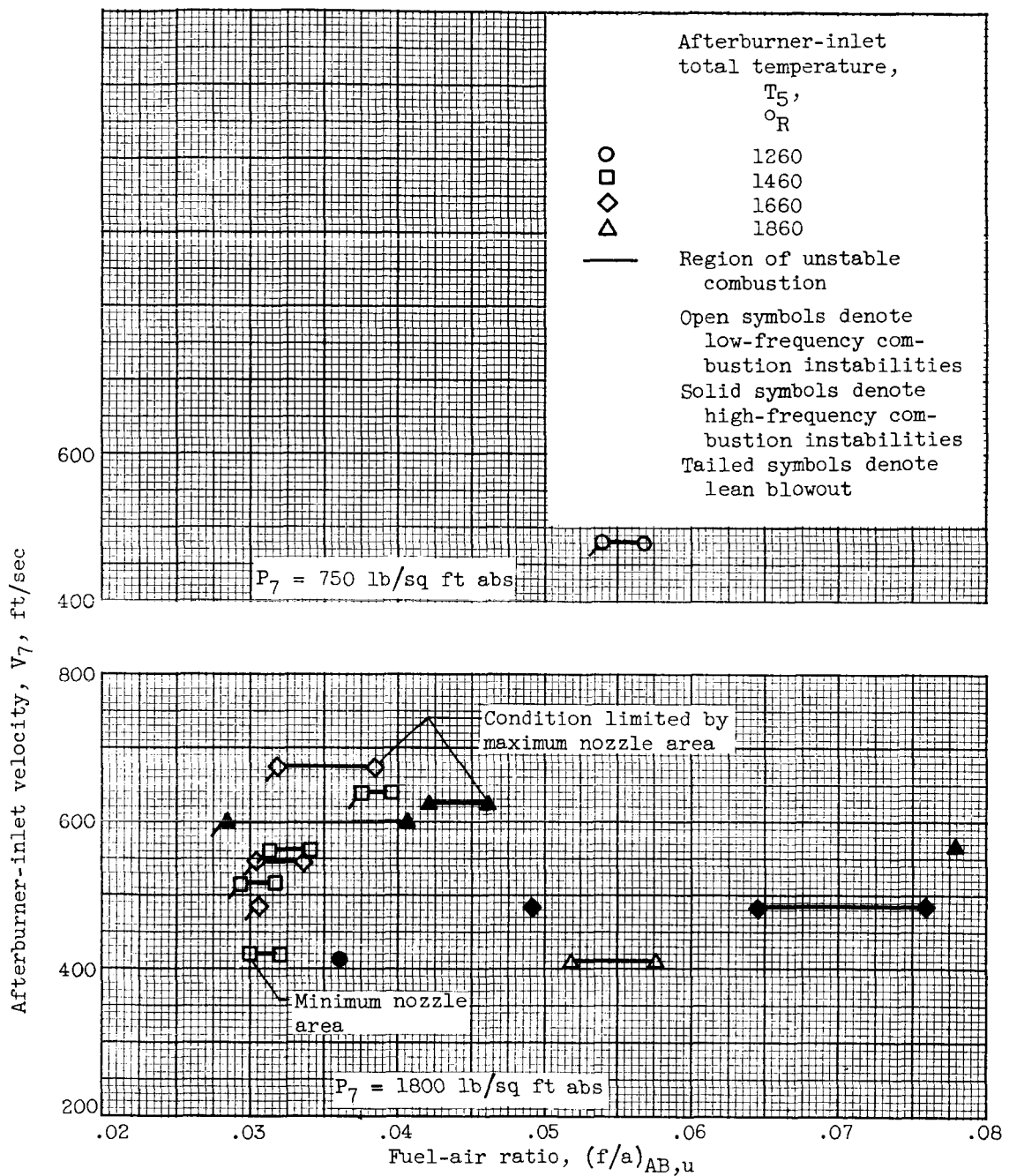
Figure 17. - Concluded. Effect of afterburner combustion-chamber length on lean blowout limits. T_5 , afterburner-inlet total temperature.

031712 200 1030



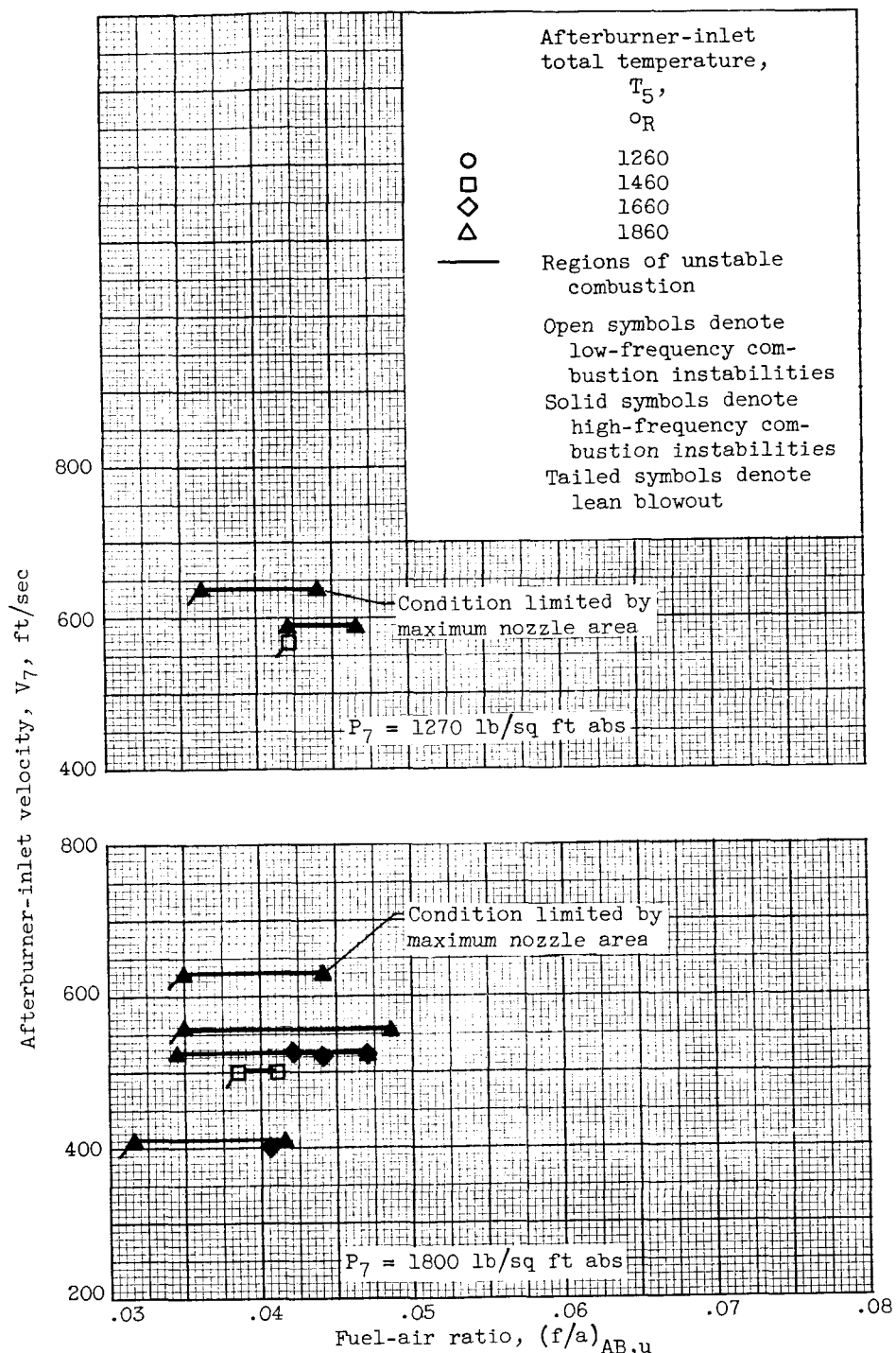
(a) Afterburner combustion-chamber length, 30 inches.

Figure 18. - Regions of combustion instabilities at several afterburner-inlet total temperatures and pressures. P_7 , afterburner-inlet total pressure.

REF ID: A6472
REF ID: A6472

(b) Afterburner combustion-chamber length, 42 inches.

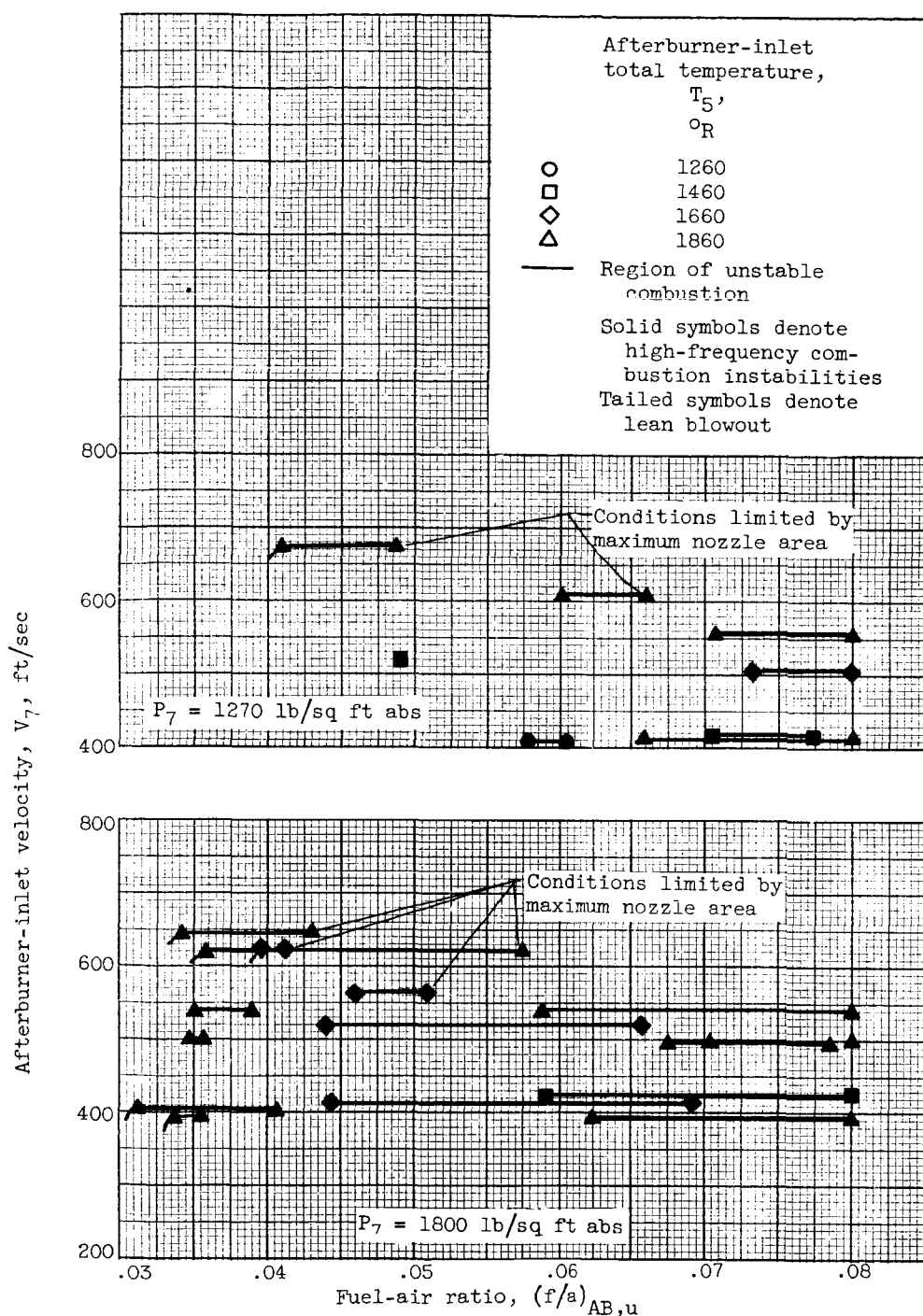
Figure 18. - Continued. Regions of combustion instabilities at several afterburner-inlet total temperatures and pressures. P_7 , afterburner-inlet total pressure.



(c) Afterburner combustion-chamber length, 54 inches.

Figure 18. - Continued. Regions of combustion instabilities at several afterburner-inlet total temperatures and pressures. P_7 , afterburner-inlet total pressure.

DECLASSIFIED



(d) Afterburner combustion-chamber length, 66 inches.

Figure 18. - Concluded. Regions of combustion instabilities at several afterburner-inlet total temperatures and pressures.
 P_7 , afterburner-inlet total pressure.

031912301500

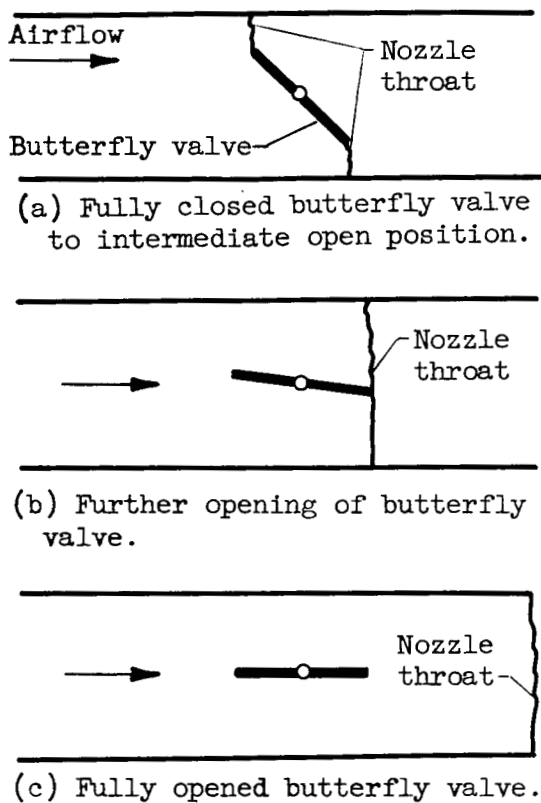


Figure 19. - Approximate position
of nozzle throat for various
positions of variable-area nozzle.